AASMUND FAHRE VIK

STRUCTURE AND SOLUBILITY OF NIOBIUM AND TANTALUM COMPLEXES IN MOLTEN ALKALI FLUORIDES

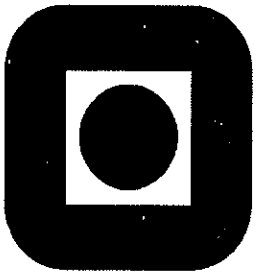

INSTITUTT FOR KJEMI

NORGES TEKNISK-
NATURVITENSKAPELIGE UNIVERSITET
NTNU

AVHANDLING NR. 99 - DESEMBER 2000

This thesis has been submitted to

Institutt for Kjemi

Norges Teknisk-Naturvitenskaplig Universitet

in partial fulfillment of the requirements for

the Norwegian academic degree

DOKTOR INGENIØR

November 2000

Acknowledgements

I would like to thank Prof. Dr. Techn. Terje Østvold for helping and guiding me through the work on this thesis. I appreciate his effort to motivate and encourage me through these four years, and for allowing me to travel to Greece, France and England. These trips have meant very much to me, both personally and scientificly. His experience on molten salts and research in general has most valuable for me. I realize how important it has been to have him around almost every day, and I thank him for always using his time to aid me. I am also grateful for his comments to this document, and for him helping me to "keep my feet at the ground" while writing it.

Most of the work on my thesis has been carried out at the Department of Chemistry, The Norwegian University of Science and Technology, Trondheim. Financial support through a scholarship from the Institute of Chemistry is thankfully acknowledged. The experimental work with Raman spectroscopy was carried out at Institute of Chemical Engineering and High Temperature Chemical Processes in Patras, Greece. Thanks are gratefully offered Vassilis Dracopoulos and George N. Papatheodorou for helping me out during my visits, and for introducing me to the Greek way of living.

I would also like to thank Heidi Mediaas for helping me out at the lab, and for teaching me all the experimental methods I have used in Trondheim. Thanks are also expressed to all the people and technical staff at the Department of Chemistry. I send my warmest greetings to the people at "Inorganic Chemistry"; you have made my years here unforgettable, and I would like to thank all of you.

Finally, for completely non-scientific reasons, I would like to thank my mother, father and my two sisters for always being there for me. My final thanks goes out to all my friends, to all those people that I have learned to know in my life. Let the light surround you...

Abstract

Alkali fluoride melts have been proposed as electrolytes for electroplating of niobium and tantalum. These and related melts have been studied extensively in order to develop a process for production of coherent deposits of these refractory metals. Special attention has been given to the influence of oxide impurities in the electrolytes. Oxide has a significant effect on current efficiency, coherence of the deposit and purity of the metal. The object of the present work has been to study the solubility and structure of different $Nb(V)$ and $Ta(V)$ complexes in $FLiNaK$ melts with varying $n_{O^{2-}}/n_{M^{5+}}$ $(M = Nb, Ta)$ ratios.

Raman spectroscopy and solubility measurements have been used to study $Nb(V)$ and $Ta(V)$ complexes in the molten LiF-NaF-KF eutectic $(FLiNaK)$. $Na_2O(s)$ was added to melts containing a given amount of K_2NbF_7 or K_2TaF_7, and samples were withdrawn at different ratios of oxide to refractory metal concentration. The samples were analyzed for oxygen and Nb/Ta, and studied by Raman spectroscopy using the windowless graphite cell technique. The solubility of both systems were studied at 700 °C.

Solubility measurements in a $FLiNaK$ melt containing 0.22 mole/kg K_2NbF_7 indicated that all the oxide and $Nb(V)$ dissolved for $n_O/n_{Nb} < 2$. Further addition of Na_2O led to precipitation of a solid compound $AlkNbO_3$ $(Alk = Li, Na, K)$, and a solubility minimum was observed at $n_O/n_{Nb} = 3$. From the Raman data, the existence of $NbF_7^{2-}(C_s)$, $NbOF_5^{2-}(C_{4v})$ and $NbO_2F_4^{3-}(C_{2v})$ at n_O/n_{Nb} ratios up to 2 were established. The spectral features indicated that a niobium trioxo fluoride complex was present in melts with $n_O/n_{Nb} \sim 3$. The complex was possibly $NbO_3F_3^{4-}$. At $n_O/n_{Nb} > 3$ the solubility data were consistent with a dissolution of the $AlkNbO_3$ solid, and formation of a $NbO_4F_x^{(x+3)-}$ species. At $n_O/n_{Nb} > 4$ an oxygen rich solid seemed to precipitate. The Raman spectra indicated the existence of $NbO_4F_2^{5-}$ species as well as $(NbO_6)_n$ network structures in these melts.

The same sets of measurements were performed with $FLiNaK$ containing 0.0956 mole/kg K_2TaF_7, and quite similar data were obtained. All the added amounts of oxide and tantalum dissolved in melts with $n_O/n_{Ta} < 1.8$, and precipitation of a solid compound $AlkTaO_3$ ($Alk = Li, Na, K$) was observed at higher ratios. A solubility minimum was observed at $n_O/n_{Ta} = 3$. From the Raman data, the existence of $TaF_7^{2-}(C_s)$, $Ta_2OF_x^{(x-8)-}$, $TaOF_5^{2-}(C_{4v})$ and $TaO_2F_x^{(x-1)-}$ at ratios up to 2 were established. The dioxo fluoro complex was probably $TaO_2F_4^{3-}(C_{2v})$, and a polarized band at 980 cm^{-1} suggested the presence of yet another tantalum oxo fluoro complex. No evidence for a tantalum trioxo fluoro complex was found. At $n_O/n_{Ta} > 3$ the solubility data were consistent with a dissolution of the $AlkTaO_3$ solid, and formation of a $TaO_4F_x^{(x+3)-}$ species. The tantalum tetra oxo fluoride complex was possibly $TaO_4F_2^{5-}(C_{2v})$. The solubility data indicated precipitation of an oxide rich solid at $n_O/n_{Ta} > 4$. The Raman spectra indicated the existence of $TaO_4F_2^{5-}(C_{2v})$ species as well as $(TaO_5)_n$ or $(TaO_6)_n$ network structures in these melts.

The major difference between the niobium and the tantalum systems was the solubility of the $AlkMO_3$ solid ($M = Nb, Ta$). The solubility of $AlkNbO_3$ in molten $FLiNaK$ at 700 °C was found to be more than 7 times larger than that of $AlkTaO_3$. The lack of a $TaO_3F_x^{(1+x)-}$ complex was probably the reason for the lower solubility of $AlkTaO_3$.

The solubility of $Nb_2O_5(s)$ in $FLiNaK$ was studied as a function of temperature. It was found that $NbO_2F_4^{3-}$ and $NbO_3F_3^{4-}$ were formed and that $AlkNbO_3$ precipitated as $Nb_2O_5(s)$ dissolved. The ratio of oxide to $Nb(V)$ was about 2.1 in saturated melts. The dissolution of $Ta_2O_5(s)$ in $FLiNaK$ was studied at 700 °C, and the ratio of oxide to $Ta(V)$ was found to be below 2. These melts contained $TaOF_5^{2-}$, $TaO_2F_4^{3-}$ and an unidentified species with a Raman active band at 980 cm^{-1}. The Ta_2O_5-$FLiNaK$ melts studied were not saturated with Ta_2O_5.

Contents

Chapter 1

Introduction

1.1 Refractory metals

The main reference in section 1.1 is : Senderoff [1].

A refractory metal is generally a metal with high melting point. There is, however, not any lower limit of melting temperature that defines this group. The main interest in refractory metals is as structural materials for high-temperature applications where iron-alloys or common non-ferrous-alloys fail. It is therefore reasonable to set the melting point of iron, 1535 °C, as a lower limit to the melting point of a metal to be considered refractory. The metals that melt above 1535 °C are those in group IV_A, V_A, VI_A in the periodic system, the six platinum metals, rhenium, technetium and some of the lanthanides and actinides. If the metal is to be used as a structural material, the platinum metals would definitely be too expensive and are excluded. The same goes for rhenium, technetium and the lanthanides and actinides because of their scarcity. This leaves the nine metals in group IV_A, V_A and VI_A: Titanium, zirconium, hafnium, vanadium, niobium, tantalum, chromium, molybdenum and tungsten. The term "refractory metal" is a matter of definition and some choose to include other elements like rhenium and osmium and exclude a metal like hafnium. In this work, only the nine metals previously mentioned will be considered as refractory metals.

1.1.1 Mechanical properties

Due to the high melting points of the refractory metals, they are interesting as potential high temperature structural materials. Their oxidation-resistance is, however, poor at elevated temperatures, and this is their mayor limitation for more widespread use in such applications. Since non of the refractory metals are particularly noble, they will be oxidized by air at even low temperatures (room temperature) and will be covered by a layer of metal-oxide. It is the stability of this oxide that determines the actual oxidation-resistance. The oxides of vanadium, molybdenum and tungsten melt or sublime below 1000 °C, and even though Cr_2O_3 is only slightly volatile, the metal itself is quite volatile at 1000 °C. Zirconium, niobium and tantalum are probably the most oxidation-resistant of the refractory metals, but they also require protective coatings for use above 600 °C.

The mechanical properties of these metals strongly depend on the amount of interstitial impurities such as oxygen, nitrogen, hydrogen and carbon. Since the removal of these impurities to acceptable levels is very difficult, there has been some disagreement concerning the measured values of mechanical properties of these elements. It is, however, clear that they all become seriously more brittle due to traces of the above mentioned impurities, and room temperature brittleness is a common occurrence. Of the nine metals, niobium and tantalum are probably those that have the best mechanical properties at low temperatures. The metal that has gained most attention as a low temperature structural metal the later years is undoubtedly titanium. This is due to its low density and high strength. It is an excellent choice for applications where weight reduction is crucial, and cost is more or less unimportant. Titanium has been used as metal implants in the human body, and is a common metal in aerospace applications.

1.1.2 Physical properties

As already mentioned, titanium is a popular material in structural applications due to its low density of 4.5 g/cm^3. Tungsten, on the other hand, is the heaviest of the nine metals with a density of 19.3 g/cm^3 and is rarely used in larger structures. The refractory metals include materials that are among both the highest and the lowest in neutron cross- section, and they are therefore suitable for a number of different nuclear applications. Their mean coefficient of thermal linear expansion varies from $4.6 \cdot 10^{-6}/°C$ for

tungsten to $10.0 \cdot 10^{-6} / °C$ for vanadium and chromium. This relatively narrow range makes it possible to use the refractory metals together without having too much strain on their interface or connecting points. The group V and VI metals are all body-centered cubic in structure in their solid state, while the group IV metals are hexagonal close packed at low temperatures and change to body-centered cubic above 800 °C.

1.1.3 Chemical properties

In addition to the mechanical and physical properties of the refractory metals, they possess chemical properties that have made them important in nuclear, aerospace and corrosion-resistance applications. The latter is interesting in electroplating since only a thin coating of the metal is needed for the metal to act as a corrosion-resistant material. Electroplating is described in more detail in section 1.3.3. Tungsten, niobium and tantalum have a corrosion-resistance similar to that of glass or quartz; they are attacked by hot alkalis and by hydrofluoric acid. Their resistance towards hot, strong acids and oxidizing acids is excellent due to the stability of their metal oxide at temperatures below 600 °C. Zirconium has similar properties, but has a lower resistance to hot mineral acids. Titanium has a high resistance towards oxidizing and chloride environments. This has led to its use for tools where corrosion may be of concern.

1.2 Niobium and tantalum

Since niobium and tantalum chemistry is studied in this work, the two metals are described in more detail than the other refractory metals. The Tantalum-Niobium International Study Center (T.I.C) [2] is an international, non profit association founded under Belgian law. It received Royal Assent in 1974, has its headquarters in Brussels, Belgium, and has more than 50 member situated in more than 20 countries across the world. The members include companies involved in raw material production, assaying, trading, capacitor manufacturing and chemical process equipment production. The main goal of T.I.C is to increase awareness of the two metals and their special properties, and to promote the use of the metals and their products. Their web site [2] has, with permission, been used as a source for this section.

1.2.1 Niobium and tantalum – dissimilar twins?

In 1801 an American chemist named Charles Hatchett analyzed a black mineral from Connecticut and found that it contained a new element which he named columbium. A year later Anders Eckberg in Sweden discovered two minerals, each containing an oxide of an unknown element. The oxide proved very difficult to dissolve in acids, and was in his opinion frustrating to work with. He therefore named it tantalum, after the king Tantalus from Greek mythology who could not reach the water to drink or the apple to eat.

In 1844 the German chemist Heinrich Rose found that another element was present in the Swedish mineral, and he named it niobium after Niobe, the daughter of Tantalus. The European niobium was later shown to be identical to the American columbium, and for nearly a century arguments raged over which name had priority. Finally in 1950 the name niobium was officially adopted by IUPAC, but a few commercial producers in America still refer to it as columbium. This is further complicated by the fact that one of the two most common minerals of niobium is universally known as "Columbite". Of the two elements, niobium is far more abundant in the earth's crust than tantalum; nevertheless they almost always occur together. This is a result of the very similar chemical properties of the their oxides, and this was also the reason why the early chemists had trouble distinguishing them from each other. The columbite mentioned above is an iron manganese niobate and there is also an iron manganese tantalate named "Tantalite". A full range of mixtures between these extremes exists, and they are all naturally occuring.

When the two elements were finally separated in 1866, and the metals were produced, it was clear that the similarity did not extend to all their physical properties. The most obvious difference is the density since tantalum is nearly twice as heavy as niobium. Due to this, and the relative abundance of niobium compared to tantalum in the earth crust, they have different applications. In some cases, in particular their use as high purity metals and their alloys, there are some overlap. The term "dissimilar twins" does indeed suit these two elements.

1.2.2 Raw materials and processing

Until recently the majority of the world's production of tantalum was from the discard slag of tin smelters. The tin mineral "Cassiterite" is frequently

associated with "Columbite" and "Tantalite" ore, especially in Thailand, Australia, Brazil and Central Africa. When the tin concentrates are melted, the tin is reduced to metal, while the tantalum remains unreduced in the slag, where it can be recovered by electric melting and/or chemical extraction. Tin slag, particularly those from the Thaisarco smelter in Phucket, Thailand, used to be an important supplier of tantalum. The decline of the tin industry in South East Asia since 1985 has led to a replacement of that tantalum source by primary mining of "Tantalite". There are a number of mines now operating, and two of the largest are open-cut operations in Western Australia (Greenbushes and Wodgina). There is also a sizeable amount (around 25%) of recycling of scrap metal and of compounds of tantalum.

Only a small part of the industry's needs for niobium is recovered during the treatment of tin slag and "Columbite"/"Tantalite" minerals which are the source of much of the world's tantalum. About 90% of all niobium is recovered as ferro niobium for use in steel-making, where the mineral "Pyrochlore", a calcium fluoro niobate, is melted by reduction of aluminum. The calcium fluoro tantalate is known as "Microlite", and is mined for similar tantalum production. Two mines in Brazil, the CBMM mine at Araxá and the Anglo-American mine at Catalão in Goiá, are the sources for 80% of all niobium, while one mine in Canada (Niobec at St Honoré) accounts for more than 10%.

The extraction of pure tantalum and niobium metal is done by chemical means rather than melting. The ores are concentrated, and leached in HF/H_2SO_4 to bring the tantalum and niobium compounds into solution. The acid solution is mixed with *methyl-iso-butyl ketone* which extracts the niobium and tantalum while leaving the impurities in the aqueous solution. The organic and inorganic phases are immiscible, and the two liquids are separated. The niobium is stripped with dilute acid, and the tantalum is subsequently extracted by acid ammonium fluoride. The tantalum is usually produced in powder form by sodium reduction of the fluoride, and can then be compacted to a final shape or melted in an electron beam furnace.

1.2.3 Applications

50% of the total tantalum usage is as powdered metal, mostly for the production of capacitors. This is due to the dielectric properties of the tantalum oxide that is formed on a tantalum compact. The amount of tantalum needed for a capacitor is reduced as the purity of the metal is increased, and

this has made the manufacturers develop a better knowledge of the process. Other important factors are particle size and shape, and all these technical advances have enabled the capacitor manufacturers to make large increases in their production. This without having a significant increase in the consumed amount of tantalum. Other important applications of tantalum are tantalum carbide used in cutting tools, pure or alloyed tantalum used as corrosion or heat resistant chemical plant equipment or in superalloys for jet engines.

As already mentioned, around 90% of the niobium usage is due to its use in structural steels, in heat resisting steels and in superalloys based on iron, nickel or cobalt. Other important alloys include tin or titanium based alloys for superconducting magnets, alloys with copper in powder metallurgy composites for components with high strength and conductivity and an alloy with zirconium for nuclear reactor fuel tubes. As for tantalum, niobium is also used as a fabricated metal for chemical plant equipment, and alloyed with zirconium or other metals for high temperature applications in aerospace. The most important non-metallic use of niobium is as the carbide in cutting tools, and the oxide Nb_2O_5 in high refractive index glass, as lead niobate in piezoelectric devices, and as single crystal $LiNbO_3$ in surface acoustic wave filters for television sets and similar equipment.

Niobium and tantalum has also gained a growing interest in medical and pharmaceutical applications later years. Tantalum is inert to the body's fluids and is an ideal metal in surgical equipment, artificial joints, plates, pacemakers and dental implants. Due to the chemical stability of the tantalum- and niobiumoxides, they are totally hypo-allergenic, and the two metals are now used as a base material in jewelry. Especially niobium, which is the cheapest of the two, is a popular choice for users with nickel-allergy, and is a safe metal even in extreme cases where gold and platinum causes an allergic reaction. Niobium looks like steel when it is exposed to air, and like platinum when it is polished. By a controlled deposition of the oxide film, the metal will appear to have all kinds of colors. By altering the thickness of the oxide surface film, the metal will shine in all the rainbow's colors.

1.3 Electrodeposition of refractory metals

The main references for this section are Sethi [3] and Senderoff [1], and the text is structured according to the latter.

The processes for electrodeposition of metals to be considered here are classified into four types: Electrowinning, electrorefining, electroplating and electroforming. All methods are widely used in aqueous systems, but this section will focus on molten salt applications. Except from chromium, non of the refractory metals can be electrodeposited in pure form in aqueous systems. These systems are therefore of little relevance to the current work. Table 1.1 was first presented by Senderoff [1] and summarizes the characteristics of the four elecrodeposition processes.

Table 1.1: Electrodeposition processes

Process	**Anode**	**Cell feed**	**Minimum required properties of cathode deposit**
Electrowinning	Not metal to be deposited	Compound of deposited metal dissolved in electrolyte	Metal in recoverable form suitable for refining
Electrorefining	Impure metal	Anodes only	Pure metal in recoverable form
Electroplating	Pure metal	Anodes only	Continuous, coherent, comparatively thin coating of metal adherent to substrate
Electroforming	Pure metal	Anodes only	Thick, continuous, coherent, freestanding metal deposit

1.3.1 Electrowinning

Electrowinning is a process where a mineral or a refined compound is converted to metal. This is commonly used for the production of non-refractory metals like aluminum, magnesium and copper, and involves the electrolysis of the metal dissolved in a proper electrolyte. The processes are used for production of metal in bulk form, and common for them all is that the anode is not the metal to be deposited. This makes electrowinning different from the other methods in concern, since the concept of the process is to convert a mineral to metal and a dissolution of the anode is not wanted.

The traditional methods for production of refractory metals have been by reduction of a halide or an oxide of the refractory metal with an active metal, carbon or hydrogen. Typical examples are the reduction of $TiCl_4$ by magnesium, which accounts for the major production of titanium metal in the world, reduction of V_2O_5 by calcium, reduction of Ta_2O_5 by carbon and reduction of WO_3 by hydrogen. The difficulties in achieving the desired purity by these methods, motivated a considerable research effort towards alternative processes. Among these, the electrowinning type process was among the most promising. All the refractory metals can be electrodeposited from molten salts, and many electrowinning routes have been developed which yielded excellent high purity metal powders, dendrites and crystals. Only a few of these have proven to be commercially successful, where the process of Balke [4] for production of tantalum is the best known. In this process K_2TaF_7 containing some Ta_2O_5 is electrolyzed at 900 °C in an iron pot (cathode) with a graphite rod as anode. The metal is formed as powder, which is separated from the electrolyte after cooling of the pot. In aluminum and magnesium electrolysis, the metal is produced as a liquid and separates from the electrolyte by a density difference. This makes it easy to tap the metal in a pure form. Due to the high melting points of the refractory metals, an electrolytic production of liquid metals is impractical. The processes for their electrowinning usually operates between 600 °C and 1000 °C, where it is possible to find suitable materials for containers, electrodes, diaphragms and insulators. The volatility of the electrolytes are also acceptable in this temperature range. Since the electrowinning of refractory metals produce metal in the solid state, it is necessary to separate the product from the electrolyte. This process require grinding, leaching, and/or sublimation, compaction and finally melting or sintering to produce the ingot. The mechanical properties of these metals are reduced drastically by only minor contamination of oxygen, nitrogen or carbon, and the recovery of the metal in a pure dense form is therefore a difficult and expensive process. It is probably these post-reduction operations that are the major limitations for commercial electrowinning of refractory metals.

1.3.2 Electrorefining

The electrorefining process is used for converting an unpure metal into a purer product. The unpure metal is used as a consumable anode and the purified metal deposits at the cathode in recoverable form. This technique is applicable for all the refractory metals. Typical examples are electrorefining of zirconium in an $NaCl$-K_2ZrF_6 solution with the use of zirconium sponge

as anode, and electrorefining of titanium in an $NaCl$-$TiCl_2$ solution utilizing scrap metal as anode. This sub-electrolysis step is also well known from the aluminum industry, where "super purity" metal is produced with superior surface and optical properties.

1.3.3 Electroplating

Electroplating is a process where a continuous and coherent metal coating is formed on a substrate. The substrate works as a cathode, and can in general be any kind of conducting material, but a metal substrate is most common. As in electrorefining and electroforming, a consumable anode of the metal to be deposited is used. The current work focuses on the tantalum and niobium fluoride systems, and these are interesting for the electroplating methods. This process will therefore be given more focus than the other three processes in table 1.1.

The main idea in electroplating is to cover a base material with another metal to enhance surface properties. A metallic coating is an effective way of improving the resistance of metals to attack by corrosive environments at either ordinary or elevated temperatures. Electroplating in aqueous solutions commonly have flaws such as porosity, and the underlying material is susceptible to pitting by galvanic processes. This problem is normally solved by applying a thicker coating, but this also increase the expenses. A thinner coating obtained by an electrolytic deposition in molten salts can often do the same job since these normally are very uniform and non-porous. Electroplating in molten salts has a few other advantages compared with electroplating in aqueous systems. These include a higher efficiency of electrolysis, better anticorrosion properties of the deposited metal, layers free of stress so that the plated part can later be deformed, and better throwing power. Throwing power is the ability to plate uniformly over an intricate surface.

Diffusion alloys

In a true electroplating process, the deposited metal forms a separate phase that adhere to another phase; the substrate material. The thickness and the properties of the plate is therefore not dependant on the substrate. A related process is metalliding, where metal ions are driven into the surface to produce diffusion alloys. The metalliding reaction normally involves the

diffusion of a more reactive metal (the anode) into a less reactive metal (the cathode) and the system will therefore contain a galvanic cell to aid the deposition. Most metalliding processes will in fact be able to sustain themselves through this internally generated e.m.f., but an external voltage is usually applied to achieve a higher and more uniform current density. The diffusion alloy has a gradient in composition, with the concentration of the substrate material decreasing as the plate builds up.

When the surface of the alloy becomes sufficiently dilute in the substrate component, the process will be strictly limited by the diffusion rate through the increasingly thicker alloy region. At some point, the alloy will no longer be formed, and the metalliding process becomes a normal electrodeposition process. The process for electrodeposition of titanium on a base metal described by Sibert and Steinberg [5] is a typical example. Their procedure involved electrolysis of K_2TiF_6 dissolved in $NaCl$, normally with a steel cathode (substrate) and a titanium anode. Only the outer layer of the electrocoating was essentially pure titanium, while a base material-titanium alloy was formed underneath. A maximum thickness of 0.127 mm were obtained of the pure titanium phase, and a continued electrodeposition resulted in "a heavy build up of crystalline titanium". This is the expression the authors use, and is probably an indication of formation of dendrites.

In the case of titanium [5] it was a drawback that electrodeposition of a coherent metal layer was only possible through the formation of a diffusion alloy. It limited the thickness and the rate of deposition, and only the outer layer had the needed properties of pure titanium. In a practical application, this will rarely be satisfactory since even small erosion of the metal will expose the less stable metal underneath. At high temperatures one would furthermore expect the diffusion of titanium into the substrate to continue, and the pure titanium surface will slowly turn into an iron-rich alloy. In other cases, metalliding is a wanted phenomena since it can increase adherence to the substrate. It is possible to form a diffusion alloy between two metals, and obtain the wanted properties from both of them. An example is an alloy of two metals that forms two metal oxides with corrosion resistance towards different environments.

The process by Senderoff and Mellors

Senderoff and Mellors [6] were the first to demonstrate that it was possible to produce coherent coatings of niobium by electroplating from a molten salt, in

this case the eutectic *LiF-NaF-KF* solvent. The work was followed by a series of publications from the same authors where they discuss the deposition of tantalum [7], zirconium [8] and molybdenum [9] in fluoride and chloride melts. Also in this series was a paper concerning the electrode reactions during deposition of niobium [10]. The method was summed up and presented for a larger selection of readers in 1966 [11] and was patented in 1969 [12]. Senderoff furthermore presented a review of older and related methods in 1966 [1]. A process for electrodeposition of coherent deposits of molybdenum by Senderoff and Brenner [13] had been known for some years, but this was highly specific for that metal. The new process was far more general. The method presented by Senderoff and Mellors was applicable to almost all of the refractory metals. By dissolving the refractory metal fluoride in mixtures of alkali metal fluorides they were able to deposit thick coherent coatings of chromium, hafnium, molybdenum, niobium, tantalum, tungsten, vanadium and zirconium. Titanium was a more troublesome metal, and could not be electroplated with unlimited thickness or without forming a diffusion alloy with the substrate metal. For the other eight metals, it was found that the deposited metal had the theoretical density, and was in some cases extremely pure. The mechanical properties were equal to or better than electron beam melted material that was commercially available at the time. There were differences between the metals in the details of the compositions of the electrolyte and the valance state of the refractory metal. A special process was described for the metal niobium [6]. A solution of 10 wt% NbF_5, added as K_2NbF_7, in the eutectic *LiF-NaF-KF* (*FLiNaK*) mixture was electrolyzed at 775 °C with a current density of about 50 mA/cm^2. Commercially pure niobium was used as anode material. Anode and cathode efficiencies were close to 100% and deposits with density of 99.8% or higher of the theoretical value were regularly obtained. The throwing power was better than what was usually associated with commercial nickel plating. The substrate material was varied and no major restrictions were found since steel, stainless steel, graphite, copper and others were used successfully. Senderoff and Mellors reported thicknesses of up to $\frac{1}{4}$ in. of electrodeposits with a surprisingly smooth surface. The microstructure of the deposits were typically columnar.

A surprising feature of the study of electrodepostion of niobium [6] was the importance of essentially pure fluoride melts. The presence of chloride caused the deposit to loose its adherence to the base material, and dendrites and powders were formed. Niobium and tantalum plating were found to have an upper tolerance of about 10 wt% chloride, while the tolerance for zirconium plating was somewhat lower. The effect of the anions were studied on a theoretical basis, explaining the results as a function of anion stability.

Senderoff and Mellors postulated that if the complex anion was too unstable, meaning that it had a too large dissociation constant, dendrites and powders would deposit since the free metal cation was available in too high concentrations at the cathode. If the anion complex was too stable, its reduction potential would become too negative and codeposition of liquid or gaseous alkali metal would occur. The fluoride melts were found to be a good intermediate between these two extremes, and the electrodeposition of niobium metal in fluoride melts was found to be a 3-step process including a direct reduction of the NbF_7^{2-} anion. This, and other proposed electroreduction mechanisms will be described in more detail in section 1.5.1. The anionic chloro complexes were found to be too unstable, and caused the production of dendrites and powders.

The composition of the electrolyte was not critical, and several mixtures with varying content of LiF, NaF and KF were used with good results. The only requirement was that the operating temperature was adjusted accordingly to the liquidus temperature of the system. The lower operating temperature limit was recommended to 25–35 °C above the liquidus since poorer deposit were obtained in "too cold" melts. This was assumed to be due to increasing viscosity of the melt, and decreasing diffusion coefficients combining to reduce the limiting current density to a very small value. The upper operating temperature limit was given by a gradual loss of coherence of the deposit, and production of dendrites and powders at even higher temperatures. This phenomenon was probably due to an increased dissociation of the anionic species at the cathode, causing the same problems as was discussed in the previous paragraph. The mean valence of niobium in the electrolyte had to be close to 4, or the cathode current efficiency would decrease dramatically. The steady state valence in baths operated over long periods of time were usually between 4.1 and 4.2 for the above mentioned conditions and the cathode current efficiency was essentially 100%. The reasons for this will be discussed in more detail in section 1.5.1. The lower limit for the current density was found to be controlled by the presence of noble impurities like iron, since the deposition of these would be favorable compared with niobium at too low rates. Extremely pure electrolytes were found not have any minimum current density. The upper current density limit increased with increasing temperature and increasing concentration of Nb^{4+} to the value of the diffusion limited current. Above this current density, the refractory metal would codeposit together with alkali metal and produce dendrites and powders. The presence of anion impurities like oxide, hydroxide, chloride, bromide and iodide was found to be undesirable. Oxide and hydroxide caused the deposit to become hard and brittle, while

the halogens reduced the operating range for the production of coherent depositions. The effect of oxide impurities is one of the main interests for the current work, and will be given more attention in later sections.

Improvements of the method by Senderoff and Mellors

After the first work by Senderoff and Mellors, there has been published a large number of articles related to the original method. Most of these are electrochemical studies of various molten salt systems that are applicable to electrolytic deposition, where alternative routes are examined and discussed. These works will be discussed later in this chapter, where an overview of the different tantalum- and niobium- chloride and fluoride systems are presented. The main reason for investigating the chloride system is due to the toxic nature of the fluorides, and it would be an environmental advantage to perform electroplating in molten chlorides. Fluoride melts are furthermore a lot more corrosive than chloride melts.

Cohen [14] developed a method for high rate electrodeposition of niobium from fluoride melts. The method used a periodic reversal technique (PR) where the cathodic deposition was followed by an anodic polishing step, that dissolved some of the deposited metal. Cohen found that it was possible to increase the deposition rate by a factor of 10 compared to the normal direct current method. Similar methods are well known for electroplating in aqueous systems, and improves the surface and bulk properties of the plate. Any unevenness on the deposit will readily be dissolved during the anodic polishing step.

1.3.4 Electroforming

Electroforming is a process where an object with simple or complex shape is manufactured by electroplating on a substrate, and the substrate is then removed. The finished piece does not have a base material to carry mechanical loads and stresses, and the required strength in the deposited metal must naturally be very high. Of the four processes mentioned in table 1.1, the electroforming process is the one that needs the highest quality of the electrodeposit. This means an absolute control of the impurities in the melt to avoid inclusions of secondary phases like metaloxides. Senderoff and Mellors [11] made an electroformed tungsten helix by plating on copper, which afterwards was removed by nitric acid. The average wall thickness of the

helix was around 0.6 millimeter. Electroforming is an elaborate and thereby expensive method, and is mainly applicable to production of small pieces of equipment for use in extreme environments.

1.4 Niobium and tantalum complexes in alkali halides

As already mentioned in section 1.3.3, Senderoff and Mellors [6] postulated that the success of the electroplating was dependant on the stability of the metal complex in the melt. Stability in this context means how easily the complexes are reduced at the cathode during the electrocoating. Some rules for predicting the most suitable stability will be given in this section.

The stability of niobium and tantalum complexes in a pure alkali halide melt is generally influenced by both the alkali and the halide ions. Lithium and sodium have the same charge, but since the atomic radius of sodium is larger, the lithium ion has a larger charge density. Lithium will therefore have a stronger attraction to the anion complex, and an enhanced ability to compete with the central refractory cation for the anions in the complex. The result is that the distance between the central and the surrounding ions in the anion complex increases, and the internal bonds are easier to break. The complex thereby becomes less stable. There is also a possibility that the complex becomes distorted and undergoes a change in symmetry. Fluoride, chloride, bromide and iodide all have the same charge, but due to the increasing radius, the effective charge is decreasing. A fluoride atom will therefore form a stronger bond to niobium and tantalum atoms than any of the larger halides, and the niobium- or tantalum-fluoride complexes will be more stable than the corresponding chloride complexes. Due to size differences between the ions, sterical effects might also have an effect on the structure of the complex ion. It should be noted that if the metalfluoride and the metalchloride complexes have a different number of ligands, the prediction of relative stability becomes a lot more complex.

Senderoff *et al.* [15] studied the activity of the cerium ion in alkali and alkaline earth chloride melts. They found the activity to increase by a factor of 20 by changing the solvent from molten KCl to $NaCl$, and an additional factor of 100 by changing from molten $NaCl$ to $CaCl_2$. It was noted that a correlation existed between the quantity Z/r^3 (Z = valence and r = crystal ionic radius) for the solvent cation and the stability of the ceriumchloride

complex. The quantity Z/r^3, a measure of the charge density, could be used to determine the expected stability of the cerium-chloride complex. The smaller the value of Z/r^3 was, the more stable the anion complex became. Mellors and Senderoff [8] used the same model to predict that the stability of fluorozirconate complexes were considerably higher in KF-LiF melts than in NaF-LiF melts.

Kuznetsov [16] studied the effect of ions in the second coordination sphere on the electrochemistry of hafnium and rhenium complexes in alkali halide melts. The term coordination sphere refers to atoms surrounding the central metal atom. The first coordination sphere consists of the negative halide ions, while the positive alkali ions are found in second coordination sphere. $HfCl_4$ was dissolved in an eqimolar mixture of $NaCl$ and KCl and the reduction of hafnium was studied by linear sweep voltammetry. The process was found to occur in two steps; a diffusion controlled reduction 1.1 and a charge transfer controlled reaction 1.2:

$$HfCl_6^{2-} + 2e^- \longrightarrow HfCl_4^{2-} + 2Cl^- \tag{1.1}$$

$$HfCl_4^{2-} + 2e^- \longrightarrow Hf + 4Cl^- \tag{1.2}$$

When $CsCl$ was added to the melt, the reduction waves corresponding to reaction 1.1 and 1.2 decreased in height, and a third wave appeared at a more negative potential. In a pure $CsCl$-$HfCl_4$ melt, only this third wave was visible. The wave was due to a single irreversible four-electron reduction process as indicated by reaction 1.3:

$$HfCl_6^{2-} + 4e^- \longrightarrow Hf + 6Cl^- \tag{1.3}$$

The presence of $CsCl$ in the melt stabilized the $HfCl_6^{2-}$ complex, and gave its reduction potential a negative shift. In addition, the reduction of the anion became a one step reaction. Similar tendencies are to be expected for the reduction of niobium and tantalum in the different alkali halide melts. The change in the reduction pathway that was observed for hafnium, is, however, not a general mechanism. The electroreduction is far more complex, and is not only affected by the stability of the original metal complex. The stability of intermediate complexes and diffusion rates will also play an important role.

The presence of oxygen in a niobium or tantalum containing alkali melt is expected to greatly affect the stability of the metal complexes. Oxygen has the ability to form strong double bonds with the central atom and create bridging bonds in dimers, and thereby stabilize the complex. The following sections will give an overview of some of the studies that has been done on the two refractory metals in molten alkali halides. The work is sorted according to the halide in the different solvents, and both oxide free and oxide containing systems are described. The majority of the work is accomplished by using electrochemical techniques, while spectroscopical and solubility studies occurs less frequently in the literature. The overview will only describe the fluoride and chloride systems since the other halides are of no interest to the electroreduction process. This is due to their large ion radius and thereby lack of ability to form stable complexes with niobium and tantalum.

1.5 Niobium in alkali fluoride melts

1.5.1 Oxygen-free alkali fluoride melts

Fordyce and Baum [17] studied $Nb(V)$ in molten KF-LiF by using infrared reflection spectroscopy, and found NbF_7^{2-} to be present in oxygen free melts. von Barner *et al.* [18] used Raman spectroscopy to determine the structure of five-valent niobium in the LiF-NaF-KF eutectic, and found the same hepta-fluoro-niobium complex in this melt. The symmetry of the complex was found to be identical with the NbF_7^{2-} entity in solid K_2NbF_7. The structure of this solid compound will be discussed in more detail in section 3.5.

The electrochemical reduction of NbF_7^{2-} to solid niobium in molten fluorides was first studied by Senderoff and Mellors [10], and they claimed the process to occur in three steps. The first two were found to be reversible and diffusion controlled, while the final step was irreversible :

$$NbF_7^{2-} + e^- = NbF_{(7-x)}^{(3-x)-} + xF^- \tag{1.4}$$

$$NbF_{(7-x)}^{(3-x)-} + 3e^- = NbF(s\ or\ l) + (6-x)F^- \tag{1.5}$$

$$NbF(s\ or\ l) + e^- \rightarrow Nb(s) + F^- \tag{1.6}$$

As indicated in reaction 1.5 and 1.6 the intermediate compound might be solid or liquid. NbF was found to react rapidly with NbF_7^{2-} to regenerate the tetravalent niobium ion $NbF_{(7-x)}^{(3-x)-}$, and thereby reduce the current efficiency at low current density. The niobium mean valence in the melt was reduced from 5 to 4.0-4.2 by a pre-electrolysis of the system, and coherent deposits of niobium was then obtained.

This first attempt to describe the reduction of niobium by Senderoff and Mellors has later been questioned in several works. Los and Joslak [19] studied the LiF-KF-K_2NbF_7 system and proposed a two step mechanism where five valent niobium was first reduced to a Nb^{3+}-fluoride complex in a reversible process. This was followed by an irreversible reduction step to solid metal. Qiao and Taxil [20] studied the LiF-KF-K_2NbF_7 system and proposed another two step mechanism as indicated in reaction 1.7 and 1.8:

$$Nb^V + e^- \rightarrow Nb^{IV} \tag{1.7}$$

$$Nb^{IV} + 4e^- \rightarrow Nb^0 \tag{1.8}$$

The first step, a reversible diffusion controlled reduction, occured at -0.06V and the second step, a (quasi)reversible diffusion controlled reduction, occured at -0.17V. A Ni/Ni^{2+} electrode was used as reference. This mechanism was further supported by later works by Taxil and Mahenc [21] in the LiF-KF-K_2NbF_7 system, and by Christensen *et al.* [22], Matthiesen *et al.* [23] and Rosenkilde *et al.* [24] in the LiF-NaF-KF-K_2NbF_7 system. The reduction potentials does, however, vary from study to study, and Christensen *et al.* point out that this might be due to high oxide concentrations in the melts that was studied by Qiao and Taxil. It should therefore be noted that the differences between the different studies is probably due to impurities in the fluoride melts. This is especially the case for the original work by Senderoff and Mellors [10] who did not use recrystallized alkali fluorides. The same is probably true for the work by Los and Joslak [19], where no purification methods are described. The main impurity in such unpurified melts is undoubtly oxygen. It is showed in section 1.5.2 that the presence of oxide in the melt will change the reduction mechanism. It is believed that

the reduction mechanism described by Qiao and Taxil [20] is correct in oxide free melts.

Rosenkilde *et al.* [24] studied the stability of the NbF_7^{2-} in liquid *FLiNaK*. They found a spontaneous reduction of $Nb(V)$ to $Nb(IV)$. It has been known since the works by Senderoff and Mellors [10] that $Nb(V)$ reacts with niobium metal to form $Nb(IV)$, but a spontaneuos reduction has only been observed recently. The reduction is probably kinetically controlled, and proceedes slowly. For electroplating purposes, it is unimportant whether this reduction occurs in the absence of niobium metal or not. During electrodepostition, there will always be elementary niobium present at the cathode and this will readily react with $Nb(V)$ and reduce the current efficiency. For this reason, a pre-electrolysis of the melt to convert most of the $Nb(V)$ complexes to $Nb(IV)$ is necessary.

Toth and Gilpatrick [25] studied the ligand-field spectrum of niobium(IV) in fluoride melts and found the presence of NbF_7^{3-} species with very low symmetry. The cubic compound K_3NbF_7 was studied by the same authors [26] using the same technique. It was found to be isostructural with $(NH_4)_3ZrF_7$ and K_3NbOF_6 of space group $O_h^5(Fm3m)$. In these compounds the transition metal is coordinated to seven anions in a distorted pentagonal bipyramid having approximate D_{5h} symmetry. The melt spectrum of $Nb(IV)$ had similar bands to those of the crystal, but were less intense. The niobium(IV)-fluoride species in a *LiF-BeF*$_2$ melt was therefore assumed to be an NbF_7^{3-} anion with no degeneracy of the 4d subshell. This results in a very low-symmetric ion.

Robin *et al.* [27] studied the effect of cathode shape and distance between the electrodes on niobium plating in *FLiNaK* at 750 °C. They found that the thickness of the deposit decreased with increasing distance between cathodic and anodic regions, and that coating were generally thicker on proturbances than on cavities. The thickness was furthermore greater in large and flat cavities than small and narrow ones. Corrosion tests on the plated material showed that the resistance towards boiling *HCl*, H_2SO_4 and HNO_3 and room-temperature *HF* were similar to that of massive niobium.

1.5.2 Oxide containing alkali fluoride melts

Fordyce and Baum [17] studied hydrolyzed $Nb(V)$ in *KF-LiF* melts by means of infrared-reflection spectroscopy. They found the $NbOF_6^{3-}$ anion to

be the predominant species in the melt, and noticed the contrast with the findings in aqueous HF solutions where $NbOF_5^{2-}$ was the stable complex. The aqueous HF system was studied by Keller [28].

von Barner *et al.* [18] used Raman spectroscopy to determine the structure of $Nb(V)$ oxo fluoro complexes in the LiF-NaF-KF eutectic. By adding Na_2O and K_2NbF_7 to the melt, they studied complexes at different ratios of oxygen to niobium, $n_{O^{2-}}/n_{Nb^{5+}}$. The NbF_7^{2-} ion in the pure melts was found to react with oxide according to equation:

$$NbF_7^{2-} + O^{2-} \rightleftharpoons NbOF_5^{2-} + 2F^- \tag{1.9}$$

This equilibrium was found to shift to the left with increasing temperature. As equation 1.9 indicates, the niobium mono oxo fluoride was identified as $NbOF_5^{2-}$, but von Barner *et al.* emphasizes that it might also be $NbOF_6^{3-}$. The complex was dominating the Raman spectra at ratios of oxygen to niobium around 1. In melts with higher concentrations of oxide, a new species was observed. $NbO_2F_4^{3-}$ was suggested. The authors carefully indicated that the number of fluorine atoms in the niobium dioxo fluoro complex might be 4. The two oxygen atoms were found to be in cis position to each other. The complex was totally dominating the Raman spectra at ratios of oxygen to niobium around 2. When this ratio increased, a new species $NbO_2F_n^{(1+n)-}$ was suggested. Furthermore, some kind of polymerization was assumed to take place in these melts and the authors indicated the presence of edge sharing distorted NbO_6 octahedra. The work by von Barner *et al.* will be discussed in more detail in chapter 3.

In a recent publication Andersen *et al.* [29] performed IR and Raman spectroscopy on molten and solidified samples of $Nb(V)$ in $FLiNaK$ at various temperatures and ratios of oxygen to niobium. They found that $NbOF_5^{2-}$ was the dominant species in melts with $n_O/n_{Nb} \sim 1$, while both $NbOF_5^{2-}$ and $NbOF_6^{3-}$ existed when the sample was solidified.

Christensen *et al.* [22] were the first to perform a systematic study on the influence of oxide on the electrodeposition of niobium in the molten LiF-NaF-KF eutectic. With cyclic voltammetry they found that the two reduction waves (R_1 and R_2) that are found in pure niobium fluorides are present also in oxide containing melts. In addition to these, a third wave (R_3) appears at a more negative potential and the height of this wave increases as the relative concentration of oxide increases. At the same time, the two first waves diminishes and dissappear at a point where a fourth wave (R_4) appears

at an even more negative potential than the third one. The excact oxide to niobium ratio in the melts are somewhat uncertain, but Christensen *et al.* indicated that R_4 appeared at $n_O/n_{Nb} \sim 1$. Christensen *et al.* claimed that R_1 and R_2 are due to reduction of niobiumfluoride as described by equation 1.7 and 1.8. R_3 was suggested to describe a one-step reduction of the $NbOF_5^{2-}$ complex to niobium metal, while R_4 was the reduction of the $NbO_2F_4^{3-}$ species. No wave corresponding to a one-electron reduction was found in these oxide rich melts, and Christensen *et al.* indicate that no oxo fluoro complexes of $Nb(IV)$ exist in major concentrations. There is, however, a possibility that this was due to passivation of the electrode by solid oxides. Such oxides has been observed by Konstantinov *et al.* [30] during electroreduction of niobium in alkali chloride-fluoride melts with high oxide content. Christensen *et al.* [22] also performed electroplating experiments of niobium in the *LiF-NaF-KF* eutectic with variation of both the oxide and niobium contents in the melt. A surprising effect was discovered. The presence of oxide did in fact have a positive impact on both current efficiency and the quality of the deposit as long as the concentration of niobium is higher than the oxygen concentration. Figure 1.1 is made from the data by Christensen *et al.* and summarizes the results obtained for the electroplating experiments:

The original figure by Christensen *et al.* was a 3D plot showing the current efficiency versus oxide and niobium concentrations. Figure 1.1 only describes the different regions that the original figure was divided into. The best quality of the deposits was obtained from melts with compositions according to the regions A and B in figure 1.1. The highest current efficiencies were obtained from melts with compositions according to the regions B and E in figure 1.1. Deposits from melts belonging to area C produced ball-like structures and potasium containing plates, while melts from area D had a characteristic feature of less well defined niobium metal crystals. In the E area, dendritic deposits were formed. The data clearly showed that there is an advantage to have a certain amount of oxide in the system. This is in contrast to earlier results presented among others by Senderoff and Mellors [10]. The results by Christensen *et al.* further showed that it was not only the concentration of oxide and niobium alone that determined the optimal electroplating conditions, but rather the ratio $n_{O^{2-}}/n_{Nb^{5+}}$. This ratio determines which complexes are present in the melt. The co-existence of NbF_7^{2-} and $NbOF_5^{2-}$ was ideal for a good metal deposit. This demonstrates the importance of the *Nb*-complexes in the melt for the reduction mechanisms.

Matthiesen *et al.* [23] studied the redox chemistry of niobium(V) fluoro and

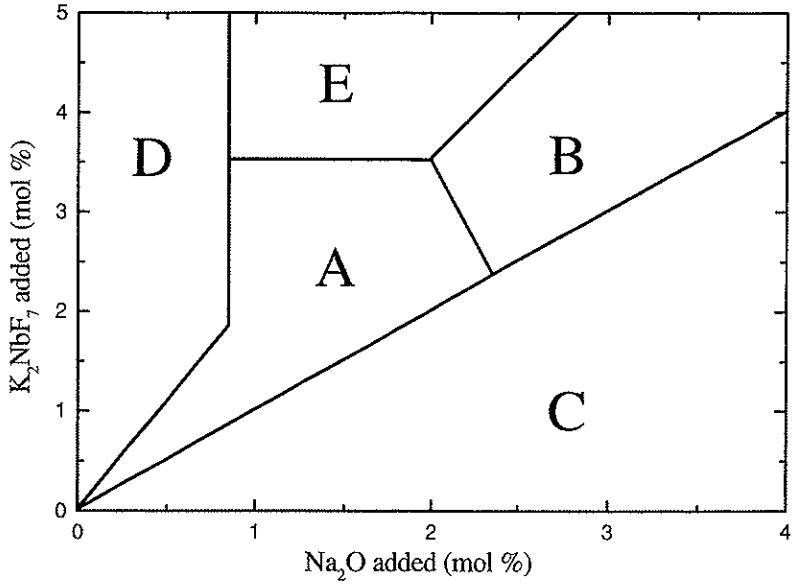

Figure 1.1: Christensen *et al.* [22] performed electroplating of niobium at different concentrations of oxide and niobium in the *LiF-NaF-KF* eutectic. Varying conditions within each of the areas marked A–F produced similar deposits with similar current efficiencies. These data are discussed in the text.

oxofluoro complexes in *LiF-NaF-KF* melts, and reproduced several of the voltametric results obtained by Christensen *et al.* [22]. Matthiesen *et al.* confirmed the temperature dependence of reaction 1.9, and identified the four reduction waves R_1–R_4. In addition, they observed a new wave R_5 at an even more negative potential than R_4 when the oxide to niobium ratio exceeded 2. The shape of the R_5 wave could have been associated with a metal deposit/dissolution process, but potentiostatic electrolysis at a cathode potential correnspondingto R_5 gave no electrode deposit.

Matthiesen, Jensen and Østvold [31] studied oxofluoro complexes of niobium(IV,V) in liquid *FLiNaK* melt at 700 °C with varying oxide to niobium ratios. *SrO* was added to *FLiNaK* containing 0.22 $molkg^{-1}$ K_2NbF_7 and the following observations were recorded: $n_O/n_{Nb} < 2$; all the Nb^V was dissolved; $n_O/n_{Nb} > 2$; a solid of the type $AlkNbO_3$ was formed; $n_O/n_{Nb} = 3$; a minimum of Nb^V and O^{2-} solubilities were observed; $3 < n_O/n_{Nb} < 4$; the $AlkNbO_3$ previously formed dissolved, and a complex ion of the type $NbO_4F_x^{(3+x)-}$ was most probably formed; $n_O/n_{Nb} > 4$; no further dissolution took place. Na_2O was used as an oxide source in the experiments with

Nb^{IV} since the lack of SrO solubility in these melts could be due to the oxoacidic character of SrO relative to Na_2O. The experiments with four valent niobium show a similar trend as for the experiment with $Nb(V)$, with one important exception. With Nb^{IV} it seems to be a partial precipitation of a solid upon additions of oxide to melts with $1 < n_O/n_{Nb} < 2.2$. This was belived to be due to precipitation of $NbOF_2(s)$. Figure 1.2 shows the differences between the solubility of Nb^{IV} and Nb^{V} in $FLiNaK$ with varying oxide to niobium molar ratios:

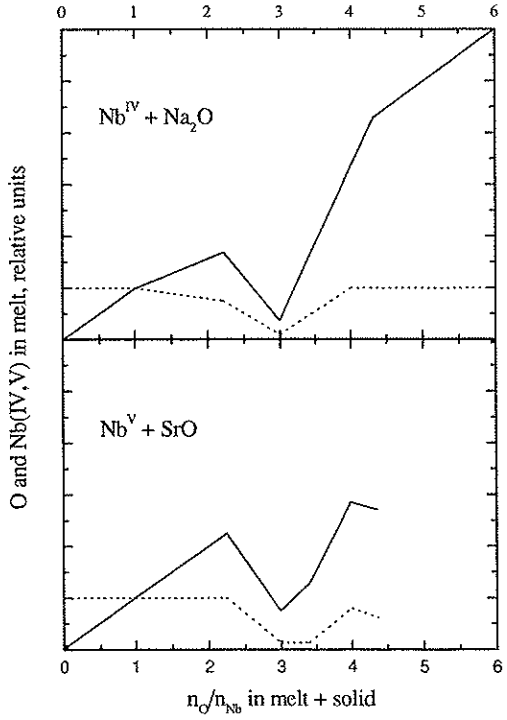

Figure 1.2: Relative oxide (filled lines) and niobium (dotted lines) concentrations in liquid LiF-NaF-KF at 700 °C versus the molar ratio of the total amount of oxide and niobium in the melt and in the solid phases. Detailed data are given by Matthiesen, Jensen and Østvold [31]

The oxide concentrations in the melts are given by the full drawn lines in figure 1.2, while niobium concentrations are given by the dotted lines. It is difficult from these data only to determine the complexes that are formed in the melts, but the authors indicates NbF_6^{2-}, $NbOF_5^{3-}$, $NbO_2F_4^{4-}$ and NbO_4^{4-} as possible Nb^{IV} complexes. In melts with $n_O/n_{Nb} > 4$ it was assumed that free O^{2-} was formed.

Rosenkilde *et al.* [24] performed electrochemical studies of the molten system K_2NbF_7-Na_2O-Nb-$(LiF$-NaF-$KF)_{eut}$ at 700 °C. By using voltammetry, the solubilities of Nb_2O_5 and $KNbO_3$ were determined to 1.8 and 0.13 mole%, respectively, in agreement with the data of Matthiesen, Jensen and Østvold. In addition to an observation of the $Nb(V)$-monooxo fluoro complex, Rosenkilde *et al.* also identified a $Nb(IV)$-monooxo fluoro complex. This complex was formed by a reaction of $Nb(IV)F_7^{3-}$ with O^{2-}. This has not been observed previously in any electrochemical work. The four valent niobium mono oxofluoride complex was found to react further with O^{2-} to form a five valent niobium complex and niobium metal in melts with $n_O/n_{Nb} > 1$. This is indicated by reaction 1.10:

$$5Nb(IV)OF_x^{(x-2)-} + O^{2-} = 4Nb(V)O_2F_4^{3-} + Nb(s) \qquad (1.10)$$

There is an obvious discrepancy between these data, and those obtained by Matthiesen, Jensen and Østvold [31]. These authors indicate a solid compound as the product of $Nb(IV)OF_x^{(x-2)-}$ and O^{2-} interaction. Rosenkilde *et al.* found no explanation for the difference.

For melts with $n_O/n_{Nb} > 3$, Rosenkilde *et al.* [24] found indications of two new niobium complexes. In the range $3 > n_O/n_{Nb} > 3.8$ there were no reductions of importance between the alkali-metal reduction and the platinum oxidation (platinum was used as working electrode), but at $n_O/n_{Nb} > 3.8$ a reduction step R_5 due to a niobium species appeared. The intensity of this wave increased with further additions of oxide, and reached a maximum intensity at $n_O/n_{Nb} = 6$. At slightly higher n_O/n_{Nb} values than 3.8, another wave appeared at a potential close to that of free O^{2-} in $FLiNaK$. This indicated the presence of free or loosely bonded O^{2-} in the melts. The R_5 wave did not show completely reversible behavior, but it was found to describe a one-electron transfer reaction. The peak was probably due to the reduction of a monomeric NbO_6 entity.

1.5.3 Summary

The chemistry of niobium in alkali fluoride and alkali oxo fluoride melts can be summed up as follows. In oxygen free melts, the NbF_7^{2-} complex is present. This complex is reduced to niobium metal in a two step reaction with a $Nb(IV)$-fluoride intermediate complex. $Nb(V)$-fluoro complexes react spontaneously with niobium metal to form a $Nb(IV)$ complex. Nb^V may also

react slowly with F^- to Nb^{IV} and $F_2(g)$. In oxygen containing melts, several niobium oxo fluoride complexes exist. For five-valent niobium, $NbOF_5^{2-}$, $NbO_2F_4^{3-}$ and at least one more oxygen rich complex exists. For four-valent niobium, $NbOF_x^{(x-2)-}$ and possibly $NbO_2F_y^{y-}$ exists. Due to a precipitation of a solid compound $AlkNbO_3$ and/or Alk_2NbO_3, a minimum in solubility is observed in systems with a total ratio n_O/n_{Nb} equal to three. The exact symmetry of the various complexes will be discussed in more detail in chapter 3

1.6 Tantalum in alkali fluoride melts

1.6.1 Oxygen-free alkali fluoride melts

Fordyce and Baum [32] studied $Ta(V)$ in molten KF-LiF using infrared reflection spectroscopy, and found TaF_7^{2-} to be present in oxygen free melts. The effect of cations upon the spectra were found to be significant, and TaF_6^- were observed in addition to TaF_7^{2-} in NaF-LiF melts. Keller *et al.* [33] studied $Ta(V)$ in aqueous NH_4F-HF solutions and found the same two complexes. Matwiyoff *et al.* [34] studied $Ta(V)$ in anhydrous HF solutions and found only the TaF_6^- complex. Varga and Freund [35] found evidence for the presence of TaF_6^-, TaF_7^{2-}, TaF_8^{3-} and TaF_9^{4-} in perchloric acid solutions containing $Ta(V)$ and HF. These results show that tantalum may form many complexes in fluoride systems.

Fordyce and Baum also studied the gas-phase above the different fluoride melts. Analysis of vapor deposits of K_2TaF_7 in a KF-LiF melt showed that both K_2TaF_7 and TaF_5 were stable gas species. The amount of K_2TaF_7 relative to TaF_5 decreased as the concentration of $Ta(V)$ in the melt increased. In lithium free melts only K_2TaF_7 were present in the gas phase. $NaTaF_6$ appeared in the vapor deposit from NaF-LiF-TaF_5 melts.

Agulyanskii [36] performed a systematic study of the influence of outer-sphere cations on $Ta(V)$ complexes in fluoride melts. He found that an equilibrium is established between six- and seven-coordinated tantalum atoms in alkali fluoride melts:

$$TaF_7^{2-} \rightleftharpoons TaF_6^- + F^- \tag{1.11}$$

Agulyanskii found that equilibrium 1.11 was shifted to the left when passing from sodium to caesium based electrolytes. TaF_6^- was found to be the dominating species in Na_2TaF_7-NaF melts with Na_2TaF_7 concentrations up to 1 mole%, while TaF_7^{2-} was the major species in Rb_2TaF_7-RbF melts of similar concentrations.

von Barner *et al.* [37] studied $Ta(V)$ in molten $FLiNaK$ by means of Raman spectroscopy, and identified the TaF_7^{2-} complex. Bjerrum *et al.* [38] studied $Ta(V)$ in solidified $FLiNaK$ with both infrared absorption and Raman spectroscopy. Their work supports the findings of von Barner *et al.* [37], but questions the conclusions drawn by Fordyce and Baum [32]. Bjerrum and coworkers furthermore exclude the presence of TaF_8^{3-} in the melts. Robert *et al.* [39] also studied $Ta(V)$ in solidified $FLiNaK$ with Raman spectroscopy. They also found the TaF_7^{2-} complex in agreement with von Barner *et al.* and Bjerrum *et al.*

The first study of electroreduction of $Ta(V)$ in fluoride melts was performed by Senderoff, Mellors and Reinhart [7]. The reduction of pentavalent tantalum to tantalum metal in molten LiF-NaF-KF was found to involve a two step mechanism as indicated by reaction 1.12 and 1.13. This was later supported by the work of Inman *et al.* [40].

$$TaF_7^{2-} + 3e^- \rightarrow TaF_2(s) + 5F^- \tag{1.12}$$

$$TaF_2(s) + 2e^- \rightarrow Ta + 2F^- \tag{1.13}$$

The proposed mechanism is somewhat similar to that of Sendeoff and Mellors [10] for the reduction of pentavalent niobium in fluoride melts. Espinola *et al.* [41] proposed a reduction mechanism for $Ta(V)$ in molten $FLiNaK$ involving two steps, but with Ta^{3+} as the intermediate. Polyakova *et al.* [42] studied the electrochemical behaviour of K_2TaF_7 in a LiF-NaF-KF eutectic melt using voltammetry. They found that $Ta(V)$ was reduced to tantalum metal in a single quasi-reversible five-electron step as shown in reaction 1.14.

$$TaF_7^{2-} + 5e^- \rightarrow Ta + 7F^- \tag{1.14}$$

This mechanism had already been proposed by Taxil and Mahenc [43] some years earlier. A similar reduction path had earlier been found by Konstantinov *et al.* [44] in the related system KCl-KF-K_2TaF_7. This will be discussed

in more detail in section 1.10.1. The mechanism described by reaction 1.14 is probably more correct than the other alternatives. Polyakova *et al.* [42] performed a systematic study of the influence of oxide on the reduction pathway, and showed that the appearance of two peaks in voltammograms of "oxygen-free" melts were due to oxide impurities. As for the case of niobium in fluoride melts, the presence of oxide in the tantalum-fluoride-melts led the above authors to propose an erroneous electrochemical reduction mechanism.

1.6.2 Oxide containing alkali fluoride melts

von Barner *et al.* [37] used Raman spectroscopy to study $Ta(V)$-oxofluoro-complexes in molten $FLiNaK$. This work is less systematic than the parallel work on niobium [18], but the spectra show the formation of mono-oxo and dioxo-fluoro complexes as Na_2O is added to the K_2TaF_7-$FLiNaK$ melt. The authors indicated that the complexes could be $TaOF_5^{2-}$ and $TaO_2F_4^{3-}$.

Apart from the work by von Barner *et al.* [37], no spectroscopic work on tantalum in molten fluoride melts has been found in the literature. There has, however, been some work done on solidified K_2TaF_7-Na_2O-$FLiNaK$ melt samples. Bjerrum *et al.* [38] developed a method to determine oxide contents of alkali metal fluoride tantalum melts using IR and Raman spectroscopy. In this work they also identified the presence of $TaOF_x^{(x-3)-}$ and a dimeric ion containing a Ta-O-Ta oxygen bridge. Robert *et al.* [39] studied solidified melts in the same system by means of Raman spectroscopy. They proposed the existence of three complexes when $n_O/n_{Ta} < 0.5$: K_2TaF_7, $K_xTa_2OF_{8+x}$ and K_2TaOF_5. They furthermore performed a systematic study on how the concentration of these species varied with the ratio n_O/n_{Ta}, and isolated the Raman spectra of each of the Ta-containing species.

Polyakova *et al.* [42] performed a systematic study of the influence of oxide on the electro reduction of tantalum in $FLiNaK$ melts. At an oxide to tantalum ratio of one, the predominant species in the melt was $TaOF_5^{2-}$, and this complex was found to be reduced to metal in a single irreversible five-electron step. At an oxide to tantalum ratio two, the $TaO_2F_x^{(x-1)-}$ complex was dominating in the melt. Electrochemical reduction of this species led to formation of an insoluble oxide, $KTaO_3$. Further additions of oxide to the melts led to a decrease of the tantalum concentration in the melt, and precipitation of $KTaO_3$ occured. In addition to their Raman spectroscopic work, Robert *et al.* [39] also studied the electrochemistry of

K_2TaF_7-$FLiNaK$-Na_2O melts with an oxide to tantalum ratio below 0.6. They plotted the integrated oxidation current versus n_O/n_{Ta}, and found a linear relationship for $n_O/n_{Ta} < 0.3$. In more oxide rich melts, a positive deviation from linearity was observed. This was explained by the presence of a bridged species of the type $K_xTa_2OF_{8+x}$.

1.6.3 Summary

The chemistry of tantalum in alkali fluoride and alkali oxo fluoride melts can be summed up as follows. In oxygen free melts, TaF_7^{2-} and/or TaF_6^- complexes are present. The alkali cations in the melts determine the concentration of each species, and only TaF_7^{2-} seems to be present in $FLiNaK$. In oxide containing melts, with $n_O/n_{Ta} < 3$, $Ta_2OF_{8+x}^{x-}$, $TaOF_5^{2-}$ and $TaO_2F_x^{(x-1)-}$ are present. The tantalum fluoride and tantalum monooxo fluoride complexes are reduced to tantalum metal in a single five-electron step, while reduction of the tantalum dioxo fluoride species leads to the formation of $AlkTaO_3$. Addition of oxide to $FLiNaK$ melts with $n_O/n_{Ta} = 2$ causes precipitation of $KTaO_3$, and a decrease of the tantalum and oxide concentrations in the melt.

1.7 Niobium in alkali chloride melts

1.7.1 Oxygen-free alkali chloride melts

Voyiatzis *et al.* [45] studied $Nb(V)$ (added as $NbCl_5$) in molten $CsCl$, $NaCl$-$CsCl_{eut}$ and $LiCl$-KCl_{eut} by using Raman spectroscopy. They found that $NbCl_6^-$ were present in all systems. The five-valent niobium species was furthermore reduced by adding niobium metal to the melt, and the presence of $NbCl_6^{2-}$ was observed in addition to $NbCl_6^-$. A valency of four was found by reduction of $NbCl_5$ with niobium metal. Dissolution of $NbCl_4$ and $NbCl_3$ led to formation of the four- and five-valent species $NbCl_6^{2-}$ and $NbCl_6^-$. The structure of $NbCl_6^-$ was studied by Bues *et al.* [46] and Kipouros *et al.* [47] who identified the species in molten $CsNbCl_6$. $NbCl_6^-$ and $NbCl_6^{2-}$ possess O_h symmetry.

A large amount of work has been done on electrochemical studies of niobium in molten alkali chlorides. There is severe disagreement in the proposed

reduction mechanisms investigated and stable oxidation states of niobium in the various chloride melts. An overview of the different alkali chloride systems of niobium will therefore be given.

$NbCl_5$ in $LiCl$-KCl melts

Kuznetsov *et al.* [48] proposed a temperature dependant reduction mechanism of $NbCl_5$ in the $LiCl$-KCl system, where Nb^{5+} was first reduced to Nb^{4+} and then to niobium metal at temperatures above 630 °C. Combining this with the spectroscopical work by Voyiatzis *et al.* [45], the electro reduction can be described by reaction 1.15 and 1.16.

$$NbCl_6^- + e^- \rightleftharpoons NbCl_6^{2-} \tag{1.15}$$

$$NbCl_6^{2-} + 4e^- \rightarrow Nb + 6Cl^- \tag{1.16}$$

Reaction 1.15 was reversible while 1.16 was irreversible. At temperatures from 400 °C to 600 °C, a three step mechanism including Nb^{2+} as an intermediate stage was proposed [48]. Zhou *et al.* [49] did a similar study of $NbCl_5$ in the molten $LiCl$-KCl melt at temperatures from 450 °C to 500 °C. They concluded that $Nb(V)$ was reduced to niobium metal in three steps with Nb^{3+} and Nb^{2+} as intermediate oxidation states. Picard and Bocage [50] investigated the same system at 450 °C, and claimed the reduction to occur in three steps with Nb^{4+} and Nb^{3+} as intermediate oxidation states. Lantelme *et al.* [51] investigated the influence of temperature on the electro reduction of $NbCl_5$ in the $LiCl$-KCl eutectic. In the temperature range 380–600 °C, solutions of $Nb(III)$, $Nb(IV)$ and $Nb(V)$ were stable, and the corresponding redox reactions were reversible. Reduction of $Nb(III)$ to niobium metal was possible, but included the formation of insoluble subhalides on the metal surface with a possible perturbation of the metal deposition. Subhalides were used as a general term for niobium chlorides where niobium had an oxidation state between 2 and 3. This phenomenon had also been reported by Kuznetsov *et al.* [48], who believed the subhalides to be a product of niobium dichloride and four-valent niobium complexes that reacted at the cathode. Mohamedi *et al.* [52] found the solubility of Nb_3Cl_8 in the $LiCl$-KCl eutectic to be below 0.8 wt% within the 400–500 °C temperature range. Lantelme *et al.* [51] found that these compounds disappeared at higher temperature, and coherent deposits of niobium were obtained above 650 °C. A

temperature increase was also found to favor the disproportionation reaction: $4Nb(III) \rightarrow 3Nb(IV) + Nb(0)$.

Dartnell *et al.* [53] studied anodic dissolution of niobium metal in molten *LiCl-KCl*, and found that only $Nb(IV)$ was formed. Saeki and Suzuki [54] performed similar experiments in the temperature range 500 °C to 600 °C, and found the apparent valence of 3.1 of the niobium ion in the *LiCl-KCl* melt immediately after anodic dissolution. After a waiting period of more than 9 hours (9–12 hours), the equilibrium composition in the melt was equal to that of Nb_3Cl_8 (2.67). The temperature range is not given explicitly in the work by Dartnell *et al.* [53], but the experiments were probably done somewhere between 420 °C and 531 °C. The solubility of $NbCl_3$ was 0.071 mole% at 531 °C [53]. In a recent publication by Gillesberg *et al.* [55], the temperature effect of the quality of the electroplated niobium was studied in the *LiCl-KCl* eutectic. At temperatures below 550 °C no coherent layers were obtained. At temperatures between 550 °C and 650 °C niobium layers were obtained, but they remained heterogeneous and contained many inclusions. At 750 °C homogeneous layers of metallic niobium were deposited from the melt.

$NbCl_5$ in *NaCl-KCl* melts

Kuznetsov *et al.* [48] compared voltammetric data obtained in the *LiCl-KCl* system and the *NaCl-KCl* melt, and found that the reduction of $NbCl_5$ occured in two steps as indicated by reaction 1.15 and 1.16. The melting point of an equimolar *NaCl-KCl* melt was 660 °C, and it was impossible to study this melt at temperatures below 600 °C, where a three step mechanism was observed in the *LiCl-KCl* melt. The same observations were confirmed in more recent publications by Kuznetsov and Grinevich [56] and Kuznetsov *et al.* [57]. The latter dealt with the solubility of Nb_3Cl_8 in the system, and it was shown that the concentration of niobium compounds with a valence below four is very low. The two step reduction mechanism was supported by the work by Khalidi and Bouteillon [58] at temperatures from 700 °C to 800 °C. Nakagawa and Hirabayashi [59], on the other hand, presented a completely different scheme for the reduction of $NbCl_5$ in the *NaCl-KCl* melt at 800 °C. This included a four step reaction with niobium in Nb^{5+}, Nb^{4+}, Nb^{3+} and Nb^{2+} valency states. This work focuses on the effect of cathode current efficency with variations of fluoride content in the melts, and the reduction process was found to be independant of the electrolyte. This is probably not correct since reduction of Nb^{5+} to niobium metal in alkali fluoride melts only includes Nb^{4+} as an intermediate oxydation step.

Lantelme and Berghoute [60] studied the $NaCl$-KCl-$NbCl_5$ system at temperatures above 670 °C, and found the reduction of niobium to occur in three steps. Below 750 °C Nb^{5+}, Nb^{4+} and Nb^{3+} were found to be the stable oxidation states, and formation of niobium metal occured directly from Nb^{3+}. At higher temperatures, Nb^{5+} tended to decompose to Nb^{4+} with evolution of chlorine gas. The authors indicated the possible presence of niobium subhalides at the cathode during the electroreduction. A spontaneous reduction of $Nb(V)$ with evolution of chlorine gas was also observed by Arurault *et al.* [61] in the $NaCl$-KCl-$NbCl_5$ system at 750 °C. Gillesberg *et al.* [55] supported the conclusions drawn by Lantelme and Berghoute, and demonstrated that both $LiCl$-KCl and $NaCl$-KCl melts are suitable electrolytes for deposition of niobium as long as the temperature is above 750 °C and the oxide concentration is kept low. Gillesberg *et al.* [55] does not specify a lower limit of oxide content. Dartnell *et al.* [53] studied anodic dissolution of niobium in molten $NaCl$-KCl. Partly soluble $NbCl_3$ was produced at low current densities, while Nb^{4+} was obtained at a high current density.

$NbCl_5$ in $CsCl$-containing melts

Elizarova *et al.* [62] and [63] studied the electrochemical behavior of niobium in $CsCl$-KCl-$NaCl$-$NbCl_5$ melts. They found that the reduction mechanism probably was of an ECE type, involving an electrochemical reaction followed by a chemical reaction and a final electrochemical reaction. Nb^{5+} was first reduced to Nb^{4+}, which again formed a dimeric species, possibly $Nb_2Cl_9^-$. Further reduction of this complex gave niobium metal. Stöhr and Freyland [64] used electrochemical impedance to investigate the reduction mechanism of niobium chloride in the $CsCl$-$NaCl$ eutectic melt at 550 °C. The reduction was found to occur in three steps, similar to the reaction scheme proposed by Lantelme and Berghoute [60] in the $NaCl$-KCl melt. The $CsCl$-$NaCl$ eutectic melt was further studied by Rosenkilde and Østvold [65] at temperatures from 550 °C to 700 °C. They also found the two one-electron steps from Nb^{5+} to Nb^{3+} via Nb^{4+}, but concluded that the reduction of the three-valent complex occured in several unidentified steps. The reduction products of Nb^{3+} were non-metallic solids at temperatures below about 650 °C, and metallic niobium at higher temperatures. Vasin *et al.* [66] studied the anodical dissolution processes of niobium in the $CsCl$-$NaCl$ eutectic melt at temperatures from 550 °C to 750 °C. They found the average valence of niobium to vary from 2.77 to 3.05, depending on the current density. A melt containing mainly $Nb(III)$ ions was left to equilibriate with niobium metal for 5–6 hours, and it was observed a weight loss of the metal piece

even if the niobium concentration in the melt was constant. This was explained by current-less transfer of metal, probably through the formation of lower-valent niobium species. The formation of a metallic coating was observed on the wall of the transparent quartz cell.

Inman *et al.* [40] studied reducion of niobium in several alkali chloride melts, and found the reduction of Nb^{4+} to occur in two steps with a Nb^{3+} intermediate. The reduction wave corresponding to the reduction of Nb^{4+} to Nb^{3+} obeyed Sand's equation (linear relationship between the square root of the sweep rate and the current density) only in the least polarising melt; the equimolar *KCl-CsCl*. For all melts, it was concluded that the reduction of the trivalent niobium species occured only by a secondary process following the deposition of alkali metal. The oxidation of niobium to $Nb(III)$ and the corresponding reduction of $Nb(III)$ to metal was found to be slow processes.

1.7.2 Oxide containing alkali chloride melts

Rosenkilde *et al.* [67] used Raman spectroscopic and *ab initio* quantum chemical methods to investigate complex formation in the molten $CsCl$-$NbCl_5$-$NbOCl_3$ system. Melts from the binary $CsCl$-$NbOCl_3$ system that were dilute in $NbOCl_3$, showed strong bands in the Raman spectra that were typical of the $NbOCl_5^{2-}$ complex. As the ratio of $NbOCl_3$ to $CsCl$ increased, new bands belonging to the $NbOCl_4^-$ species appeared, and were totally dominating the spectra in an equimolar mixture of $CsCl$ and $NbOCl_3$. An equilibrium was therefore present in the binary system for $X_{CsCl} > 0.5$:

$$Cs_2NbOCl_5 = CsCl + CsNbOCl_4 \tag{1.17}$$

The equilibrium constant of reaction 1.17 was close to unity. Bands due to a possible $NbOCl_6^{3-}$ complex could not be detected, even in the most $CsCl$ rich melts. The remaining parts of the work deals with melts having $X_{CsCl} \leq 0.5$. Data for these melts are therefore not directly comparable with data for electrolytes used for deposition of niobium, where the niobium concentration is less than 5 mole%.

Except from the work of Rosenkilde *et al.* [67], no work concerning spectroscopic measurements of niobium oxochloro complexes in molten alkali chloride has been found in the literature. The structure of the $NbOCl_5^{2-}$ ion has however been studied in solid Rb_2NbOCl_5 and Cs_2NbOCl_5 by Sabatani

and Bertini [68] using IR spectroscopy and by Wendling [69] and Brown [70] using XRD methods. The spectroscopic work on these solids supports the findings of a $NbOCl_5^{2-}$ complex with C_{4v} symmetry in molten alkali halides.

Ivanovskii and Plekhanov [71] were probably the first to study the electrochemistry of molten chloride melts containing niobium oxochlorides. Their work describes anodic dissolution of NbO in an equimolar $NaCl$-KCl mixture at 700 °C, and the formation of $Nb(V)$-oxo complexes was observed. Electrolytic reduction of such oxygenated melts led to formation of NbO (or an other niobium oxide with a composition close to that of NbO) at the cathode. These solutions were found unfit for production of metallic niobium. Similar conclusions were drawn by Lantelme *et al.* [51] who noticed a rapid decrease of the wave (cyclic voltammetry) corresponding to the redox reaction $Nb(V)/Nb(IV)$ at the presence of oxide ions in the system. This furthermore induced the formation of niobium oxides during the electrodeposition of niobium. Gillesberg *et al.* [55] found that the niobium suboxides were more stable in pure chloride melts than melts containing fluoride ions. This means that electrolysis from a chloride solution requires a more oxide-free electrolyte than electrolysis from a fluoride or a chloride-fluoride solution. This is probably due to the stabilizing effect fluoride ions have on niobium-oxo-halide complexes.

As mentioned in section 1.7.1, Picard and Bocage [50] found the electroreduction of $Nb(V)$ in oxygen-free $LiCl$-KCl eutectic to take place in three steps. This included one-electron steps through $Nb(IV)$ and $Nb(III)$ and a three-electron step to niobium metal. When oxide was introduced to the system, it was further found that $Nb(II)$ was stable in the form of $NbO(s)$. Picard and Bocage [50] presented a potential-oxoacidity diagram of niobium in the molten $LiCl$-KCl eutectic. This plot summarizes the stability regions for $LiNbO_3$, Nb_2O_3 and NbO under various potentials and oxide activities in the melt.

Bachtler *et al.* [72] recorded electronic absorption spectra of niobium in various alkali chloride and oxychloride melts. By reducing $NbCl_5$ with niobium metal, they were able to study the stability of lower valent niobium complexes in the various media. The results showed no indication of niobium in II- or III-states in the oxychloride containing melts. This conclusion was also made in the work of Rosenkilde and Østvold [65] (co-authors of [72]) who performed voltametric studies of niobium oxochlorides in the $CsCl$-$NaCl$ eutectic melt. $NbOCl_5^{2-}$ ions were found to be reduced in two steps: $NbOCl_5^{2-} + e^- = NbOCl_x^{(x-2)-} + (5-x)Cl^-, (x = 3, 4 \text{ or } 5)$ followed by reduction of $NbOCl_x^{(x-2)-}$ to a solid, probably $NbO(s)$. $NbO_2Cl_x^{(x-1)-}$ ions

probably also existed in $NbCl_5$-containing melts saturated with Nb_2O_5. This ion was probably reduced to $NbO_2(s)$. In melts containing Cs_2NbOCl_5, Nb_2O_5 and Nb-metal, $Nb(IV)$-mono oxochlorides were the main niobium-containing ions in the solution. The electrodeposition of niobium on steel was also studied in this work. In order to obtain pure, dense and coherent deposits the following criteria had to be met. An equilibrium had to be established between the niobium-containing ions in the melts and the metal, the temperature had to be higher than about 920K and the molar ratio of oxide to niobium had to be less than 1 in the melt. The latter is surprising when the conclusions by Ivanovskii and Plekhanov [71], Lantelme *et al.* [51] and Gillesberg *et al.* [55] is considered. These authors found that even traces of oxide in the electrolyte would cause oxygen inclusions in the metal deposit from $NaCl$-KCl and $LiCl$-KCl melts. It is possible that the stabilizing effect of the Cs-ion on the niobium monoxide complex allows a higher oxide content for successful niobium plating. This will favor the reduction of niobiumchloride to niobium metal compared to reduction of niobium mono oxochloride to $NbO(s)$.

Stöhr and Freyland [64] confirmed the findings of Rosenkilde and Østvold [65] in a recent publication. With electrochemical impedance measurements they found the presence of niobium mono oxochloride complexes that are reduced to niobium metal or metal oxide in two steps. They also found clear indications for niobium dioxo complexes in melts with a ratio $n_O/n_{Nb} = 2$. At high oxide concentration they found a reduced activity of the niobium containing species that was probably due to precipitation of $CsNbO_3$ or $NaNbO_3$. This is similar to what has been observed in the corresponding fluoride systems (see section 1.5.2).

Rosenkilde and Østvold [73] studied the solubility of Nb_2O_5 and SrO in the $CsCl$-$NaCl$ eutectic melt with additions of $NbCl_x$ (x = 4, 5). $NbCl_5$ reacted with Nb_2O_5 according to reaction 1.18 and 1.19.

$$3NbCl_6^- + Nb_2O_5(s) + 7Cl^- = 5NbOCl_5^{2-} \tag{1.18}$$

$$3NbOCl_5^{2-} + Nb_2O_5(s) + (3x-5)Cl^- = 3NbO_2Cl_x^{(x-1)-} \tag{1.19}$$

Reaction 1.18 was completely shifted to the right, while reaction 1.19 had an equilibrium constant $K = 5 \times 10^{-5}$. $NbCl_4$ reacted with $Nb_2O_5(s)$ according to reaction 1.21, and the $NbOCl_5^{2-}$ formed from this reaction reacted further with $Nb_2O_5(s)$ as shown in reaction 1.19.

$$3Nb(IV)Cl_6^{2-} + Nb(V)_2O_5(s) = 3Nb(IV)OCl_x^{(x-2)-} + 2Nb(V)OCl_5^{2-} + (8-3x)Cl^- \quad (1.20)$$

In the presence of excess $SrO(s)$, $Nb(IV)$ and $Nb(V)$ precipitated probably as $NbO_2(s)$ and $MNbO_3(s)$ ($M = Na, Cs, \frac{1}{2}Sr$) respectively.

1.7.3 Summary

The chemistry of niobium in alkali chloride and alkali oxochloride melts can be summed up as follows. In oxygen free melts, $NbCl_6^-$ is the only stable $Nb(V)$ containing complex regardless of the cation composition. A lot of studies has been done on the reduction mechanism of this species, and the results varies a lot from work to work. A three step mechanism through $NbCl_6^{2-}(IV)$ and $NbCl_x^{3-x}(III)$ does, however, seem most likely for most of the systems, but the temperature of the bath will probably also affect the reduction scheme of $NbCl_6^-$. The final reduction step of $NbCl_x^{3-x}(III)$ to niobium metal does probably occur through multiple steps with a possible formation of niobium subchlorides like Nb_3Cl_8. The large variation between the different studies on this matter is probably due to insufficient control of the oxide level in the electrolytes.

In oxide containing melts dilute in $Nb(V)$, $NbOCl_5^{2-}$ and $NbO_2Cl_x^{(x-1)-}$ are stable, while $NbOCl_4^-$ coexists with $NbOCl_5^{2-}$ in more $Nb(V)$ rich melts. $NbOCl_5^{2-}$ is reduced to $NbO(s)$ through an $NbOCl_x^{(x-2)-}(IV)$, (x = 3, 4 or 5) intermediate complex. $NbO_2Cl_x^{(x-1)-}$ is probably reduced in one step to $NbO_2(s)$. In the presence of excess of oxide, $Nb(IV)$ and $Nb(V)$ precipitates as $NbO_2(s)$ and $MNbO_3(s)$ (where M is any of the non-refractory cations in the system) respectively.

1.8 Tantalum in alkali chloride melts

1.8.1 Oxygen-free alkali chloride melts

Voyiatzis *et al.* [45] studied $Ta(V)$ (added as $TaCl_5$) in molten $CsCl$, $NaCl$-$CsCl_{eut}$ and $LiCl$-KCl_{eut} by using Raman spectroscopy. They found that

$TaCl_6^-$ was present in all the systems. The five-valent tantalum species was furthermore reduced by adding tantalum metal to the melt, and the presence of $TaCl_6^{2-}$ was observed in addition to $TaCl_6^-$. A valency of four was found to be the lowest possible by reduction of $TaCl_5$ with tantalum metal. *In situ* Raman spectroelectrochemical measurements on amorphous carbon electrodes in $LiCl/KCl_{eut}$ containing about 5mol% $TaCl_5$ indicated that $TaCl_6^{2-}$ was formed during the reduction process. Another tantalum chloride species with valence state lower than four was also detected from the spectra. The structure of $TaCl_6^-$ was studied by Kipouros *et al.* [47] who identified the species in molten $CsTaCl_6$. $TaCl_6^-$ and $TaCl_6^{2-}$ possess O_h symmetry. The $TaCl_6^-$ species was also found by Rosenkilde *et al.* [74] in an equimolar $CsCl$-$TaCl_5$ melt.

Polyakova *et al.* [75] have presented a summary of the electrochemistry of tantalum in alkali chloride melts. This comparative study of anodic and cathodic processes during electrolysis shows that Ta^{5+}, Ta^{4+} and probably also Ta^{2+} are stable states of tantalum in these systems. Suzuki [76] studied the electrolytic reduction and oxidation of $TaCl_4$ in the $LiCl$-KCl eutectic melt by chronopotentiometric and coulometric measurements. They found that Ta^{4+} was oxidised to Ta^{5+} in one reversible step. Reduction of Ta^{4+} occured in two steps; a reversible two-electron reaction to Ta^{2+} and an irreversible reaction from Ta^{2+} to tantalum metal. Bailey *et al.* [77] studied the same melt, and found that Ta^{2+}, Ta^{4+} and Ta^{5+} were produced during anodical dissolution of tantalum. The reduction of Ta^{4+} was however found to occur in one step. Baimakov *et al.* [78] studied Ta^{5+} reduction in the $LiCl$-KCl melt. They claimed that Ta^{5+} first is reduced to Ta^{3+} and then to metal at temperatures in the range 400 to 550 °C. At increased temperatures, the reduction potentials of the two steps approached each other, and merged into one five-electron step above 550 °C.

Bachtler *et al.* [79] used impedance and *in-situ* Raman spectroscopy in addition to cyclic voltammetry, and found a three step mechanism for the reduction of Ta^{5+} in the $LiCl$-KCl eutectic melt. This is shown by the reactions below.

$$Ta^{5+} + e^- = Ta^{4+}, \tag{1.21}$$

$$Ta^{4+} + e^- = Ta^{3+}, \tag{1.22}$$

$$Ta^{3+} + e^- = Ta \tag{1.23}$$

Bachtler *et al.* [79] also studied $NaCl$, KCl and $NaCl$-KCl melts and found that the Ta^{3+} species could no longer be observed. The reduction of Ta^{5+} now proceeded as indicated below:

$$Ta^{5+} + e^- = Ta^{4+}, \tag{1.24}$$

$$Ta^{4+} + e^- = Ta \tag{1.25}$$

1.8.2 Oxide containing alkali chloride melts

Rosenkilde *et al.* [74] studied the binary $CsCl$-$TaOCl_3$ by means of Raman spectroscopy. $TaOCl_4^-$ and $TaOCl_5^{2-}$ were found in the melts at temperatures from 650 to 750 °C, and the equilibrium:

$$TaOCl_4^- + Cl^- = TaOCl_5^{2-} \tag{1.26}$$

was established. The spectra showed that $TaOCl_5^{2-}$ was the dominant species in melts dilute in tantalum (16 mole%). The close resemblance of the Raman spectra of $TaOCl_5^{2-}$ and $NbOCl_5^{2-}$ indicated that both species belonged to the same symmetry group, C_{4v}. The spectra furthermore showed that the $CsCl$-$TaOCl_3$ system had a greater ability to form bridging oxygen than the corresponding $CsCl$-$NbOCl_3$ system. The Ta-O-Ta bands were observed at wavenumbers between 700 and 850 cm^{-1}.

Stöhr *et al.* [80] studied the influence of oxide (Na_2O) on the reduction mechanism of tantalum in a $TaCl_5$-$CsCl$-$NaCl$ melt. By using cyclic voltammetry and electrochemical impedance spectroscopy they found that the one-electron reduction from Ta^{5+} to Ta^{4+} in reaction 1.24 was totally suppressed in melts with $n_O/n_{Ta} = 1$. A new peak was observed in the voltammograms, 100 mV cathodic to the metal deposit peak. Additions of oxide to $n_O/n_{Ta} = 2$ in a melt containing four-valent tantalum, indicated that no tantalum dioxochloride complexes are formed in the system. A further addition of oxide to $n_O/n_{Ta} = 3$ led to precipitation of a solid oxide and all waves dissapeared in the voltammograms. Ping-hsin *et al.* [81] measured the solubility of Ta_2O_5 in molten KCl at 950 °C and found 0.04 wt%.

1.8.3 Summary

The chemistry of tantalum in alkali chloride and alkali oxochloride melts can be summed up as follows. In oxygen free melts, $TaCl_6^-$ is the only stable $Ta(V)$ containing complex regardless of the cation composition. The reduction of this species has been subject to several electrochemical investigations. The work by Bachtler *et al.* [79], where three independent analyzing techniques have been used, is probably most reliable. Their work concluded with a three step reduction scheme of $Ta(V)Cl_6^-$ through $Ta(IV)Cl_6^{2-}$ and $Ta(III)$ to tantalum metal in the $LiCl$-KCl eutectic melt. In less polarizing melts, not containing $LiCl$, the reduction of $Ta(IV)Cl_6^{2-}$ proceeded directly to tantalum metal according to Bachtler *et al.*

$TaCl_6^-$ reacts with oxide to form $TaOCl_5^{2-}$ and $TaOCl_4^-$ in $CsCl$ melts. $TaOCl_5^{2-}$ is the dominant species in melts dilute in tantalum. The reduction mechanism of the $TaOCl_5^{2-}$ species has not been studied in detail, but seems to be a one step reaction to an unknown product. The solubility of tantalum oxochlorides for $n_O/n_{Ta} = 3$ is probably very low.

1.9 Niobium in mixed alkali chloride-fluoride melts

1.9.1 Oxygen-free alkali chloride-fluoride melts

von Barner *et al.* [82] studied KCl-$NaCl$-K_2NbF_7 melts by means of Raman spectroscopy, and found that NbF_7^{2-} were the main niobium carrying species in oxide free melts. The work by von Barner *et al.* is less systematic than their earlier work on $Nb(V)$ in $FLiNaK$, and contains no Raman spectra of oxide free melts. Alimova *et al.* [83] and [84] recorded IR spectra of solidified $CsCl$-KCl-$NaCl$-K_2NbF_7, and found bands characteristic of both NbF_7^{2-} and NbF_6^-.

As mentioned in section 1.3.3, the presence of chloride in the fluoride electrolyte was undesirable for electroplating as described by Senderoff and Mellors [6]. Since then, a considerable amount of work has been done to understand the chemistry of these chloride-fluoride melts. A review of the most important studies will be given in the following.

Wong and Kirby [85] studied the KCl-KF-K_2NbF_7-Nb_2O_5 system in order to find the optimal operating parameters for electrowinning of niobium. The most important result of this old work is probably that the presence of oxide (Nb_2O_5) seemed to have a positive effect on the current efficiency without contaminating the deposit with oxide. A mixture of KCl and KF was also found to be more beneficial than either pure KCl or KF. A more recent study on electrowinning of niobium from chloride-fluoride melts has been done by Kuznetsov [86].

The first systematic study on the mechanism of electrochemical reduction of $Nb(V)$ in a chloride-fluoride melts was done by Chemla and Grinevitch [87]. They found that NbF_7^{2-} was reversibly reduced to $Nb(IV)$ and then irreversibly to niobium metal in a $NaCl$-KCl melt. This is similar to the reduction scheme for NbF_7^{2-} in alkali fluoride melts. The same reduction mechanism has been found by Kuznetsov *et al.* [88], [89], [90], [91] and [92], Barhoun *et al.* [93] and [94], von Barner *et al.* [82], Arurault *et al.* [95] and Lantelme *et al.* [96] in the $NaCl$-KCl-K_2NbF_7 melt, by Konstantinov *et al.* [97] and Kuznetsov [86] in the KCl-KF-K_2NbF_7 melt, by Alimova *et al.* [84], [83] and [98] in the $CsCl$-KCl-$NaCl$-K_2Nb_7 melt, by Polyakov *et al.* [99] in the $CsCl$-KCl-$NaCl$-NaF-K_2Nb_7 melt, and by Khalidi and Bouteillon [58] in the $NaCl$-KCl-KF/NaF-$NbCl_5$ melt. Conflicting views exist on the reversibility of the second step, and even for the same melt there are different opinions whether the four-electron reaction is reversible, quasi-reversible or irreversible. According to Polyakov *et al.* [99] this is due to the presence of oxide in the melts. They claim the second step to be irreversible.

None of the studies that were mentioned in the previous paragraph concerns melts with lithium. The reduction mechanism of niobium in $LiCl$-KCl-KF-K_2NbF_7 melts with $n_{F^-}/n_{Nb} = 8$ was studied by Gillesberg *et al.* [100] at temperatures from 370 °C to 725 °C. They found that $Nb(V)$ was reduced to $Nb(III)$ in two reversible steps at temperatures below 520 °C, and that niobium subhalides were formed on further reduction of $Nb(III)$. At temperatures above 660 °C, metallic niobium was formed during reduction.

The presence of the NbF_7^{2-} in these melts does of course require that the molar ratio of fluorine to niobium is 7 or larger. Lantelme and Berghoute [60] studied niobium anodically dissolved in $NaCl$-KCl melts with small additions of NaF. The temperature was varied from 680 °C to 870 °C. In the pure chloride system at temperatures below 750 °C, the reduction of niobium occured in a three step reaction as mentioned in section 1.7.1. At higher temperatures $Nb(V)$ tended to decompose to $Nb(IV)$ with chlorine

evolution. By introducing fluoride to $n_{F^-}/n_{Nb} > 2$, the higher oxidation states of niobium were stabilized up to 870 °C. The $Nb(III)$ species were not stable anymore, and $Nb(IV)$ was reduced directly to niobium metal. The presence of fluorine ions were found to have a beneficial effect on the quality of the niobium deposit. These results suggest that $Nb(V)$ may form other complexes than NbF_7^{2-} or NbF_6^- in mixed chloride-fluoride melts.

$Nb(V)$ is known to react with niobium metal to form $Nb(IV)$ in alkali fluoride and alkali chloride melts, and this reaction has also been found in mixed alkali chloride-fluoride melts. This is reported in several of the studies mentioned above. Alimova *et al.* [84] and [98] found that $Nb(IV)$ was also formed in $CsCl$-KCl-$NaCl$-K_2NbF_7 melts before any electrochemical reduction took place. This spontaneous reduction was accompanied by evolution of fluorine gas from the melt. The process was rather slow, and a complete conversion to $Nb(IV)$ required several hours. The rate depended on the temperature of the bath and initial concentration of $Nb(V)$. IR spectra of solidified melts indicated that the reduced species was $Nb(IV)F_7^{3-}$ or $Nb(IV)F_6Cl^{3-}$. The ratio n_{F^-}/n_{Nb} changed from the original value 7 to about 6 upon complete transition of $Nb(V)$ to $Nb(IV)$. A similar phenomenon was observed by Arurault *et al.* [95] and [101] in $NaCl$-KCl-K_2NbF_7 melts. They observed a spontaneous reduction of $Nb(V)$, but assumed the process to be accompanied by evolution of chlorine gas. Arurault *et al.* furthermore assumed K_2NbF_7 to dissolve and react in the melt as follows:

$$NbF_7^{2-} + nCl^- \leftrightarrow NbF_{7-n}Cl_n^{2-} + nF^- \tag{1.27}$$

or

$$NbF_6^- + nCl^- + F^- \leftrightarrow NbF_{6-n}Cl_n^- + (n+1)F^- \tag{1.28}$$

$Nb(V)$ ions were then slowly reduced to $Nb(IV)$ under the action of Cl^-. Oxidation of $Nb(IV)$ occured in two different processes, corresponding to oxydation of one fluorine-rich complex and one chlorine-rich complex respectively. It is somewhat strange that fluorine gas should be formed in these chlorine rich melts. Chlorine gas is far more stable than fluorine gas when potentials of reduction to their respective ions are compared. The concentration of chloride ions is also higher. It is, however, difficult to explain the loss of fluorine ions from the melts of Alimova *et al.* with an evolution of chlorine gas.

Nakagawa and Hirabayashi [59] measured the cathodic current efficiency as a function of melt composition, and found that the relative yield increased

with increasing number of fluoride ions in the system. Quite the opposite was observed by Kuznetsov *et al.* [102] who found a slight decrease in the cathodic current efficiency when KCl was substituted with KF in a KCl-K_2NbF_7 melt. This probably indicates that melt impurities are determining the current efficiency in at least some of these investigations.

1.9.2 Oxide containing alkali chloride-fluoride melts

The Raman work by von Barner *et al.* [82] on KCl-$NaCl$-K_2NbF_7 melts showed Raman spectra of a melt with $n_O/n_{Nb} \sim 1$. This was compared with a spectrum of $NbOF_5^{2-}$ in $FLiNaK$. Since the same bands were observed in both spectra, the oxofluoro complex was believed to exist also in the chloride-fluoride melt. Konstantinov *et al.* [97] assumed that the $Nb(V)$ mono-oxo fluoro complex in chloride-fluoride melts was $NbOF_6^{3-}$, while Grinevitch *et al.* [103] and Kuznetsov *et al.* [90] and [56] believed $NbOF_4^-$, $NbOF_5^{2-}$ and $NbOF_6^{3-}$ could be present. Neither the conclusions by Konstantinov *et al.* or by Kuznetsov *et al.* are drawn on the basis of vibrational spectroscopy, but rather on chemical analysis of frozen baths.

Konstantinov *et al.* [97] studied the electroreduction of $Nb(V)$ in KCl-KF-K_2NbF_7-Nb_2O_5 melts. They found that the two waves corresponding to reduction of niobium fluoride complexes were replaced by a single five-electron step at a ratio $n_O/n_{Nb} = 1$. This was claimed to be due to reduction of a niobium mono oxo fluoro complex to niobium metal. On further addition of Nb_2O_5 to $n_O/n_{Nb} = 2$, this wave was replaced by three new waves. These were ascribed to a three-step reduction of a niobium dioxo fluoro complex to niobium metal. The formation of $KNbO_2F$ and $KNbO_3$ impurities was also possible due to the excess of O^{2-} at the cathode during electrolysis. Further addition of Nb_2O_5 to the melt resulted in new peaks that were assumed to be due to a niobium tri oxo complex.

Kuznetsov *et al.* [90] studied the less fluoride rich melt $NaCl$-KCl-K_2NbF_7-Nb_2O_5, and claimed that Nb_2O_5 and K_2NbF_7 at a ratio of 1 to 3 reacted as follows :

$$3K_2NbF_7 + Nb_2O_5 \rightleftarrows 4KNbOF_4 + K_2NbOF_5 \qquad (1.29)$$

The reduction of niobium complexes in this melt appeared as one broad peak. This peak could, by mathematical analysis, be differentiated into two

peaks; the first about four times higher than the other. Adding fluoride ions to the melt gradually led to a decrease of the first and an increase of the other. The first peak was therefore ascribed to the presence of $NbOF_4^-$ and the second to $NbOF_5^{2-}$. Further addition of fluoride to the melt led to a negative shift in the reduction potential, and this was believed to be due to the $NbOF_6^{3-}$ complexes. The interaction of $NbOF_4^-$ and $NbOF_5^{2-}$ with niobium metal was studied by Kuznetsov and Grinevich [56]. Both complexes were found to react with metal to form NbO, Nb_2O, $Nb(IV)F_5^-$ and F^- ions. The presence of $Nb(IV)F_5^-$ was also found after NbF_7^{2-}-niobium metal interaction. The $Nb(IV)F_5^-$ complex had a reduction potential more positive than that of the niobium mono-oxo fluoride complexes. The reduction of $NbOF_4^-$ and $NbOF_5^{2-}$ would therefore appear as one peak in the voltammogram. Kuznetsov *et al.* [92] presented another electrochemical study of the $NaCl$-KCl-K_2NbF_7-Nb_2O_5 melt, this time in more oxide rich melts. The presence of niobium mono-oxo, dioxo and tri oxo species were observed. The solubility of the dioxo complex was found to be ten times larger than that of the tri oxo complex. A recent study of niobium in oxide containing $NaCl$-KCl-K_2NbF_7 melts was performed by Grinevitch *et al.* [103]. This work contains much of the same material as was presented by Kuznetsov *et al.* [90], [56] and [92]. The electrochemical part of the work by von Barner *et al.* [82] contains similar conclusions as those drawn by Kuznetsov *et al.*, but concerns melts with $n_O/n_{Nb} < 2$

Lantelme *et al.* [96] studied the influence of oxide on the electrochemical processes in K_2NbF_7-$NaCl$-KCl melts. They found the same reduction mechanisms as Kuznetsov *et al.* [90]. At $n_O/n_{Nb} < 1$, niobium metal deposition was perturbated by formation of niobium suboxides like NbO or Nb_4O_5. In melts with higher oxide content, a black layer of NbO_2 appeared at the electrode surface.

Gillesberg *et al.* [100] showed that the reduction mechanism of niobium in lithium containing, oxide free melts were somewhat different from those without lithium (see section 1.9.1). When oxide was introduced to give a ratio $n_O/n_{Nb} = 1.1$, only minor changes were observed on the voltammograms. It was suggested that oxide addition mainly led to precipitation of oxide containing compounds.

$$NbOF_6^{3-} + TaF_7^{2-} = NbF_7^{2-} + TaOF_6^{3-} \tag{1.30}$$

Kuznestov *et al.* [88] showed that hydrolysis of niobium could be suppressed by addition Ta^{5+}, Zr^{4+} or Al^{3+} ions to the chloride-fluoride melt. As an

example, the equilibrium of reaction 1.30 was shifted to the right, and any free oxide would react with tantalum instead of niobium.

1.9.3 Summary

The chemistry of niobium in alkali chloride-fluoride and alkali oxochloride-fluoride melts can be summed up as follows. In oxygen free melts, $Nb(V)$ is reduced to $Nb(IV)$ in a reversible step and further to niobium metal, probably in an irreversible step. This is valid for lithium free melts with a ratio $n_F/n_{Nb} > 7$. $Nb(III)$ seems to be a stable oxidation state in lithium based melts. The structural properties of the niobium complexes are somewhat uncertain. $Nb(V)F_7^{2-}$ and $Nb(V)F_6^-$ have been proposed. Mixed $Nb(V)$-chloride-fluoride complexes have also been proposed for the highest oxidation state. NbF_5^- has been proposed for the four-valent niobium species. A spontaneous reduction of $Nb(V)$ to $Nb(IV)$ accompanied by evolution of chlorine or fluorine gas has been observed in these melts.

Introducing oxide to the system seems to lead to a stabilization of the higher oxidation states of niobium. Reduction of $Nb(V)$ mono oxo fluoro complexes seems to occur in a single five-electron step to niobium metal. $Nb(V)$ dioxo and tri oxo complexes of niobium is also present in alkali chloride-melts with high concentrations of oxide. Electrolysis of such melts leads to formation and precipitation of solids like $KNbO_2F$ and $KNbO_3$.

The chemical properties of an alkali chloride-fluoride melt is naturally dependant on the ratios F/Cl and F/Nb in the melt. An alkali chloride melt with small traces of fluoride will posses the typical characteristics of a pure chloride melt. A melt with $F/Nb > 7$ seems, however, to perform much like a pure alkali fluoride melt. The reduction mechanisms are generally the same (except for the case of lithium containing melts) and similar structural entities have been proposed.

1.10 Tantalum in mixed alkali chloride-fluoride melts

1.10.1 Oxygen-free alkali chloride-fluoride melts

Agulyanskii *et al.* [104] studied K_2TaF_7-KCl-KF melts by means of IR spectroscopy and found that TaF_7^{2-} and TaF_6^- were present. TaF_7^{2-} was dominating species in melts dilute in tantalum. A TaF_6Cl^{2-} complex was also proposed, but its existence was not proved.

Drossbach and Petrick [105] studied electrolysis of tantalum from a K_2TaF_7-KCl-$NaCl$ melt, and considered the reduction of Ta^{5+} to be a two step reaction with Ta^{3+} as an intermediate. Their melt was, however, probably strongly contaminated with oxide impurities and an evolution of CO and CO_2 from the anode was reported. Konstantinov *et al.* [44] studied the electrochemical reduction of Ta^{5+} in a K_2TaF_7-KCl-KF melt, and found it to be a fast reversible one step reaction to tantalum metal. This work includes systematic measurements of the influence of oxide on the reduction mechanism.

Baimakov *et al.* [78] studied the influence of KF additions to a $TaCl_5$-$LiCl$-KCl melt. They observed a transformation of their voltammograms, going from a two step reduction in the pure chloride melt to a one step reduction in melts with $n_F/n_{Ta} > 6.6 - 6.8$. TaF_7^{2-} was therefore assumed to be the major complex in this chloride-fluoride melt, but TaF_6^- and TaF_6Cl^{2-} were probably also present.

Polyakova *et al.* [75] found the same five-electron reduction mechanism for tantalum in liquid $CsCl$-KCl-$NaCl$-K_2TaF_7. They furthermore studied anodic dissolution of tantalum in this melt, and found evidence for formation of several complexes. The small amount of free F^- ions in the vicinity of the anode could indicate a formation of $Ta(IV)$ and $Ta(V)$ chloro complexes in addition to the $Ta(V)$ fluoro complex. On the other hand, only TaF_7^{2-} were assumed to be discharged at the cathode since the Ta chloro complexes reacted with the excess of free F^- ions liberated when $Ta(V)$ was reduced. As was shown in section 1.6.1 and 1.8.1, $Ta(V)F_7^{2-}$ is the only stable tantalum fluoride complex while both four and five-valent tantalum chloro complexes are known. A reaction between the $Ta(IV)$ chloro complexes and fluoride ions was therefore found to cause a disproportionation reaction with the formation of TaF_7^{2-} and a suspension of metallic tantalum. The suspension

contributed to formation of sludge and a metallic film growing out from the electrodes on the surface of the electrolyte. The introduction of sufficient amounts of fluoride ions to the melt suppressed these unwanted side reactions.

Lantelme *et al.* [106] studied electrodeposition of tantalum from a $NaCl$-KCl-K_2TaF_7 melt, and found the same reduction mechanism as Konstantinov *et al.* [44], Baimakov *et al.* [78] and Polyakova *et al.* [75].

As mentioned in section 1.2.2, tantalum powder for production of capasitors is manufactured by reducing K_2TaF_7 with molten sodium. K_2TaF_7 is commonly dissolved in a KF-KCl electrolyte and sodium is added in portions to have a controlled reaction rate. An example of such a process is given by Bergman and Mosheim [107]. The tantalum powder is pressed into a pellet, sintered in a furnace to form a porous body and anodized in a suitable electrolyte to form a continous dielectric film of Ta_2O_5 on the sintered body. The capasitive potential of this compound is a direct function of the surface area. Since tantalum is an expensive metal, efforts are made to produce small particles with a high area to weigth ratio.

1.10.2 Oxide containing alkali chloride-fluoride melts

As mentioned in section 1.10.1, Konstantinov *et al.* [44] studied the effect of oxide additions upon electroreduction of tantalum in a K_2TaF_7-KCl-KF melt. Ta_2O_5 dissolved in the chloride-fluoride melt and reacted with $Ta(V)$ fluoride to form mono oxo fluoride complexes such as $TaOF_6^{3-}$ and to a small extent dioxo fluoride complexes such as $TaO_2F_4^{3-}$. No spectroscopic evidence for the exact structure of these complexes were given. The electrochemical reduction of the tantalum oxo fluoride complexes occured at more negative potentials than the $Ta(V)$ fluoride complex, and the deposits obtained at such potentials were still tantalum metal.

During the electrochemical studies of a $NaCl$-KCl-K_2TaF_7 melt, Lantelme *et al.* [106] observed that the potential of a pure tantalum electrode slowly shifted when it was immersed in the bath. In addition, a thin layer of tantalum oxides were formed on the surface and later an additional layer of tantalum subhalides. This formation became more rapid with increasing overpotential. At low overpotentials, metallic tantalum could not be generated and the electrode was covered with a thin layer of tantalum rich oxides and tantalum subhalides. Pure metallic tantalum was, however, produced at

more negative overpotentials, but too much negative potential increased the formation of subhalide cluster complexes. Electrolytic production of tantalum could therefore only be accomplished in a very narrow potential range. Addition of NaF was shown to be beneficial for the reduction processes, and the previously formed insoluble layer disappeared when the concentration of NaF reached 5–10 wt%. Lantelme *et al.* furthermore studied the influence of oxide added as Na_2O and BaO to the $NaCl$-KCl-K_2TaF_7 melt. A new peak was observed negative to the reduction of $Ta(V)$ fluoride in their voltammograms, and was attributed to the reduction of a tantalum mono oxo complex like $TaOCl_xF_y^{(x+y-3)-}$. The size of the peak increased up to $n_O/n_{Ta} = 1$, but no change was observed upon further addition of oxide up to $n_O/n_{Ta} = 2$. Electrolytic deposition of these melts led to formation of a black powdery layer that was identified as metallic tantalum with inclusions of oxides like Ta_2O and TaO.

1.10.3 Summary

The chemistry of tantalum in alkali chloride-fluoride and alkali oxochloride-fluoride melts can be summed up as follows. In oxygen free melts, $Ta(V)$ is reduced to tantalum metal in a reversible step in melts with $n_F/n_{Ta} > 7$. TaF_7^{2-} is the major tantalum species in these melts, but mixed tantalum chloride-fluoride complexes have also been proposed to exist. Less fluoride rich melts contain tantalum chloride complexes that are reduced in a more complex mechanism (see section 1.8.1). The KF-KCl-K_2TaF_7 system is an important melt for production of tantalum powder for capacitor manufacturing.

Introducing oxide to the system leads to a formation of oxide containing tantalum complexes. No spectroscopic measurements of such melts were found in the literature, but species like $TaOF_6^{3-}$ and $TaO_2F_4^{3-}$ have been proposed. Electrochemical reduction of these complexes results in formation of metallic tantalum with inclusions of oxides like Ta_2O and TaO.

1.11 Scope of the present work

As allready mention in section 1.4, the majority of the work on niobium and tantalum in alkali halide melts has been accomplished by using electrochemical techniques. Most of the reduction mechanisms for both "oxide free" and

oxide containing systems have been found, and appropriate conditions for electroplating have been proposed. It was therefore natural to focus on other experimental methods in the present work. The choice of methods will be given more attention later in this section.

The scope of the present work is to gain a better understanding of the influence of oxide on niobium and tantalum complexation in systems related with electroplating of the two metals. As was shown in the current chapter, the presence of oxide in the alkali halide systems has a large impact on several electroplating parameters. Coherence of the deposit, current efficiency and purity of the metal are some examples. The current work will therefore focus on the impact of oxide concentration in the electrolyte, to gain a better understanding of how the two metal ions behave in such systems. It should be emphasized that the scope of the present work is not to gain a better understanding of the electroreduction processes, since this has been studied well by other authors. Electrochemical methods were therefore not used.

The choice of the *FLiNaK* electrolyte for performing the experiments was done at an early stage. Both chloride, fluoride and mixed chloride-fluoride systems have their advantages. The chloride electrolytes are low melting and are cheap, but the electroplating process require very low oxide contents in order to be successful. This will make the preparation of the electrolyte expensive. As was shown by Rosenkilde and Østvold [65], the presence of *CsCl* reduces the problems associated with oxide contamination, but *CsCl* is probably a too expensive compound for commercial use. Replacing the niobium or tantalum chloride compound with K_2NbF_7 or K_2TaF_7, thus making it a mixed chloride-fluoride system, is another way to improve the process. Such mixed systems offers better conditions for electroplating than the pure chloride melts, but not as good as the pure fluoride electrolytes. Even though the fluoride melts are more toxic and corrosive than chlorides, they still seem to be the best media for an industrial electroplating process. The *FLiNaK* melt has a low eutectic melting point compared to the pure alkali fluorides, and makes it possible to operate the process at a temperature where suitable cell-materials can be found. The *FLiNaK* melt has, as shown in the previous sections, been studied in several other works, and was a natural choice as electrolyte for the current experiments.

Matthiesen, Jensen and Østvold [31] were the first to perform a systematic study of solubility of oxide and niobium(IV,V) in *FLiNaK* with varying molar oxide to niobium ratios, n_O/n_{Nb}, in the melt. von Barner *et al.* [18] studied the complex formation by Raman spectroscopy in the same melt, but

due to the lack of solubility data some of their conclusions were probably incorrect. Both these works have been described in section 1.5.2. The scope of the present work is to combine solubility measurements with spectroscopy. It is then possible to know the exact composition of the melts and to see if there are solids present in the system. This will make it possible to understand what complexes that are formed in the melts, and how the equilibria between these are established. As shown by Christensen *et al.* [22], it is only melts with $n_O/n_{Nb} < 1$ that are interesting for electroplating. The current work will also focus on more oxide rich melts for scientific reasons. The work will try to find similarities and differences between the two twin-elements and how they form metal-oxofluoride complexes in molten *FLiNaK*.

Chapter 2

Experimental

2.1 Chemicals

The chemicals used are listed in Table 2.1.

Table 2.1: Chemicals

Compound	Quality	Manufacturer	Comments
LiF	99.5%	Alfa, Germany	
KF	99%	Merck, Germany	
NaF	99%	Merck, Germany	
Nb_2O_5	99.95%	Cerac, USA	
Ta_2O_5	99.95%	Cerac, USA	
NbO_2		See section 2.1.1	
NbO		See section 2.1.1	
K_2NbF_7	99.9%	Alfa, Germany	
K_2TaF_7	99.9%	Alfa, Germany	
Na_2O_2	$< 95\%$	Merck, Germany	
Ar	99.996%	AGA, Norway	
He	99.998%	AGA, Norway	
N_2	99.999%	AGA, Norway	
HF, p.a. 40%		Merck, Germany	Concentrated

2.1.1 Preparation of chemicals

Preparation of Na_2O

Na_2O was made by decomposing Na_2O_2 in an Al_2O_3 crucible at 600 °C under a vacuum of 10^{-3} mbar for 12 hours. The apparatus shown in figure 2.1 was used. The product, a hard lump with green colour, was transfered immediately to a glove-box where it was mortared to fine powder. The procedure was repeated twice, and the compound was used within a few days. The oxide reacts quickly with air (oxygen and water), and could not be stored for longer periods of time unless kept in a sealed ampoule.

By dissolving the oxide in water and titrating with HCl, it was possible to find the purity of the compound. Assuming the reaction $Na_2O + H_2O = 2NaOH$ to take place upon contact with water, the solution was titrated until neutrality. A typical result after double decomposition showed a purity of 98% compared to pure Na_2O. This is however a simplified way of calculating the purity, as it is assumed that deviation from 100% is due to the presence of unreacted Na_2O_2. The latter will also react with water: $Na_2O_2 + H_2O = H_2O_2 + 2NaOH$; forming the monoprotic acid hydrogen peroxide in addition to sodium hydroxide. Hydrogen peroxide, that has $pK_a = 11.65$ is not dissociated at $pH = 7$ (titration end point) and will not have any effect on the titration. The increased molar weight of Na_2O_2 compared to that of Na_2O will, however, affect the results. Taking 1 gram oxide, this will contain x gram Na_2O_2 and y gram Na_2O, or rather $(x/78)$ moles of Na_2O_2 and $(y/62)$ moles of Na_2O. If the oxide had been perfectly pure ($x = 0$) the titration endpoint would have been reached after addition of $(2y/62)$ moles of HCl since each mole of Na_2O produces two moles of $NaOH$. Instead, neutrality is reached after addition of $(2x/78) + (2y/62)$ moles of HCl. Thus, when a purity of 98% is reported one gets: $(2x/78) + (2y/62) = 0.98(2y/62)$ giving $x = 0.0975$ and $y = 0.9025$ (since $x + y = 1$). More generally $(2x/78) + (2y/62) = p(2y/62) \Rightarrow x = 78(1-p)/16)$ and $y = (78p - 62)/16$, where p is the purity and is a number from 0 to 1. By adding 1 gram of an oxide with a reported purity of 98% to a melt, one actually adds 0.00125 moles of Na_2O_2 (7.9 mole%) and 0.0146 moles of Na_2O (92.1 mole%). Knowing that Na_2O_2 is stable in $FLiNaK$ up to at least 600 °C [108], the presence of the sodium peroxide should be taken into account when using the synthesized (Na_2O) compound.

Preparation of NbO and NbO_2

The oxides NbO and NbO_2 were prepared by Sergey Kuznetsov as described by Grinevitch *et al.* [103].

2.1.2 Purification of chemicals

Purification of alkali fluorides

The alkali fluorides LiF, NaF and KF have low vapor pressures at their respective melting points, and were therefore purified by recrystallization. A water cooled tubular furnace with an inner Pythagoras (commercial available Al_2O_3-SiO_2 based ceramic) lining was used for this purpose. The furnace was connected to a vacuum pump, and had valves at the top and bottom to allow a continuous flow of nitrogen during the recrystallization. A crucible containing the salt was placed in the middle of the furnace, with radiation shields above and below to obtain a better temperature gradient over the crucible.

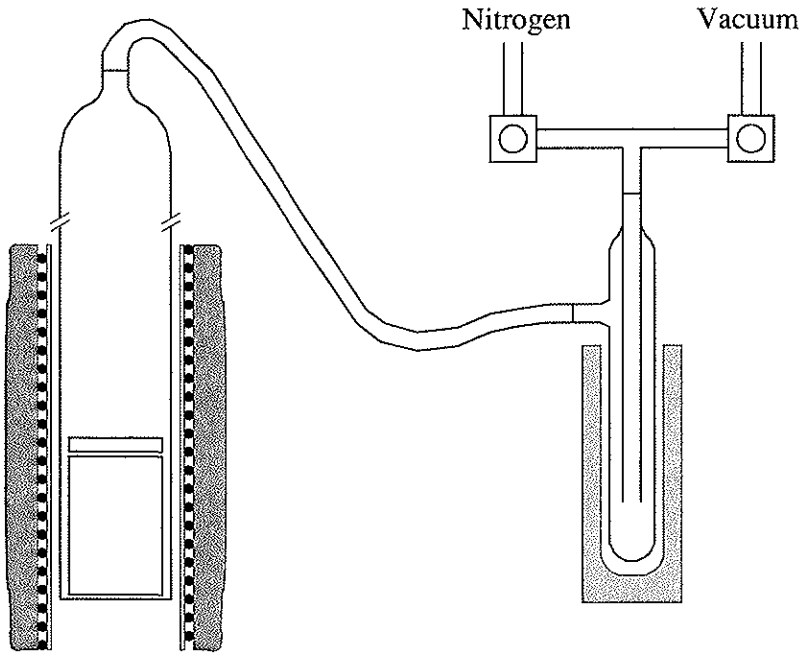

Figure 2.1: Apparatus used for high-temperature, vacuum experiments

The alkali fluorides were first dried under vacuum at 400 °C for 4 hours. The furnace was then filled with nitrogen to 1 atm. A constant small flow of nitrogen was allowed through the furnace. The temperature was raised to 20 °C above the melting points and kept at 2 hours to make sure that the salt was completely melted. The actual recrystallization was done from this temperature by cooling the melt at 3 °C/hour to a temperature 10 °C below the melting point. The furnace was then cooled to 150 °C and kept at this temperature until the crucible was transfered to a glove-box. The impurities (mainly alkali oxides) were concentrated in the middle of the crucible, and could easily be removed. The alkali fluorides were recrystallized twice and stored in closed containers inside a glove-box.

The crucible was normally made of platinum (5cm high, slightly coned from top to bottom). LiF made in this way sometimes showed impurities in the crystals after the recrystallization. The salt had a red color, that was first believed to be iron, but an analysis of the fluoride on ICP (See section 2.2.4 showed traces of aluminum and silicon. It is difficult to say for sure why the recrystallization of LiF failed, but it could be that the high wetting of the melt with platinum made the salt make a film on the crucible which reacted with the inner ceramic lining of the furnace. When a glassy carbon crucible was used, there was never any problems with the recrystallization of LiF; probably due to the pour wetting of LiF on this material. It should be mentioned that the situation is the opposite for CsF, where recrystallization in glassy carbon was impossible due to wetting. This compound was successfully purified in a platinum crucible, but was not used for experiments described in this work.

Drying of Nb_2O_5 and Ta_2O_5

The niobium- and tantalum-pentoxide were only dried before use. The apparatus shown in figure 2.1 was used for this purpose. Both oxides were dried in a glassy carbon crucible under vacuum at 600 °C for at least 12 hours, and then transfered to a glove box.

2.2 Solubility experiments

2.2.1 Apparatus

The equilibrium studies at different oxide to niobium ratios were carried out in a furnace mounted vertically under an argon filled glove box, making it possible to access the experimental cell from inside without introducing moisture to the cell. The water and oxygen contents in the box were ≈1 and ≈3 PPM, respectively. All handling of purified salts and samples were performed in the box. The cell and furnace assembly is shown in figure 2.2. A graphite lid was mounted on the top of the glassy carbon crucible, and 8 graphite radiation shields were possitioned above the lid at regular distances of 3 cm to decrease the vertical temperature gradient. A glassy carbon tube surrounded the radiation shields to reduce the corrosive actions of fluorides on the quartz cell. The lid and the shields had holes for sample extraction (see figure 2.3) and feeding of salts, stirring unit and thermocouple. There were also holes for two electrodes, but these were not used under the solubility experiments. Melt samples for chemical analysis were extracted from the melt using graphite ladles (see figure 2.4), while stirring was performed with a graphite blade connected to an electrical motor via a steel rod. The whole setup was mounted inside a quartz tube, and lowered into a Kanthal cell surrounded by a furnace. A brass lid, with holes similar to those in the graphite lid and the radiation shields, was mounted on the top of the quartz tube to prevent impurities from falling into the melt.

2.2.2 Procedure

Sample extraction and salt addition methods

The sample extraction and salt addition methods applies to all the solubility measurements and is described below. The hole in the radiation shields used for this purpose was plugged with a long graphite rod during the experiment, and was only removed when it was needed for addition or extraction of salts. The rod prevented evaporation and heat loss from the melt surface to some extent.

The charging tube was inserted into the cell only seconds before the actuall additon took place. The salt crystals were in the form of small pieces and

could stick to the tube wall and melt if it became too hot. Since the molten fluorides are very corrosive towards quartz, this could lead to introduction of SiO_2 in the melt. The tube was quickly withdrawn from the hot cell after addition. Before a sample was taken from the melt, it was necessary to turn off the stirrer at least 15 minutes in advance to allow possible solid particles to settle at the bottom of the crucible. The possible solids were generally more than twice as dense as the melt. Molten $FLiNaK$ has a density of about 2 g/cm^3. The density of the following solids are measured at room temperature and are found in the CRC Handbook of Chemistry and Physics [109] : Nb_2O_5 : 4.6 g/cm^3, $LiNbO_3$: 4.3 g/cm^3, $NaNbO_3$: 4.55 g/cm^3, $KNbO_3$: 4.64 g/cm^3 and Ta_2O_5 : 8.2 g/cm^3. Melt samples were normaly taken with graphite ladles. In some cases a graphite filter was used to separate the melt from solid particles when taking a sample.

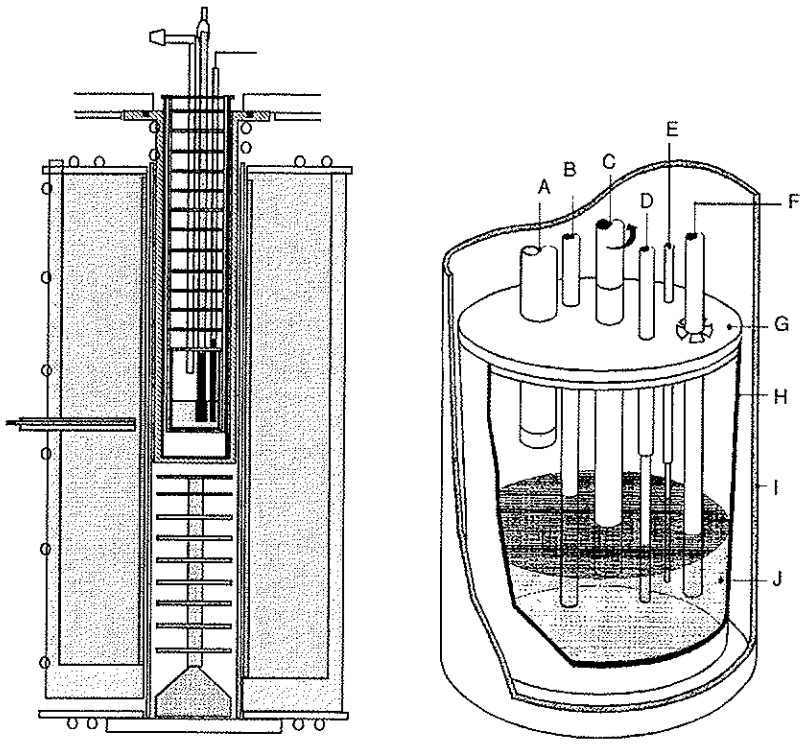

Figure 2.2: Experimental cell and furnace mounted to glove box: (A) quartz sampling tube; (B) electrode, not in use; (C) stirrer; (D) electrode, not in use; (E) electrode, not in use; (F) thermocouple, type K; (G) graphite lid; (H) glassy carbon crucible; (I) quartz container; (J) melt.

This sampling device never failed. It was, however, much more expencive and was mainly used to control the analysis obtained from the samples that were taken using the graphite ladle. The ladle and the filter system is shown

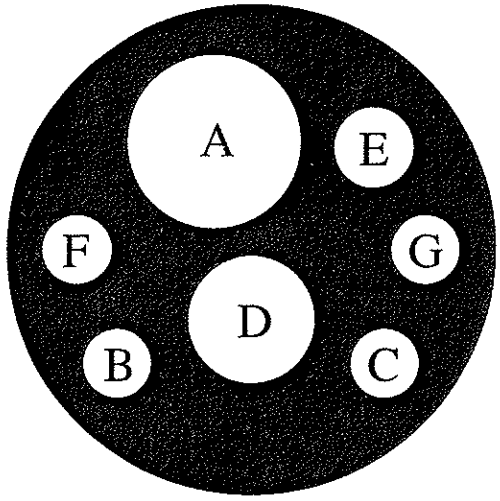

Figure 2.3: Radiation shields of graphite. The graphite lid and brass lid has similar holes: (A) addition and sample extraction; (B) and (C) electrode; (D) stirring; (E) thermocouple; (F) and (G) graphite rods connecting and seperating the 8 shields

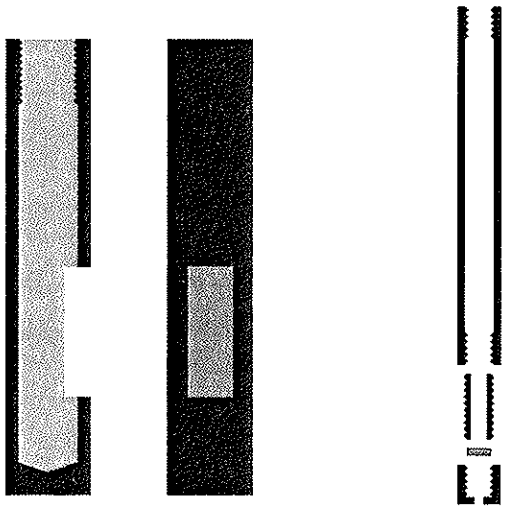

Figure 2.4: Equipment for extraction of samples from the melt.

in figure 2.4. The ladle was connected to a steel rod, and slowly inserted into the cell. It was important that the graphite became sufficently hot before it was imersed into the melt. In this way no salt would freeze on the ladle before it was filled. This could possibly have altered the composition of the sample and caused analytical errors. It was noted that some melts (e.g. pure $FLiNaK$) vetted graphite very poorly. The melt level had to be around 1.5 cm above the inlet level to force the melt into the ladle. Normally, the ladle was kept 3 cm above the melt for 5 minutes to heat it properly. It was then dipped into the crucible and quickly pulled up into the glove box to cool. Since the melt samples were not quenched very rapidly inhomogenity in the samples might have occured.

The graphite filter device is also shown in figure 2.4. The graphite assembly was connected with a steel tube, which again was connected to a manual pump. Each filter was tested with distilled water in advance to check how fast liquid would flow through, and this was used to estimize how long the pump should be used in each case (the porosity of the filters had a tendency to vary). Like for the graphite ladles, the filter system was slowly lowered into the cell to be heated before the actual extraction was performed. Once down in the melt, a negative pressure was applied for a gived period, and the filter assembly was lifted out of the cell to cool.

Experiments with *Niobium*

All the graphite parts, including ladles and filter system for sample extraxtion, was cleaned by boiling in dilute HCl and subsequent boiling in distilled water. The graphite was also heated under vacuum at 900 °C in the aparatus shown in figure 2.1. The cell was kept in the glove box furnace at 500 °C for 24 h in order to remove adsorbed water, before the LiF, NaF, KF and K_2NbF_7 were added to the glassy carbon crucible in given amounts. The crucible was normally filled with enough salt to get a melt level of 2.5 cm. It was necessary to add the salts in two batches by melting down the first batch at 700 °C before the next addition. A sample was then extracted and pellets of Na_2O added to obtain a given n_O/n_{Nb} ratio. Equilibrium was established at 700 °C by carefully stirring the melt for at least 8 hours.

Two solubility experiments were performed; series 1 covering the compositions $0 < n_O/n_{Nb} < 4.6$, and series 2 covering $2 < n_O/n_{Nb} < 8.7$. In series 2, the first addition of Na_2O was done directly into the crucible before it was lowered into the cell for further additions of fluorides and Na_2O. The saturation experiments with the 3 oxides Nb_2O_5, NbO_2 and NbO were performed

by adding a certain amount of the oxide to pure $FLiNaK$. The samples were extracted and analyzed at regular intervals until two samples contained the same concentration of oxygen. By comparing the added and the measured amounts, it was possible to know whether saturation was reached or not. For Nb_2O_5, the saturation levels were measured at different temperatures.

Experiments with *Tantalum*

The experiments with tantalum were performed in a similar way as those with the niobium. For the system LiF-NaK-KF-$K_2TaF_7 - Na_2O$, compositions were studied at 700 °C in the range $0 < n_O/n_{Ta} < 6.1$. The dissolution experiment with Ta_2O_5 was performed at 700 °C, by adding small amounts of the solid to $FLiNaK$. Stirring was applied, and samples were withdrawn from the melt before each addition of Ta_2O_5.

2.2.3 Oxygen analysis

The oxide content of the extracted samples was determined by the carbothermal reduction method using LECO TC–436, as described by Mediaas *et al.* [110] and [111]. The oxygen in a sample reacts with carbon powder in an electrically heated graphite crucible to form CO. The CO is oxidised to CO_2 with CuO, and the amount of CO_2 is detected by infrared absorption (IR) at a frequenzy characteristic for CO_2. The detection limit and accuracy are reported to be 0.1 ppm (at 1 gram sample weight) and 1% of oxide present, respectively.

Preperation of samples

The handling of samples was important since the salts could easily absorb water forming hydroxides and oxides upon heating. All the preperations for the analysis were therefore performed inside the argon filled glove box. Salt pieces, rather than powder, were added to small tin capsules, which were closed. The capsules were transfered to marked glass containers with plastic caps. The glass containers were transfered from the glove box to the LECO TC–436 apparatus some minutes before the actual analysis. The sample were transfered directly to the loading mechanism of the instrument. The exposure to atmospheric moisture was therefore very small.

4 parallels were normally run from each sample. It should be emphazised that these were from different parts of the extracted salt. It was then possible to monitor inhomogenity in the samples resulting from insufficent quenching. If the oxygen content in the four paralells were different by a standard deviation more than 20% of the average value, more parallels were normally run to get a more reliable oxygen content of the extracted sample. In extreme cases, all the extracted salt had to be analyzed in order to have a trustable average value. Large deviations from parallel to parallel was in some cases observed, and indicated that there were solid particles in the sample as mentioned above. By analyzing 10 paralells only 2 or 3 were far from the average of the other 8–7. The remaining paralells showed a normal deviation which was +/- 10% of the average value.

Analysis procedure

The analysis method could be performed in different ways. Three standard procedures; scan, automatic and step ramp that were provided by the instrument will be discussed here. Common for all was: An analysis was initiated by loading the sample in the tin capsule. A graphite crucible about 2cm tall, with a diameter of about 1cm was filled with graphite powder. The powder was used to improve contact between carbon and sample. When the furnace was closed, the crucible was positioned between the upper and the lower electrodes. The instrument, including the furnace with the crucible, was flushed with helium to remove oxygen in the furnace chamber. This normally took 30–60 seconds. While still flushing, power was applied to the electrodes to heat the crucible to a temperature well above the analyzing temperature. This lasted for 30–60 seconds, and would effectively remove any oxygen from the crucible. The crucible was cooled down to the starting analysis temperature, and the system was held like this for 10–30 seconds in order to let any of the formed CO_2 pass through the detector.

The tin capsule containing the sample automatically dropped into the crucible after this cleaning procedure, and both the salt and the tin capsule would melt, mix and react with the graphite powder. Normally, the "scan" procedure was chosen for new samples. The temperature is raised by a rate set by the operator, starting and ending at preset temperatures. With this method the different oxides in the sample will react with the carbon at different temperatures, indicating their respective carbothermal decomposition temperatures. The output of the analysis is a graph showing produced amount of CO versus time, and the total oxide content of the sample is

found by integration of this curve. If the sample contains different kinds of oxides and if these oxides decompose at different temperatures, it is also possible to determine their respective amounts. The major drawback of this method is that it is rather timeconsuming. It is therefore an advantage to use the faster "automatic" mode. Then the sample is analyzed at a constant high temperature and it normally takes about 40–50 seconds to decompose all the oxide in the sample, compared to 200–300 seconds for "scan". There is, however, a danger that oxide that would normally react at lower temperature could evaporate at the high temperature. The method will in these cases indicate too low oxide content in the sample. It is therefore important to do both the "scan" and the "automatic" method on a new sample to make sure the same result is obtained in both cases. The "step ramp" method is a combination of the two other methods. It provides the operator with 9 different analysis temperatures. It is possible to "step" or "scan" from one "ramp" to another. Common for all methods is that the maximum analysis time is 400 seconds.

2.2.4 Elemental analysis

The *Nb* and *Ta* concentrations were obtained by ICP (Inductive Coupled Plasma emission spectroscopy). ICP has the advantage of analyzing several elements at the same time. This was not needed in the present work. A solution was pumped into the spectrometer and mixed with argon to form a fluid of small droplets in relatively large amounts of gas. The fluid was led into an inductive coupled plasma, where the liquid phase evaporated. The valence electrones of the ions would be exited into higher energy states due to the high temperature of the plasma, and the emission lines as the ions regain their ground states were measured. Since each element has their own characteristic lines (or frequencies), it is possible to obtain both a qualitative and quantitative measure of the concentrations of an ion in solution. The instrument, a Thermo Jarrell Ash–Atom Scan 16, was equipped with a Teflon mixing chamber, where the solution was mixed with the argon and a sapphire tube that led the fluid into the plasma. These materials were chosen due to the corrosive nature of the solutions used.

The samples, 0.2 g each, were dissolved in 10 ml HF (40%) and 1 ml HNO_3 (68%), and distilled water was added to a volume of 100 ml. In order to dissolve the fluorides completely, it was necessary to keep the solutions at 50 °C, and this temperature was also kept during analysis to avoid precipita-

tion. The solutions were mixed and stored in plastic containers. Caution was taken during handeling of these liquids due to the high *HF* concentration.

2.3 Raman spectroscopy

Raman spectra of the melts were recorded at the "Institute of Chemical Engineering and High Temperature Chemical Processes (ICE/HT)", Patras Greece in colaboration with Vassilis Dracopoulos and George Papatheodorou. The samples had been prepared in Norway. Both niobium and tantalum containing fluoride salt were studied with the Raman technique.

2.3.1 Apparatus

The experimental setup of the Raman equipment is shown in figure 2.5. The 488 nm line of an argon ion laser (Spectra Physics, Model 2017, Power: 600mW) was used to obtain the spectra. For analysing and collecting the spectra the T-64000 (Jobin Yvon) Raman system, equipped with a Spectraview - 20 2DTM liquid N_2 - cooled CCD detector was used, in the triple configuration. The spectral resolution was 5-6 cm^{-1} and the integration time was 5–20 sec. The spectral window centred at 450 and 850 cm^{-1} in the Stokes region in order to record a spectrum from 50 up to 1200 cm^{-1}.

Before each experiment two liquid samples were used for adjusting the optics and the polarization characteristics of the spectra ; CCl_4 at room temperature and a mixture of $0.3ZnCl_2$-$0.7CsCl$ at 800 °C. The system was interfaced with a personal computer and the spectra were saved in digital form. Two different polarization directions were used for recording the spectra namely VV and HV.

Some IR measurements were additionally performed on a Bruker IFS 66V.

2.3.2 Procedure

Due to the high corrosivity of *FLiNaK* melts, the windowless graphite cell technique was used for recording the spectra. The cell design was described by Gilbert *et al.* [112] and by Gilbert and Materne [113], and the high

temperature furnace was described by Dracopoulos *et al.* [114]. The graphite cells were degassed at 1000 °C for ten hours before use, and transfered into a glove-box. Each cell was filled with 0.11–0.12 g of a salt, and put into a quartz tube. The tube was connected to a stop-cock that was closed before taking the cell out of the box. Each cell was evacuated and refilled with N_2 twice, the last time only to about 0.4 atm. When mounting the cell in the furnace, the gas would naturally expand, giving a pressure around 1 atm. at high temperature. The reason for choosing an inert atmosphere instead of vacuum was to reduce the diffusion of corrosive gases that otherwise would attack the quartz glass tube.

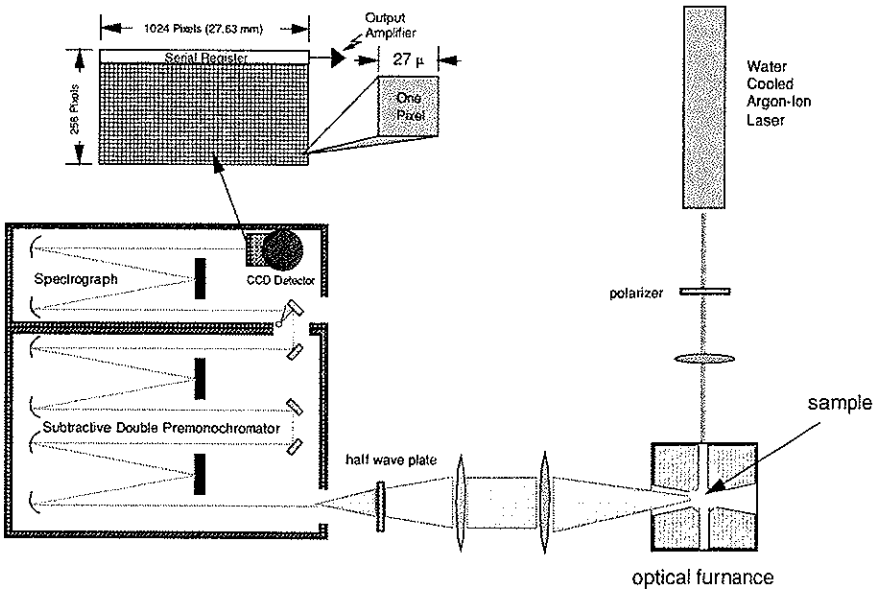

Figure 2.5: Schematic figure of the Raman spectrometer and the experimental setup. The quartz tube containing the graphite cell with a sample is positioned in the centre of the furnace. The laser beam is focused to obtain a maximum intensity in the middle of the sample, and the scattered Raman light is collected at an angle of 90 °C. The spectrometer is divided into a double and single monochromator, and works like a tripple monochromator when used in serial configuration.

Chapter 3

Niobium

3.1 Solubility of $Nb(V)$ and O^{2-} in $FLiNaK$ with variations in oxygen content

The influence of Na_2O concentration on oxide and $Nb(V)$ solubility, and $Nb(V)$-F-O complexation in $FLiNaK$ melts containing a given amount of K_2NbF_7, was studied as a function of the n_O/n_{Nb} molar ratio at 700 °C. The niobium and oxide concentration in the melt is plotted versus the molar ratio n_O/n_{Nb} in figures 3.1 and 3.2, where the content of oxygen and niobium in both the melt and in the possible solid Nb-O-containing compounds are included in the ratio. The dotted lines indicate the total concentration of oxide in the systems; the theoretical values of oxygen that is expected if all the added Na_2O goes into solution. Values used to plot the figures are given in appendix A.

The measured oxide content in samples with $n_O/n_{Nb} > 4$ has a rather high standard deviation, and this is probably due to inhomogeneity of the quenched melts. The mean value of the analyzed data will, however, be fairly accurate, since most of the sample was used for analysis or the samples for analysis were taken from representative parts of the quenched melt in order to compensate for the gradient in concentration through the salt. It is possible to give an evaluation of the stoichiometry of the precipitating species as well as the complexes formed from the data below. The n_O/n_{Nb} data are based on added amounts of Na_2O and K_2NbF_7 (0.22 mole/kg melt). Corrections are made for the measured oxygen and niobium content in the salt due to samples withdrawn for analysis.

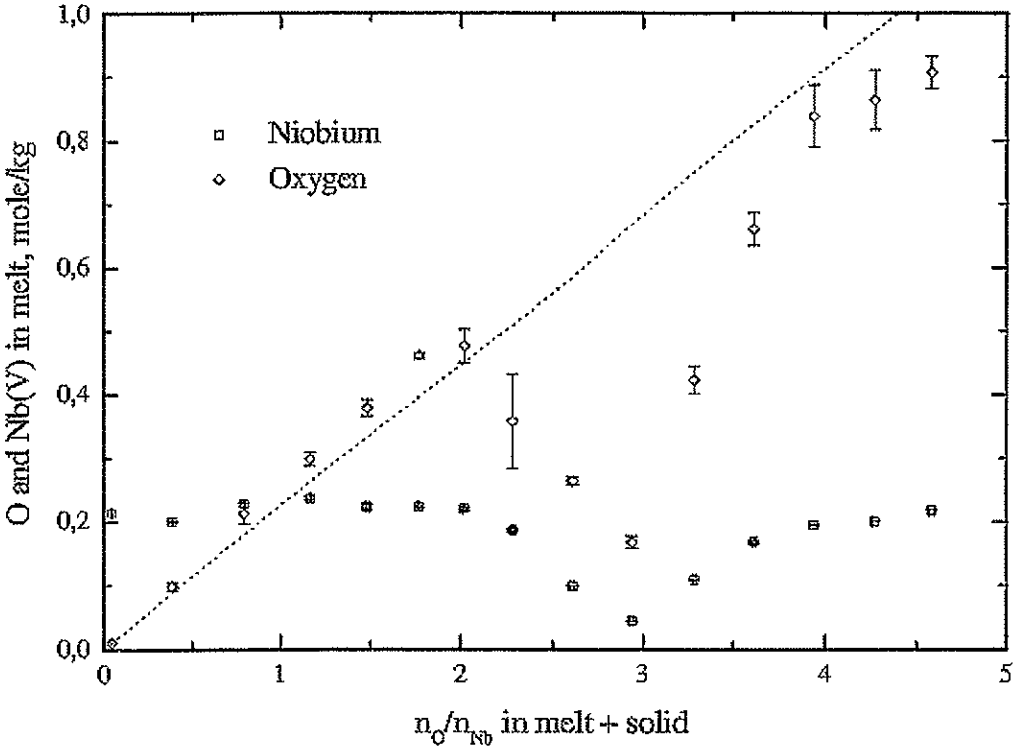

Figure 3.1: Oxide Na_2O and $Nb(V)$ concentrations in the liquid LiF-NaF-KF eutectic at 700 °C versus the molar ratio, n_O/n_{Nb}, in the melt and in the solid phases. Series 1: $0 < n_O/n_{Nb} < 4.7$.

$\mathbf{0 < n_O/n_{Nb} < 2}$: The niobium concentration in the melt is constant, and the oxygen concentration increases linearly as the ratio n_O/n_{Nb} increases. All the added oxide goes into solution. In fact, a higher concentration is observed than that corresponding to the added amounts of Na_2O. A similar effect was reported by Christensen *et al.* [22] also that in a K_2NbF_7-Na_2O-$FLiNaK$ melt, and was explained by "experimental difficulties". The oxide that was used in series 1 indicated a purity of about 96.5 mole% Na_2O by titration with HCl. As mentioned in section 2.1.1, the enhanced oxide concentration is probably due to Na_2O_2. An addition of the 96.5 mole% Na_2O will indeed produce a too high oxygen concentration due to the Na_2O_2 content. One gram of Na_2O will give $(1/62) = 0.0161$ moles of oxygen while addition of one gram Na_2O_2 will give $(2/78) = 0.0256$ moles of oxygen to the melt. A purity 96.5 mole% indicates that the oxide may contain 17.1 wt% of Na_2O_2 and 82.9 wt% and Na_2O. One gram of this oxide will therefore contain

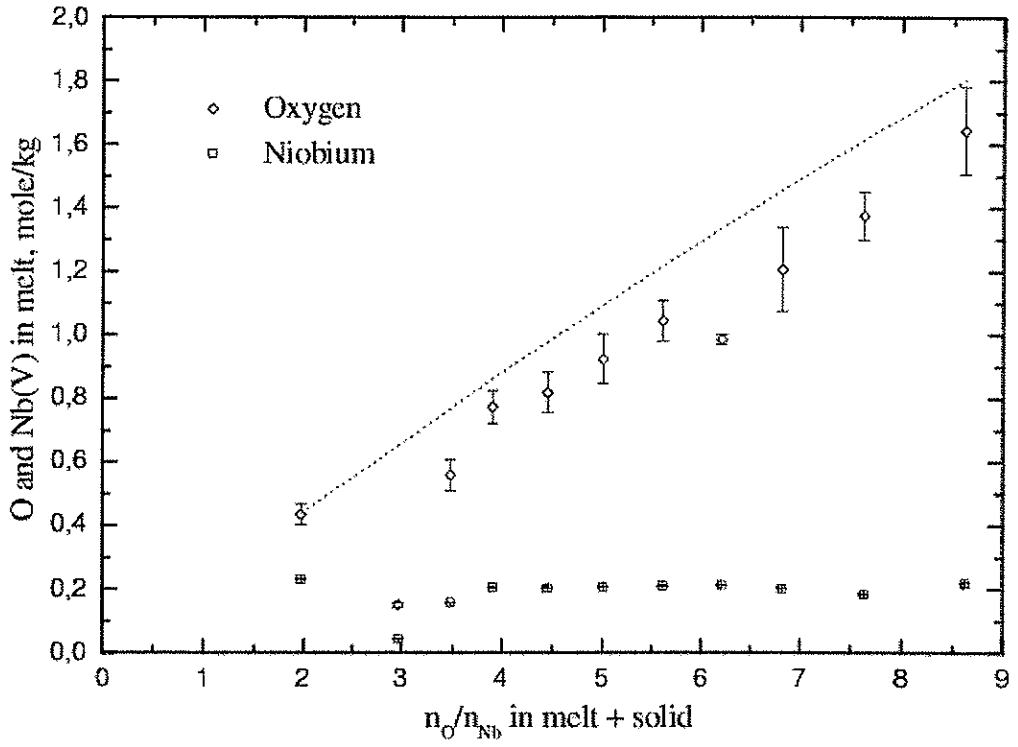

Figure 3.2: Oxide Na_2O and $Nb(V)$ concentrations in the liquid LiF-NaF-KF eutectic at 700 °C versus the molar ratio, n_O/n_{Nb}, in the melt and in the solid phases. Series 2: $2 < n_O/n_{Nb} < 8.7$.

0.0178 moles of oxygen; about 10% more than the oxygen content in one gram of pure Na_2O. In series 2 an oxide with a measured purity of 98.5 mole% was used; an oxide containing about 4.3 mole% more oxygen than pure Na_2O. The measured oxygen concentration at $n_O/n_{Nb} = 2$ is, within the experimental errors, equal to the added amount of oxide.

It is difficult to say how the presence of Na_2O_2 will affect the chemistry of the system, but it seems to be a reasonable explanation for the high oxygen content in the melt. The values for n_O/n_{Nb} in the figures 3.1 and 3.2 are based on the assumption that the added oxide is pure Na_2O. The solubility minimum is probably due to the precipitation of a solid with a ratio of oxgen to niobium equal to 3, and the minimum is expected where the total ratio n_O/n_{Nb} in the system is 3 if a pure Na_2O is used. The minimum in solubility is found close to the ratio $n_O/n_{Nb} = 3$, and not at a lower ratio.

This is somewhat surprising in the view of the Na_2O_2 content in the Na_2O used.

It is impossible to say anything definite about the species in the melt just based on these solubility data, but it is clear that no solid salts are present in the system for $n_O/n_{Nb} < 2$. The results are consistent with reaction 3.1 and the formation of $NbOF_5^{2-}$ and $NbO_2F_4^{3-}$ complexes in the melt as suggested by von Barner *et al.* [18]:

$$yO^{2-} + NbF_7^{2-} = NbO_yF_x^{(2y+x-5)-} + (7-x)F^- \tag{3.1}$$

$\mathbf{2 < n_O/n_{Nb} < 3}$: As shown in figure 3.1, the concentration of both oxygen and niobium decreases as the ratio n_O/n_{Nb} increases above 2. A solubility minimum is reached at $n_O/n_{Nb} = 3$. Precipitation of a solid compound $AlkNbO_3$ seems to occur as indicated by reaction 3.2; similar to the one presented by Matthiesen *et al.* [31]:

$$NbO_2F_4^{3-} + O_2^- + Alk^+ = AlkNbO_3(s) + 4F^- \tag{3.2}$$

Rosenkilde *et al.* [24] measured the solubility of $KNbO_3$ in $FLiNaK$ by using cyclic voltammetry, and found a solubility 0.032 mole/kg at 700 °C. This is in reasonable agreement with the data in figures 3.1 and 3.2.

According to equation 3.2, the slopes of the lines for the decreasing $Nb(V)$ and O_2^- concentrations in the region $2 < n_O/n_{Nb} < 3$ should be close to -1 and -2, respectively. The lines in figure 3.1 show slopes of about -0.75 and -1.3. The results indicate that another reaction takes place simultaneously, possibly the formation of a soluble Nb-O-F-complex with $n_O/n_{Nb} = 3$. It is, however strange that precipitation of $AlkNbO_3(s)$ should occur simultaneously with the formation of the dissolved specie $NbO_3F_x^{(1+x)-}$. Figure 3.3 is a closeup of figure 3.1 and shows the oxide concentrations in the range $1.8 < n_O/n_{Nb} < 3.2$:

It is expected that precipitation starts as soon as the dissolved specie reaches a critically high concentration, and that this concentration should remain constant as long as the precipitated solid is present in the system. If this solid oxide is totally insolubly in the melt, the oxygen concentration will follow the dashed line in figure 3.3. Precipitation starts imidiately as the ratio n_O/n_{Nb} exceeds 2, and the oxygen concentration is given by the line

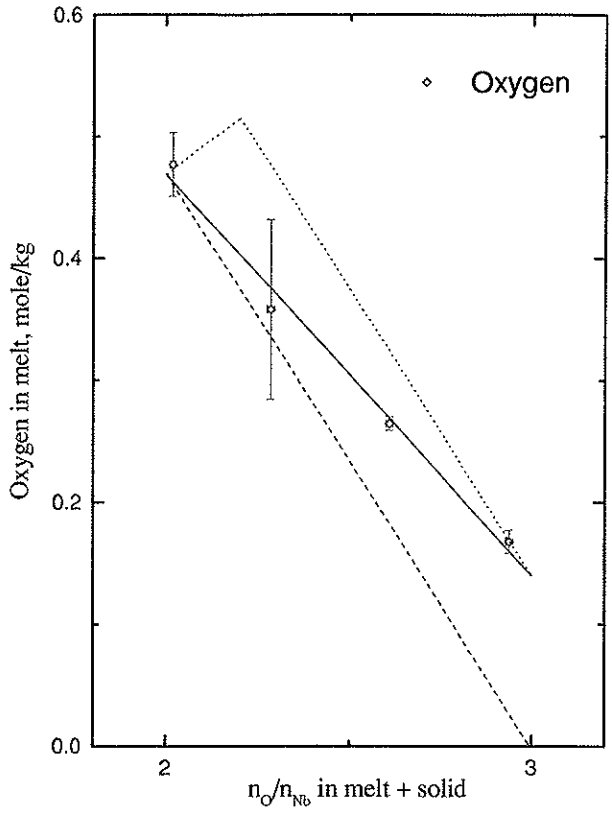

Figure 3.3: Closeup of figure 3.1 in the range $1.8 < n_O/n_{Nb} < 3.2$. The solid line is a regresion line based on the four data-points, while the dotted and dashed lines are theoretical lines based on reaction 3.2

with slope $= -2$. If the solid oxide has a solubility corresponding to the measured oxygen concentration at the ratio $n_O/n_{Nb} = 3$, the solubility will follow the dotted line in figure 3.1. Precipitation does not start before a limiting concentration of the dissolved specie is reached, but once the melt is saturated, the oxygen concentration descends along the line with slope $= -2$. Neither of these options fits with what is actually beeing observed.

Matthiesen *et al.* [31] performed a similar experiment when studying the influence of SrO in K_2NbF_7 containing $FLiNaK$ melts. As previously mentioned they reported a precipitation of a solid compound $AlkNbO_3$ for $2 < n_{SrO}/n_{Nb^V} < 3$, but more importantly; the oxygen concentrations followed a trend similar to the dotted line in figure 3.3. It is therefore likely that the data observed in the present system is due to the presence of Na_2O_2 in the melt. It is however difficult to understand why Na_2O_2 has this effect.

The minimum in solubility was measured at $n_O/n_{Nb} = 2.94$ in series 1 where the concentrations of oxygen and niobium were 0.17 mole/kg melt and 0.044 mole/kg melt respectively. In series 2 the minimum in solubility was measured at $n_O/n_{Nb} = 2.97$, and oxygen and niobium concentrations were 0.15 mole/kg and 0.045 mole/kg respectively. This means that the solubility of the solid compound $AlkNbO_3$ is equal to or lower than 0.045 mole/kg at $n_O/n_{Nb} = 3$ and 700 °C. Rosenkilde *et al.* [24] found the solubility of $KNbO_3$ in $FLiNaK$ at 700 °C to be 0.13 mole%. This equals 0.031 mole/kg melt. Matthiesen et al [31] did not report the solubility at $n_O/n_{Nb} = 3$ in their $FLiNaK$-K_2NbF_7-SrO melt, but the value seems to be 0.04–0.05 mole/kg at 700 °C.

$3 < n_O/n_{Nb} < 8.7$: Dissolution of the solid $AlkNbO_3$ occurs. The concentration of both oxygen and niobium increases to $n_O/n_{Nb} = 4$ indicating that all the added compounds are dissolved at this point. Matthiesen *et al.* [31] propose formation of a $NbO_yF_x^{(2y+x-5)-}$ complex, probably with $y = 4$. It is not possible to draw any further conclusions based on the solubility data only. When the ratio n_O/n_{Nb} exceeds 4, the niobium concentration remains more or less constant while the oxygen composition in the melt increases slightly . The increase is less than what would have been expected if all the added oxide had gone into solution. This indicates a formation of an oxygen rich solid compound. A small precipitation of a solid containing distorted NbO_6 octahedra will not have a large influence on the niobium concentration in the melt, and the analyzed niobium concentration is also almost constant.

3.2 Solubility of Nb_2O_5, NbO_2 and NbO in $FLiNaK$

Matthiesen *et al.* [31] studied the solubility of Nb_2O_5 in $FLiNaK$ at 700 °C, and indicated that the $NbO_2F_x^{(x-1)-}$ complex was responsible for the measured solubility (see equation 3.4). It is important to note that, even with very low additions of Nb_2O_5 there seemed to be a precipitation of $AlkNbO_3$, and the concentrations of niobium and oxygen increased linearly as a function of the added amounts until saturation was reached. From the slopes of their concentration v.s. addition plots, the ratio n_O/n_{Nb} in the melt seemed to be 2.2. Unable to determine the structure of the soluble species, Matthiesen *et al.* [31] assumed the presence of $NbO_2F_4^{3-}$ and

$Nb_2O_5(dissolved)$ to account for the ratio n_O/n_{Nb} in the melt. Based on the known [18] and the present spectroscopic data it is unlikely that Nb_2O_5 is present as a dissolved specie. It is more appropriate to assume that $NbO_2F_x^{(x-1)-}$ and $NbO_3F_x^{(1+x)-}$ is present. It is reasonable to assume that all the added oxide goes into solution until a saturation ratio of $AlkNbO_3$ is reached. Reaction 3.3 will then be dominating.

$$Nb_2O_5(s) + (x+y)F^- = NbO_2F_x^{(x-1)-} + NbO_3F_y^{(1+y)-} \qquad (3.3)$$

When the saturation limit of $AlkNbO_3$ is reached, reaction 3.4 will be dominating.

$$Nb_2O_5(s) + xF^- + Alk^+ = NbO_2F_x^{(x-1)-} + AlkNbO_3(s) \qquad (3.4)$$

In the present work, the solubility of Nb_2O_5 in $FLiNaK$ has been studied as a function of temperature. Samples at different temperatures were withdrawn and analyzed for oxygen and niobium. Results are given in figure 3.4. Values used to plot the figure are given in appendix A.

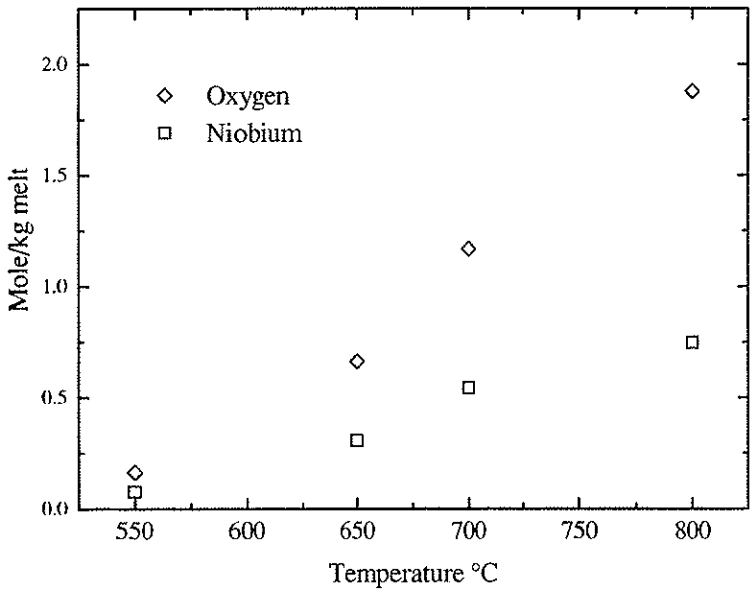

Figure 3.4: O^{2-} and $Nb(V)$ concentrations as a function of temperature in the liquid LiF-NaF-KF eutectic saturated with Nb_2O_5

Except for the sample withdrawn at 800 °C, the n_O/n_{Nb} ratio in the melt varies between 2.11 (at 550 °C) to 2.14 (at 700 °C), while the n_O/n_{Nb} ratio at 800 °C is close to 2.5. This final sample could indicate a complete dissolution of Nb_2O_5 with no formation of a solid $AlkNbO_3$. This is not reasonable due to the low solubility of $AlkNbO_3$ at the other temperatures. The measured melt composition at 800 °C is probably not correct, and it is not included in the calculations of ΔH°_{sol} of Nb_2O_5 in $FLiNaK$. The activity of Nb_2O_5 and $AlkNbO_3$ is set equal to one (present as solids in the melt), and the concentrations of $NbO_2F_x^{(x-1)-}$ and the possible $NbO_3F_x^{(1+x)-}$ complexes are calculated from the n_O/n_{Nb} ratio in the melt. These data are then used to calculate the equilibrium constant K for equation 3.4 at the different temperatures. K is based on molal concentrations and ideality for all dissolved species. By plotting $-(lnK) \times R$ as a function of $1/T$, the molar enthalpy of dissolution ΔH°_{sol} can be found as the slope of the curve as shown by equation 3.5:

$$-R \ln K_{eq} = \frac{1}{T} \Delta H^\circ_{sol} - \Delta S^\circ_{sol} \tag{3.5}$$

By assuming temperature independent ΔH°_{sol} and ΔS°_{sol}, ΔH°_{sol} was found to be $84.2 \pm 1.2\ kJmol^{-1}K^{-1}$. The estimated error is calculated directly from the standard deviation of the regression analysis.

The attempts to measure the solubility of NbO and NbO_2 in $FLiNaK$ failed due to decomposition of the two oxides during the experiment. The dissolution of the oxides proceeded very slowly, and a stable level of oxygen was never reached in the melts. The solidified melts had a dark blue colour, indicating the presence of niobium with oxidation state less than 5. For both compounds a metallic film was found on the crucible after the experiment was finished. A black crystalline solid was also found on the stirring rod. Elemental analysis with a scanning electron microscope (SEM) indicated that the metallic film was pure niobium, while the black solid on the rod seemed to be an alloy of potassium and niobium. Neither oxygen nor carbon was found in any of the deposits. These observations indicate a decomposition of the niobium ions to $Nb(0)$ and $Nb(V)$. It is know from previous work [31] that the reaction:

$$4Nb^{5+} + Nb(0) = 5Nb^{4+} \tag{3.6}$$

is nearly completely shifted to the right for niobium in $FLiNaK$ with low oxide content. Rosenkilde *et al.* [24] studied the electrochemistry of $Nb(IV)$-

O-F complexes in $FLiNaK$ at different n_O/n_{Nb} ratios, and found very low anodic limiting currents in melts with $n_O/n_{Nb} = 1.6$. It was in other words impossible to oxidize the niobium containing specie. They therefore concluded that $Nb(IV)$-O-F complexes decompose to form elementary niobium and $Nb(V)$ dioxo fluoride complexes when the ratio n_O/n_{Nb} exceed 1. This result fits well with the decomposition of NbO_2 observed in the present work, but does not fit with the results of Matthiesen *et al.* [31]. It should, however, be noted that Matthiesen *et al.* studied complexes in the $FLiNaK$-K_2NbF_7-Na_2O system, while the present work concerns the $FLiNaK$-NbO_2 melt. It is not yet clearly understood why the dissolution of NbO_2 in $FLiNaK$ leads to decomposition and formation of elementary niobium. One early explanation was that the presence of carbon in the system allowed formation of NbC (or another niobium carbide), in a reaction like:

$$5Nb^{4+} + C(s) = NbC(s) + 4Nb^{5+} \tag{3.7}$$

This reaction has been reported to take place in $FLiNaK$ between carbon and four-valent niobium by Kuznetzov *et al.* [115]. There was, however, no carbon in the present deposits, and reaction 3.7 can not explain the data. It is likely that the niobium(IV) dioxo fluoride complex is thermodynamically unstable, and that its decomposition reaction is kinetically controlled, leading to the different results reported by Matthiesen *et al.* [31] and Rosenkilde *et al.* [24].

The failure to obtain NbO solubilities can simply be explained by the fact that $Nb(II)$ is not stable in $FLiNaK$. It probably decompose to the more stable $Nb(0)$, $Nb(IV)$ and $Nb(V)$ states.

3.3 Raman spectroscopic analysis of $Nb(V)$ in molten $FLiNaK$ with variations in oxygen content

Table 3.1 lists the main observed frequencies at different ratios and temperatures of all the fluoride mixtures observed in the Raman spectra. Fluorescence background was not detected. A large number of spectra were recorded but only some are presented in order to give an overall picture of the liquid systems. Figures 3.5–3.9 show representative Raman spectra

obtained for a series of $FLiNaK$-K_2NbF_7-NaO_2 liquid mixtures at different n_O/n_{Nb} ratios. From this study the following general observations can be made:

Table 3.1: Observed Raman bands in K_2NbF_7-$FLiNaK$-Na_2O mixtures at different n_O/n_{Nb} ratios and temperatures

n_O/n_{Nb}	T/°C	Main frequencies						
0.04	750		303		630		922	
0.39	610		302	(588)	630		923	
0.80	750		305	585	(631)	881/817	922	
1.16	670	(296)	(368)	585	(633)	878/815	921	
1.48	670	291	(360)			878/815	(922)	
1.76	700	289	(364)			877/815		
2.02	720	292	(368)			880/816		
2.28	700	(277)	(355)			877/(808)		
2.60	740	(277)	(355)			877/(810)		
2.98	840		(304)			(818)/(756)	844	
3.28	750		306			826/(751)	841	(1045)
3.61	760		300			820/(749)	(841)	(1045)
	820		300			820/(749)	(841)	(1045)
	850		300			820/(749)	(841)	(1045)
3.94	780		300			820/(745)	(840)	1045
4.27	750		302			820/745		1045
4.58	740		300			820/745		1045
5.03	780		310			824/745		1052
5.64	780		310			824/748		1051
6.24	780		310			824/749		1052
6.83	860		309			822/748		1050
7.64	830		310			822/747		1049
8.65	860		310			822/746		1049

$0 < n_O/n_{Nb} < 0.5$: In this range the Raman spectra are characterized by four main bands; three polarized at 922, 630 and 585 cm^{-1} and a depolarized at 304 cm^{-1} (figure 3.5). As the oxide content increases the intensity of the 922 and 585 cm^{-1} bands increases, while the band at 630 cm^{-1} decreases.

$0.5 < n_O/n_{Nb} < 1.5$: The intensity of the 630 cm^{-1} band is continuously decreasing, and disappears at ratios above 1.2. The intensity of the bands

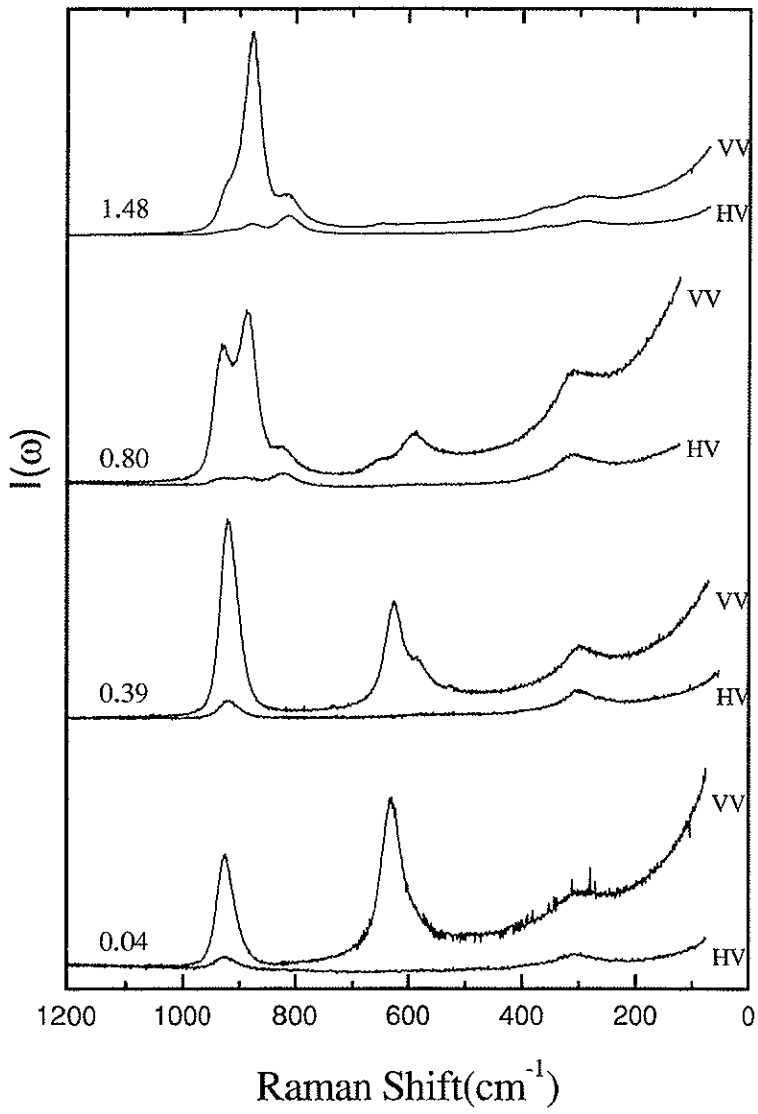

Figure 3.5: Raman spectra of 0.22 mole/kg $Nb(V)$ in $FLiNaK$ melts with n_O/n_{Nb} ratios varying between 0.04 and 1.48

at 922 and 585 cm^{-1} increases up to $n_O/n_{Nb} = 1$ and decreases with further addition of oxide. At $n_O/n_{Nb} \sim 0.8 - 1.2$ four new bands are observed in the spectra; one polarized at 878 and three depolarized at 815, 368 and 290 cm^{-1} (figure 3.5). The intensity of the 878 and 815 cm^{-1} bands increases as the ratio n_O/n_{Nb} increases.

$1.5 < n_O/n_{Nb} < 2.5$: The Raman spectra are dominated by four bands; the

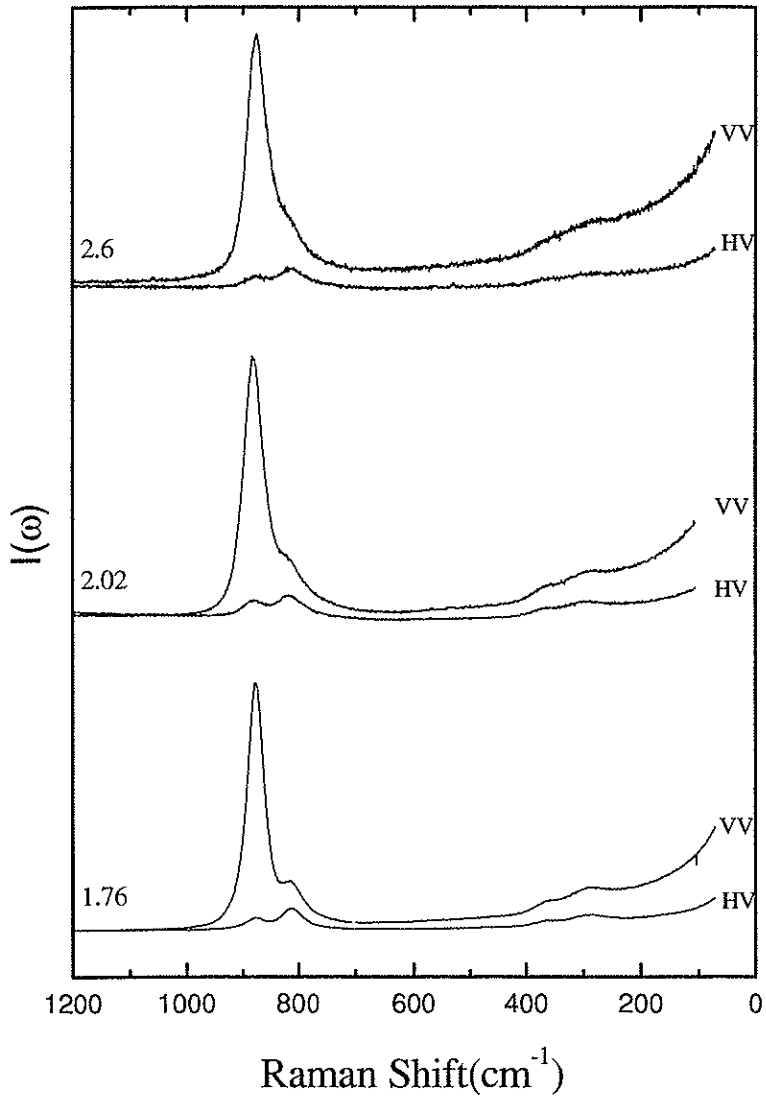

Figure 3.6: Raman spectra of 0.22 mole/kg $Nb(V)$ in $FLiNaK$ melts with n_O/n_{Nb} ratios varying between 1.7 and 2.6

three depolarized at ~290, 370 and ~812 cm^{-1} and one polarized at ~877 cm^{-1} (figure 3.6). Above ratio 2 the overall intensity of the spectra decreases as the ratio n_O/n_{Nb} increases. The last observation fits very well with the solubility measurements, in which both oxide and niobium concentrations were found to decrease in the liquid.

$3 < n_O/n_{Nb} < 8.7$: New bands are observed in the Raman spectra at

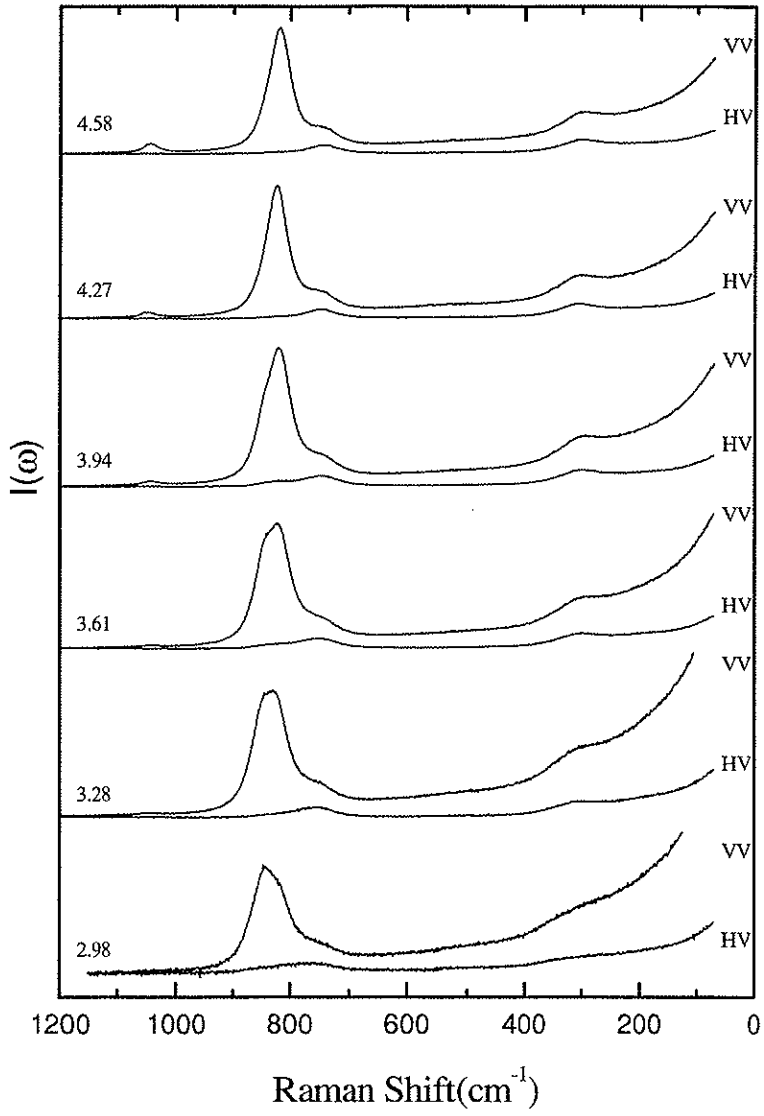

Figure 3.7: Raman spectra of 0.22 mole/kg $Nb(V)$ in $FLiNaK$ melts with n_O/n_{Nb} ratios varying between 2.98 and 4.6

$n_O/n_{Nb} \sim 3$; two polarized at 840 and 820 cm^{-1} and two depolarized at 750 and 300 cm^{-1}. The intensity of the 840 cm^{-1} band decreases as the oxide content increases and disappears at ratios above 4. Furthermore, with increasing temperature and at a given composition, the intensity of the 840 cm^{-1} band increases relative to the corresponding 820 cm^{-1} band (figure 3.9). The three remaining bands have constant frequency for ratios up to

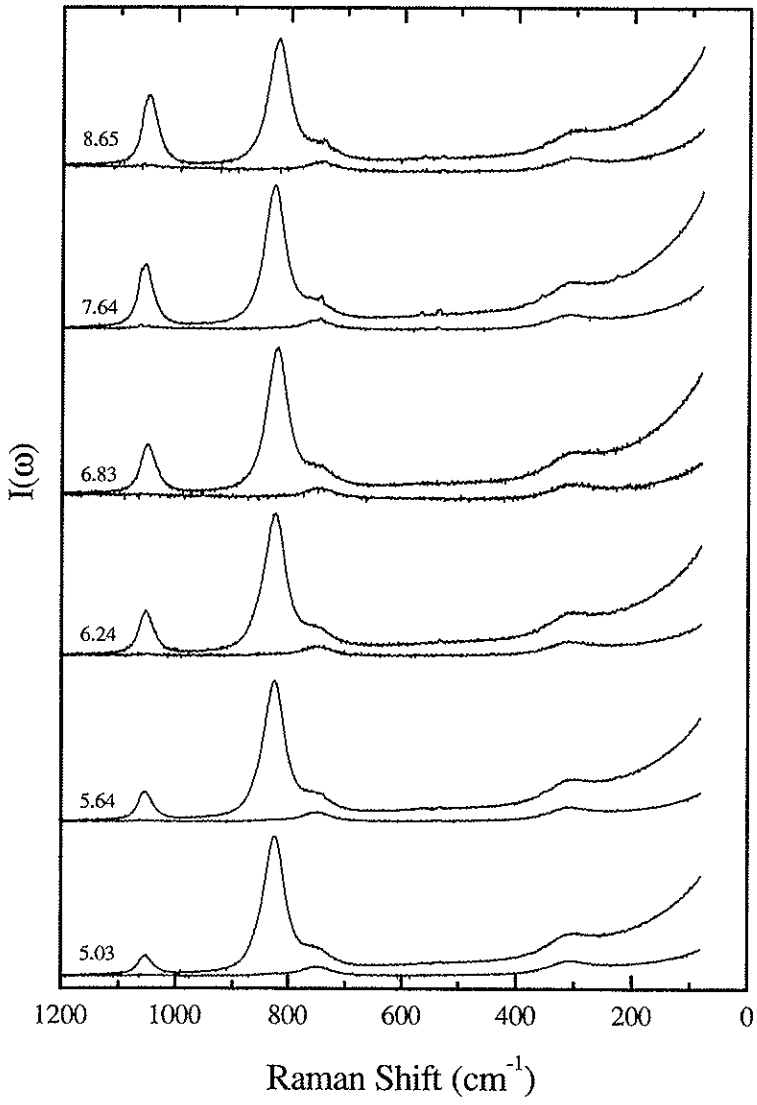

Figure 3.8: Raman spectra of 0.22 mole/kg $Nb(V)$ in $FLiNaK$ melts with n_O/n_{Nb} ratios varying between 2.98 and 4.6

$n_O/n_{Nb} = 8.7$. At ratios close to 4 a new polarized band is observed at $\sim$1045 cm^{-1}, and its intensity increases as n_O/n_{Nb} increases.

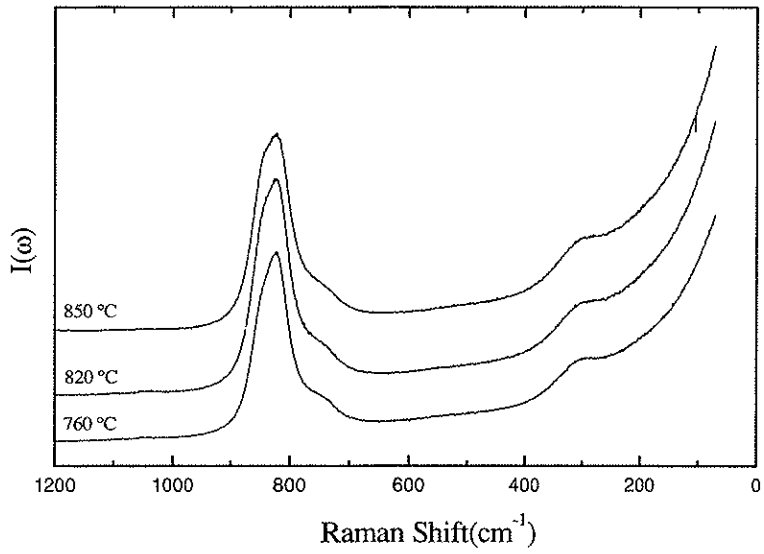

Figure 3.9: Raman spectra of 0.22 mole/kg $Nb(V)$ in $FLiNaK$ melt with $n_O/n_{Nb} = 3.61$ at different temperatures

3.4 Raman and IR spectroscopy of solidified melts in the $FLiNaK$-K_2NbF_7-Na_2O system

Some of the solidified melts were analyzed by means of IR spectroscopy, to better distinguish between possible symmetries of the niobium oxo fluoro complexes. The results are presented in figure 3.10, where the transmittance spectrum of pure $FLiNaK$ is added to show the "background" of the analysis. To be able to compare the spectra from molten salt solutions with solid samples, one has to be certain that the structural properties are preserved upon quenching of the melts. The Raman spectra of some of the solidified samples were therefore recorded to prove this, and the results are shown in figure 3.11.

The sample with a ratio of oxygen to niobium $n_O/n_{Nb} = 0.8$ has a band at around 920 cm^{-1} that is both IR and Raman active, while none of the other bands appear in both the IR and the Raman spectrum. The broad shoulder from 550 to 650 cm^{-1} in the IR analysis is difficult to assign to a specific band. For the sample with $n_O/n_{Nb} = 2.02$ there is at least two vibrations at around 880 cm^{-1} and 600 cm^{-1}, and possibly one at 810 cm^{-1} being

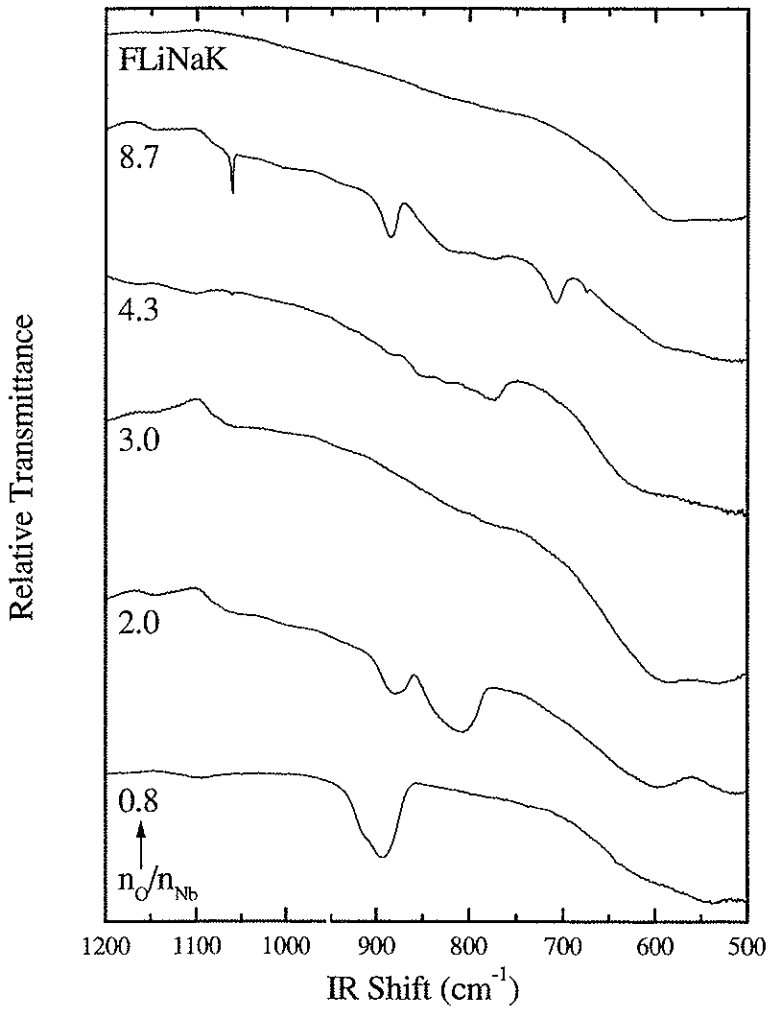

Figure 3.10: FT-IR spectra of solidified samples of 0.22 mole/kg $Nb(V)$ in *FLiNaK* melt with n_O/n_{Nb} ratio varying between 0.8 and 8.7. The spectrum of pure *FLiNaK* is included for comparison

present in both the IR and the Raman spectrum of the solidified melt. At the ratio $n_O/n_{Nb} = 2.98$, the IR signal is very weak, and no bands can be clearly identified in the spectrum under 1000 cm^{-1}. The Raman spectrum, however, shows a weak band at around 830 cm^{-1}, possibly with the same origin as the 840 cm^{-1} band in the molten salt (figure 3.7). For the most oxide rich sample with $n_O/n_{Nb} = 8.7$, a sharp peak at around 1060 cm^{-1} is found to be both Raman and IR active. The remaining bands does either not appear in both the spectra, or are too diffuse or weak to be determined.

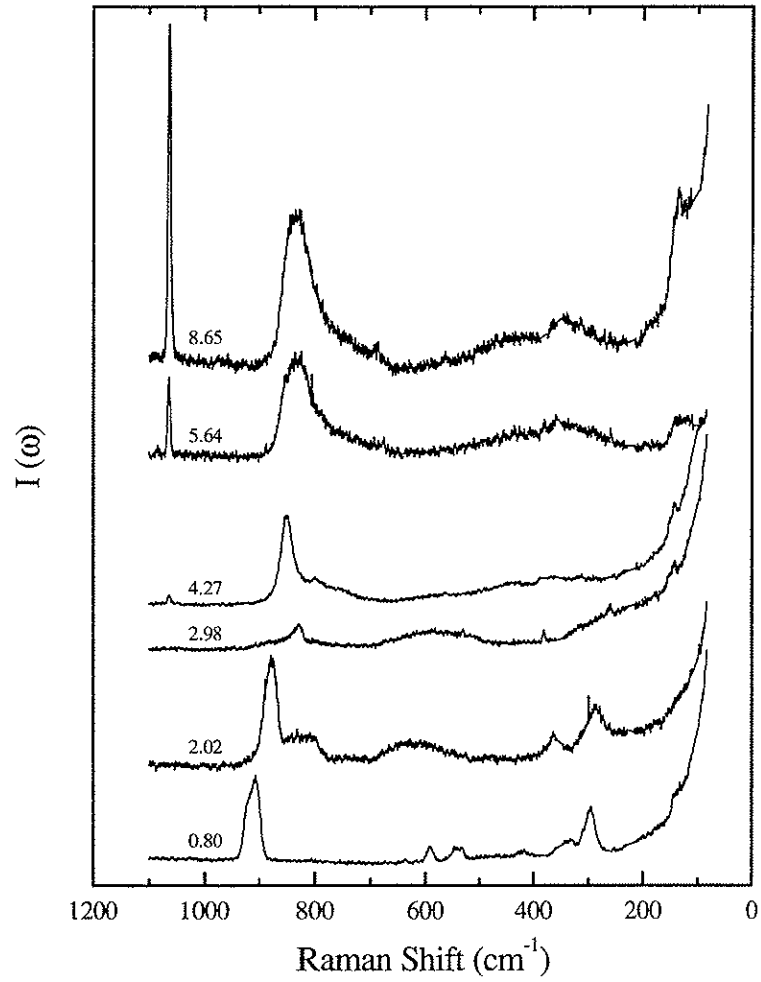

Figure 3.11: Raman spectra of solidified samples of 0.22 mole/kg $Nb(V)$ in $FLiNaK$ melt with n_O/n_{Nb} ratio varying between 0.8 and 8.7.

3.5 The niobium(V) fluoride complex in molten $FLiNaK$

Due to a reaction between niobium fluoride and the fused silica envelope of the experimental cell, samples containing very small amounts of oxide were very difficult to analyze. The spectrum of a "pure" fluoride melt shown in figure 3.5 is therefore of a rather mediocre quality, but it is shown to present the trend when oxide is added to a melt where the niobium fluoride species is dominating. The band at 630 cm^{-1} in figure 3.5 is associated with the

niobium fluoride complex in these melts, while all the other bands are due to some niobium oxo-fluoride complexes that will be described later. This is in agreement with the previous measurements by von Barner *et al.* [18]

To determine the symmetry of the niobium(V) fluoride complex in *FLiNaK*, it is reasonable to compare the measured spectra with bands in related systems. This was done properly by von Barner *et al.* [18], and will only be covered briefly here. Keller [28] recorded the Raman spectra of K_2NbF_7 dissolved in concentrated *HF*, and found bands at 685 cm^{-1} and 280 cm^{-1}. By comparison with the spectra of solid $CsNbF_6$, this band was ascribed to the presence of a NbF_6^- complex in these solutions. The presence of octahedral NbF_6^- units in $CsNbF_6$ was verified by a comparison with other molecules of symmetry O_h, like the isoelectronic MoF_6. Keller further examined solid K_2NbF_7, and found a sharp and strong band at 630 cm^{-1}, and two weaker bands at 388 cm^{-1} and 782 cm^{-1}, and this was later confirmed by von Barner *et al.* [18] who in addition found a band at 275 cm^{-1}. Solid K_2NbF_7 was studied with X-ray diffraction by Hoard [116], and was shown to possess a monoclinic structure with discrete NbF_7^{2-} anions of C_{2v} symmetry. Neutron diffraction studies by Brown and Walker [117] on the same compound indicated that the NbF_7^{2-} ion had a lower symmetry (C_s). The structure of NbF_7^{2-} ion can be described by a four member fluorine square put on top of a 3 member fluorine triangle, with the central niobium atom placed between them.

Since the band at 630 cm^{-1} in figure 3.5 is also found in solid K_2NbF_7, it is reasonable to assume that NbF_7^{2-} is present in the melts with low oxide content, with a similar symmetry as in the solid. von Barner *et al.* [18] who also measured bands at 290 and 371 cm^{-1} made a similar conclusion. It is, however, difficult to decide whether the symmetry of the NbF_7^{2-} anion in molten *FLiNaK* is C_s or C_{2v}; none of the symmetries can be completely ruled out due to the broadness of the 630 cm^{-1} band. The presence of NbF_7^{2-} in molten *FLiNaK* is further supported by Fordyce and Baum [17] who found this anion in the *LiF-KF* binary by using IR-reflection spectroscopy.

3.6 The niobium(V) mono oxo fluoride complex in molten *FLiNaK*

When oxygen is added to the melt the band at 630 cm^{-1} decreases in intensity as n_O/n_{Nb} increases and disappears at $n_O/n_{Nb} = 1.2$ The intensity

of the bands at 304, 585 and 922 cm^{-1} becomes stronger. The spectral features indicate the presence of oxo fluoro complexes in these melts. The 922 cm^{-1} polarized band is in close agreement with recent studies in molten fluorides by von Barner *et al.* [18] as well as with earlier vibrational studies of $K_2NbOF_5 \cdot H_2O$ by Keller [28] and in $A_2NbOF_5(A : Rb, Cs)$ solids by Pausewang *et al.* [118], and is assigned to the $Nb = O$ symmetric stretching vibration. The A_2NbOF_5 solid compounds were found to be isostructural with K_2GeF_6 by Pausewang [119], [120] and by Srivastava and Ackerman [121] containing isolated $NbOF_5^{2-}$ species having an ideal C_{4v} molecular symmetry. In both IR and Raman spectra of these solids, the $Nb - F$ stretching frequency was found at 577 cm^{-1} for the caesium compound and at 586 cm^{-1} for the Rb_2NbOF_5 solid [118]. The polarized band at 585 cm^{-1} (figure 3.5) is very close to these bands and could therefore be associated with the *Nb-F* stretching frequency of $NbOF_5^{2-}$ species in the melts. This is further supported by early Raman studies of tungsten and molybdenum fluoride by Burke *et al.* [122] and tungsten and molybdenum mono oxo fluoride by Alexander *et al.* [123]. The substitution of two fluoride ions by one oxygen in these compounds leads to a red shift of about 40 cm^{-1} of the symmetric stretching vibration of the metal-fluorine band in the metal-mono-oxo-fluoro complexes. A similar trend is also observed in this work by a decrease of 45 cm^{-1} in the *Nb-F* stretching frequency when comparing NbF_7^{2-} with $NbOF_5^{2-}$.

The origin of the depolarized band at 304 cm^{-1} is more difficult to explain. In previous Raman spectroscopic studies of molten fluoride media by von Barner *et al.* [18] as well as of the $K_2NbOF_5 \cdot H_2O$ solid by Keller [28], this band was attributed to the $Nb - F$ vibration due to E and/or B_2 vibrational modes of the C_{4v} $NbOF_5^{2-}$ complex. Eleven fundamental modes are expected for such C_{4v} molecules; eight are both Raman and IR active ($4A_1$, $4E$) while the last three modes ($2B_1$, B_2) are Raman active only. According to the description of the vibrational modes of C_{4v} molecules by Holloway *et al.* [124], these modes are the result of either an NbF_4 scissoring type of vibration ($\nu_7(B_2)$) or an *Nb-O-F* bending mode ($\nu_9(E)$) of the $NbOF_5^{2-}$ species. In the Cs_2NbOF_5 solid a band at around 300 cm^{-1} was present in both the Raman and IR spectra and was assigned to the *Nb-O-F* bending mode of the $NbOF_5^{2-}$ isolated complexes in that crystal (done by Pausewang *et al.* [118]). This in turn indicates that the band at 304 cm^{-1} in figure 3.5 could be associated with the *Nb-O-F* bending mode of the same species.

Since there are no bands observed in the frequency region between 304 and 585 cm^{-1}, a possible fluoride bridging is unlikely. Such bands were observed in the gas-phase Raman spectrum of $NbOCl_3$ by Beattie et al [125] where

double chains of *Nb-Cl-Nb* produce a strong polarized band at 395 cm^{-1}. The same goes for the absence of bands between 600 and 800 cm^{-1}; thus no oxygen bridging takes place in these liquids. This implies that the $NbOF_5^{2-}$ species is a monomer.

The above suggestions are close to that of the study in similar fluoride melts by von Barner *et al.* [18]. The difference in assignment of the low frequency band could be resolved by further Raman measurements on a Cs_2NbOF_5 single crystal at elevated temperatures. Also the spectral changes upon melting of the later compound as well as an IR study in the low frequency region would help in resolving this discrepancy.

3.7 The niobium(V) dioxo fluoride complex in molten *FLiNaK*

From the data in figure 3.5 and 3.6, the appearance of four new bands in the spectra could be associated with the existence of new oxo fluoro complexes as n_O/n_{Nb} exceeds 0.8. The present spectra (figure 3.6 and 3.7) are in good agreement with previously reported data by von Barner *et al.* [18] where the bands were assigned to the existence of $NbO_2F_4^{3-}$ monomers in the liquid. The band at 290 cm^{-1} is ascribed to an asymmetric *Nb-F* vibration in the dioxo fluoro complex, while the symmetric band at 880 cm^{-1} and the asymmetric bands at 815 and 370 cm^{-1} are ascribed to *Nb-O* stretching. The arguments for this assignment is as follows.

As for the niobium mono oxo fluoride complex, the strongest symmetric band is assigned to a *Nb-O* vibration where the high frequency reflects the character of a strong double bond. Replacing a fluorine atom with a second oxide atom in the complex causes a decrease in this frequency, indicating that the bond becomes weaker. This is because the electron density around the central niobium atom increase, and this leads to a reduction in the attractive forces between the central and the surrounding atoms. In this case, the reduction in bond strength causes a decrease in frequency of 42 cm^{-1}. This is a trend that can be observed in other refractory metal oxo halides (like vanadium, niobium, molybdenum and tungsten oxo halides), when a second oxide is introduced into the complex. When a second oxide is introduced into a MOX_4 complex to form $MO_2X_n(n = 3, 4)$ a shift of about 100 cm^{-1} is observed in the symmetrical stretch frequency (comparing for example VOF_4^- and $VO_2F_4^{3-}$ studied by Howell and Moss [126] and Griffith

and Wickins [127] respectively). For species with an octahedral structure, MOX_5, the effect is smaller and the frequency normally drops about 30-50 cm^{-1} when going to MO_2X_4 (in the niobium complexes, the frequency drop is about 45 cm^{-1}). This has been pointed out by von Barner *et al.* [18].

The other high frequency band at 815 cm^{-1} that was observed in the Raman spectra of the melt and the IR spectra of the corresponding solidified melt, is also likely to be due to a niobium-oxygen vibration. As suggested by von Barner *et al.* [18], the band is ascribed to an asymmetric stretch vibration of the NbO_2^+ entity. The band does not appear in the mono oxo complex, and is therefore probably due to a vibration involving two oxide in addition to the central niobium atom. An important feature of the vibration is that it is both IR and Raman active, and the niobium dioxo fluoro complex can therefore not have a center of symmetry.

The band at 290 cm^{-1} is probably due to an asymmetric *Nb-O-F* vibration in the dioxo fluoro complex. In accordance with the reduction in the symmetrical stretching frequency that was observed when a second oxide was introduced, it is also possible that the frequency of the asymmetric *Nb-O-F* vibration is reduced. As the electron density around the central atom is increased, the bonds to the surrounding atoms will weaken, and result in a red shift of the vibrations. In the case of the depolarized *Nb-O-F* band, a reduction of about 15 cm^{-1} is observed.

The origin of the band at 370 cm^{-1} is more uncertain. Because of its low frequency and depolarized nature, it is probably not due to a *Nb-F* symmetric stretch like the bands at 630 and 585 cm^{-1} in the niobium fluoro and oxo fluoro complexes. The same argument further excludes *Nb-O-Nb* bridging vibrations, as these are expected to be polarized and at a higher frequency. The most likely possibilities are an asymmetric *Nb-F* vibration, a low frequent deformation mode of the NbO_2^+ entity or a bridging fluorine mode like Burke *et al.* [122] found in WOF_4. As for the latter, the bridging fluorine vibration was almost invisible in the Raman spectra while it appeared clearly in the IR spectrum of solid WOF_4. Since this bridging frequency is as high as 555 cm^{-1} it is unlikely that the band at 370 cm^{-1} has the same origin. Griffith and Wickins [127] investigated a series of *cis* dioxo fluorides of molybdenum and tungsten and found in general three bands in the Raman spectra; one strong polarized near 950 cm^{-1}, one moderate intense and depolarized near 900 cm^{-1}, and finally one weakly polarized band at 370 cm^{-1} with moderate intensity. All the bands further appeared as strong absorptions in the IR spectra of the solid complexes. The low frequency band was ascribed to the deformation $\delta(MO_2)$, an A_1 mode in the dioxo complex.

Even though none of the three possibilities can be excluded, it is assumed that the latter is the most probable due to the many similarities between the trends and structures in the molybdenum and niobium oxo fluorides.

Having a possible assignment of the bands of the niobium dioxo fluoride does not mean that the molecular formula of the dioxo fluoride is given. There is always an uncertainty of the number of fluorine atoms, but the most probable answer fits with the suggestion that was presented by von Barner *et al.* [18]; $NbO_2F_4^{3-}$. This fits well with the above mentioned trend of replacing one fluorine with one oxide to achieve a red shift in the symmetric *Nb-O* stretch of about 40 cm^{-1}. The measured high frequency bands at 880 and 815 cm^{-1} further fits well with the bands in solid $Rb_2KNbO_2F_4$ that was observed by Pausewang and Rudorf [128]. Such a complex will be an octahedral molecule with a C_{2v} symmetry where the two oxides are in *cis* position, and thus having no center of symmetry.

Any oxygen bridging in the form of a *Nb-O-Nb* band seems unlikely also in this case, due to the absence of visible vibrations in the Raman spectra between 815 and 600 cm^{-1}. This does not go for the possible fluorine bridges since the band intensity from this mode is expected to be weak in Raman spectra. In the IR spectrum (figure 3.10), there might be a weak band at around 520 cm^{-1}, which is not found in the corresponding solid state Raman spectrum. IR spectra of the molten samples would in this case give valuable information regarding possible fluorine bridges, but such measurements were not performed due to the complicated experimental setups needed for such investigations. An IR spectrum of a melt with $n_O/n_{Nb} = 2$ was measured by Andersen *et al.* [29], but the spectrum is very noisy at frequencies below 700 cm^{-1}. It is therefore unfit for determination of possible fluorine bridging bands.

3.8 The niobium(V) trioxo fluoride complex in molten *FLiNaK*

When approaching $n_O/n_{Nb} = 3$, the intensity of the bands at 290, 370, 812 and 880 cm^{-1} decreases. As the minimum in solubility is reached, all these bands are gone, and peaks at around 310, (750), 822 and 840 cm^{-1} appear. From these observations it seems that new structural entities are formed in the melt. In their work, von Barner *et al.* [18] assumed that the melt was saturated with oxide and found four bands at 300, 745, 820, and 1044 cm^{-1}.

The solubility data presented in the present work show that no absolute saturation exists above the ratio $n_O/n_{Nb} = 3$; on the contrary the solubility increases with further addition of Na_2O. The first three bands were by von Barner *et al.* [18], assigned to the possible existence of $NbO_3F_3^{4-}$ species in the melts and the high frequency band at 1044 cm^{-1} to edge sharing NbO_6 octahedra. They also claimed that another hidden band located at the wing of 820 cm^{-1} band could be associated with the presence of corner sharing octahedral NbO_6 units in that molten media. This hidden band is probably the 841 cm^{-1} polarized band which is clearly observed in the present data. The spectra at $n_O/n_{Nb} = 4.28$ looks like the one reported by von Barner *et al.* [18] for their "saturated" melt.

Since the bands at 822(p), 750(dp) and 310(dp) cm^{-1} are present in the liquid spectra at ratios $n_O/n_{Nb} > 4$, the species that could be associated to these bands are probably complexes with 4 oxygens for each niobium. The origin of the polarized band at 840 cm^{-1} must be different since this band no longer is present at $n_O/n_{Nb} = 4.27$, and it seems likely that the band is due to a complex with an oxide to niobium ratio of 3. The polarized character of the band, and the fact that it appears at a high frequency indicates that it is an *Nb-O* symmetric stretch; similar to the bands at 920 and 880 cm^{-1} that was found for complexes at lower n_O/n_{Nb} ratios. For the mono and dioxo fluoro complexes it was observed that a replacement of one fluorine with one oxygen atom caused the symmetric stretch frequency to drop by approximately 40 cm^{-1}. If the same phenomenon is valid also for further substitution of fluoride by oxide, a frequency of about 840 cm^{-1} would be expected for the complex $NbO_3F_3^{4-}$.

Griffith *et al.* [127] measured IR spectra of the related molybdenum oxo fluoro complexes, and found a decrease in the symmetrical $\nu^s(MoO_2)$ frequency of 49 cm^{-1} when going from $K_2[MoO_2F_4], H_2O$ to $K_3[MoO_3F_3]$. A similar trend was observed in the Raman spectra, but there with different cations in the two solids compared. The observations made by Griffith *et al.* [127] fit well with the shift that was found in the present work, and it is therefore likely that the band at 840 cm^{-1} is due to a $NbO_3F_x^{(1+x)-}$ complex. As for the number of fluorine that is attached to the complex, a value of 3 seems most likely due to the previously mentioned trend; substitution of one fluorine by one oxygen causes a decrease in the symmetric stretch frequency of about 40 cm^{-1}. It should however be stated that this is just an assumption that seems more likely than other possibilities, and since no bands are associated to *Nb-F* vibrations in this complex, the value of x will be uncertain.

The complex $NbO_3F_x^{(1+x)-}$ will not contain a center of symmetry, no matter what the value of x is, and it should therefore be possible to find the vibration at 840 cm^{-1} in both the IR and the Raman spectrum. As already mentioned, the concentrations of niobium and oxygen were very low in the sample that was analyzed by means of IR, and the spectrum shows more or less only the characteristics of solidified *FLiNaK*. If x is set to 3, there are two possible configurations for the complex : The $trans(1,2,6)$- and the $cis(1,2,3)$-trioxo complex. It is not possible to distinguish between these from the spectroscopic results, but according to Griffth *et al.* [127] the *cis* configuration is preferred over the trans in d^0-complexes; complexes where the central atom lacks d-electrons. This is the case for $Nb(V)$, and it is therefore assumed that the band at 840 cm^{-1} is due to the complex $cis(1,2,3) - NbO_3F_3$ with a C_{3v} symmetry. Any oxygen or fluoride bridging is impossible to determine due to the lack of bands that can be attributed to the complex.

It should also be mentioned that the solid precipitate that is formed at $n_O/n_{Nb} = 3$, has a typical perovskite structure, build up by corner sharing NbO_6 octahedra with the alkali ion placed in the cavity between 8 octahedra (structure of $KNbO_3$ studied by Fontana *et al.* [129]). It is uncertain which of the three possible alkali niobium oxides that is formed, but they all possess a similar structure. This is a very stable structure, and any dissolved species can not possess a similar structure without having several terminal oxygen (this would require a ratio n_O/n_{Nb} above 3). The actual solubility of the oxide in *FLiNaK* is instead due to the above mentioned specie that seems to be a lot less stable than the perovskite solid.

3.9 Niobium(V) oxo fluoride complexes with a ratio of n_O/n_{Nb} above 3 in molten *FLiNaK*

As already mentioned, the bands at 820(p), 750(dp) and 310(dp) cm^{-1} are ascribed to a complex with $n_O/n_{Nb} > 3$. As the solid oxide starts to dissolve, with increasing n_O/n_{Nb} ratio above 3, all these bands become more intense due to the increasing concentration of species in the melt. In addition, a new band appears at around 1045 cm^{-1}. The polarized band at 820 cm^{-1} and the depolarized band at 750 cm^{-1} are probably of a similar origin as the two bands at 880 and 815 cm^{-1} that were observed for the dioxo fluoro complex.

The bands appear as a pair, and are due to symmetric and asymmetric Nb-O vibrations, in this case probably in the NbO_4^{3-} entity. The intensity of one band relative to the other remains constant regardless of the value of n_O/n_{Nb} and the temperature of the melt. The bands furthermore seem to be present in both the IR and the Raman spectra of the solidified melts, which excludes a center of symmetry in the species they originate from.

It is tempting to ascribe the band at 310 cm^{-1} to a Nb-O-F vibration in the new complex, since this band appears at a similar frequency, with similar characteristics as the band at 305 cm^{-1}. This band was connected to such a vibration in the niobium mono oxofluoride complex. In that case it was possible to compare the vibration with known assignments in solid compounds like $A_2NbOF_5 (A : Cs, Rb)$. For the 310 cm^{-1} band this becomes more difficult. Spectral data are not available in the litterature from solid niobium oxofluoro compounds with a sufficiently high oxygen to niobium ratio, and that makes the origin of the band at 310 cm^{-1} uncertain.

Again, any possible oxygen bridging in the form of an Nb-O-Nb band seems unlikely due to the absence of bands in the Raman spectra between 750 and 600 cm^{-1}. As already stated, bands due to fluorine bridging modes are expected at lower frequencies. By comparing the IR spectra of solidified $FLiNaK$ with the solidified samples at ratios of $n_O/n_{Nb} = 4.3$ and 8.7, there seems to be a broad band at around 500 cm^{-1}. This could possibly indicate that these very oxygen rich species contain bridging fluoride, but in the absence of IR spectra of the molten samples no definite conclusion can be made.

Rosenkilde *et al.* [24] investigated these very oxide rich melts of $Nb(V)$ in molten $FLiNaK$ by means of electrochemistry, and found evidence for the existence of at least two different species in the melts for $n_O/n_{Nb} > 4$. The first species appears at $n_O/n_{Nb} > 3.8$, while the other species appears at slightly higher ratios. This fits well with the present results, where the bands at 820, 750 and 310 cm^{-1} are ascribed to the species giving a reduction wave observed at $n_O/n_{Nb} > 3.8$, and the very high frequency band at around 1045 cm^{-1} to the second specie. The fact that the intensity of the high frequency band increase relative to the others as the oxide content is increased, does indeed indicate the presence of two species. It further implies that this latter specie is a more oxide rich complex than the first. The symmetrical high frequency band is ascribed to an $Nb = O$ vibration.

It has been shown earlier in this chapter that NbF_7^{2-}, $NbOF_5^{2-}$, $NbO_2F_4^{3-}$ and possibly $NbO_3F_3^{4-}$ are present in the melts for $0 < n_O/n_{Nb} < 4$. When

new bands are found at even higher ratios, it seems likely that new species with an even higher ratio of oxygen to niobium are stable in such melts. Such species have not been found in the litterature in any solvent. An attempt will therefore be made to determine the stoichiometry of these complexes. Considering the first specie, $NbO_4F_x^{(3+x)-}$. This ion is obviously the reason for the increased solubility in the melts as n_O/n_{Nb} increases above 3. If the number of x is 0, one obtains an NbO_4^{3-} complex very similar to the other MO_4^{n-} complexes that are formed by most other elements in group III_A, IV_A, V_A and VI_A. These tetrahedral complexes are stable in both solids and different solvents, except that they are extremely rare for the case of niobium and tantalum. In fact, $MNbO_4$ and $MTaO_4$ $(M = Sc, Y, La, Ln)$ are the only examples for the two latter elements. In all the different polymorphs of solid Nb_2O_5, the tetrahedral configuration is in clear minority versus the dominating octahedral groups of distorted NbO_6 units (as shown by Mc Connel *et al.* [130]). It is therefore highly unlikely that the very rare NbO_4^{3-} tetrahedron is present in molten $FLiNaK$, and the value of x is thus more likely to be higher than 0.

Adopting the above arguments, it now remains to determine how many fluorine atoms are present in the $NbO_4F_x^{(3+x)-}$ species. It might be the dimer $Nb_2O_8F_2^{8-}$ with two bridging fluorine bands since the IR measurements could not exclude such bridges. The complex would then possess a D_{2h} symmetry, much similar to the dimeric Nb_2Cl_{10} that was investigated by Edwards and Ward [131]. This is, however, just a speculation. There might be several possible answers to what the structure of $NbO_4F_x^{(x-3)-}$ looks like. All the other complexes that have been observed at lower n_O/n_{Nb} ratios seem to be monomeric. The new species is therefore also assumed to be a monomer since there is no clear evidence for bridging bands. The most probable solution then seems to be an $NbO_4F_2^{5-}$ complex with the two fluorine in *cis* position to avoid a center of symmetry. The complex will then have a C_{2v} symmetry, and the band at 310 cm^{-1} is probably due to a bending vibration of the Nb-O-F entity. It further has a remarkably high charge; a good examples of the extreme complexing abilities of the heavy metals like niobium, tantalum, tungsten and molybdenum. Going from $NbO_3F_3^{4-}$ to $NbO_4F_2^{5-}$ a reduction in the symmetrical $Nb = O$ stretch of about 20 cm^{-1} is observed, which is only half of what has been observed earlier in substitution of one fluorine with one oxygen. This might be explained by the fact that the electron density around the central niobium atom is already rather large, and that the substitution now has a smaller effect.

The temperature dependence of the melt with $n_O/n_{Nb} = 3.6$ (figure 3.9), showed that the band at 840 cm^{-1} became stronger relative to the band at

around 822 cm^{-1} at higher temperatures. The equilibrium:

$$NbO_3F_3^{4-} + O^{2-} = NbO_4F_2^{5-} + F^- \tag{3.8}$$

therefore seems to be established. Figure 3.9 indicates that the equilibrium shifts towards the left side of equation 3.8 when the temperature increase, and the standard enthalpy ΔH° must be negative for the reaction. The sign of the standard entropy can not be determined from these data, but the value is probably not large since there is no change in the number of species. The negative enthalpy is therefore the driving force of the reaction, and causes any free oxide to react with the niobium trioxo complex until the concentration of this is negligible. This seems to occur at $n_O/n_{Nb} \sim 4$.

The very high frequency band at around 1045 cm^{-1} has already been assigned to an even more oxide rich specie in the melts, but the structure of this complex is yet to be determined. It is believed to be an NbO_6 polyhedron, but not necessarily with a O_h symmetry. The high frequency indicates the presence of a strong Nb=O band, and the other Nb-O bands must be weaker in order to stabilize the unit. The polyhedron is thus a distorted octahedron, and probably consists of one or two terminal oxygen while the remaining oxygen forms bridges to similar units. The presence of this high frequent band in the IR and Raman spectra of the solidified melts supports the existence of non-centro-symmetric species in the melt. Balachandran and Eror [132] studied spectra of the high temperature solid Nb_2O_5 and found that the vibration corresponding to edge sharing NbO_6 units appeared at 992 cm^{-1}. It is probably a related structure that causes the band at around 1045 cm^{-1}. It should be emphasized that the distorted octahedra is not an ion like NbO_6^{7-}, but rather an oxide bridged network of loosely bonded NbO or NbO_2 units, with an overall ratio of oxide to niobium of 6. This network like structure of NbO_6 is consistent with recent Raman spectroscopic studies in the Nb_2O_5-$K_2S_2O_7$ system by Boghosian *et al.* [133].

Rosenkilde *et al.* [24] analyzed pure $FLiNaK$ with additions of Na_2O by means of electrochemistry, and found that the oxidation/reduction peaks for the oxide ion appeared at a similar potential as the peaks in melts with $n_O/n_{Nb} \sim 6$. This further indicates that the bridging oxygen is not bonded to the niobium like the Nb-O bands that were found in complexes for melts with a lower ratio of oxide to niobium. Neither is it a bridging oxygen like those Beattie *et al.* [125] found in $NbOCl_3$ since no bands were found in the range 600 to 800 cm^{-1}. The oxygen atoms must therefore be loosely bonded.

3.10 Raman spectroscopic analysis of Nb_2O_5 dissolved in $FLiNaK$

Nb_2O_5 dissolved in $FLiNaK$ gave spectra of the same shape and showed the same peaks and relative intensities as the samples with a n_O/n_{Nb} ratio between 2 and 3 (see figure 3.6). This is in agreement with the solubility data, indicating formation of a $NbO_2F_x^{(x-1)-}$ complex together with a solid compound, $AlkNbO_3$.

3.11 Conclusions

Raman spectroscopy and oxide and Nb solubility measurements of Na_2O-$FLiNaK$-K_2NbF_7 melts show that at least four different niobium oxo fluoro species are formed. The solubility data are indicating the formation of different $NbO_yF_x^{(2y+x-5)-}$ species where y and x take values depending on the n_O/n_{Nb} ratio in the melt. From the Raman measurements, the existence of NbF_7^{2-} (C_s), $NbOF_5^{2-}$ (C_{4v}) and $NbO_2F_4^{3-}$ (C_{2v}) at n_O/n_{Nb} ratios up to 2 are well established. At $n_O/n_{Nb} = 3$ the solubility data indicate the precipitation of a solid compound such as $AlkNbO_3$. At this ratio the spectral features implies that formation of trio-oxo fluoro complexes in the melt is possible. At $n_O/n_{Nb} > 3$ the solubility data are consistent with a dissolution of the $AlkNbO_3$ solid, and formation of a $NbO_4F_x^{(x+3)-}$ species. At $n_O/n_{Nb} > 4$ an oxygen rich solid seems to precipitate. The Raman spectra indicate the existence of $NbO_4F_2^{5-}$ species as well as $(NbO_6)_n$ network structures in these melts.

Chapter 4

Tantalum

4.1 Solubility of $Ta(V)$ and O^{2-} in $FLiNaK$ with variations in oxygen content

The influence of Na_2O concentration on the oxide and $Ta(V)$ solubilities, and $Ta(V)$-F-O complexation in $FLiNaK$ melts containing a given amount of K_2TaF_7, were studied as a function of the n_O/n_{Ta} molar ratio at 700 °C. The tantalum and oxide concentrations in the melt are plotted versus n_O/n_{Ta} in figure 4.1, where the content of oxygen and tantalum in both the melt and in the possible solid Ta-O-containing compounds are included in the n_O/n_{Ta} ratio. The dotted line indicates the total concentration of oxide in the system; the theoretical value of oxygen that is expected if all the added Na_2O goes into solution. Values used to plot the figure are given in appendix B.

The measured oxide content in samples with $n_O/n_{Ta} > 4$ has a rather high standard deviation, and this is probably due to inhomogeneity of the quenched melts. The mean value of the analyzed data will, however, be fairly accurate, since most of the sample was used for analysis or the samples for analysis were taken from representative parts of the quenched melt in order to compensate for the gradient in concentration through the salt. It is possible to give an evaluation of the stoichiometry of the precipitating species as well as the complexes formed from the data below. The n_O/n_{Ta} data are based on added amounts of Na_2O and K_2TaF_7 (0.0956 mole/kg melt). Corrections are made for the measured tantalum and oxygen content in the salt due to samples withdrawn for analysis.

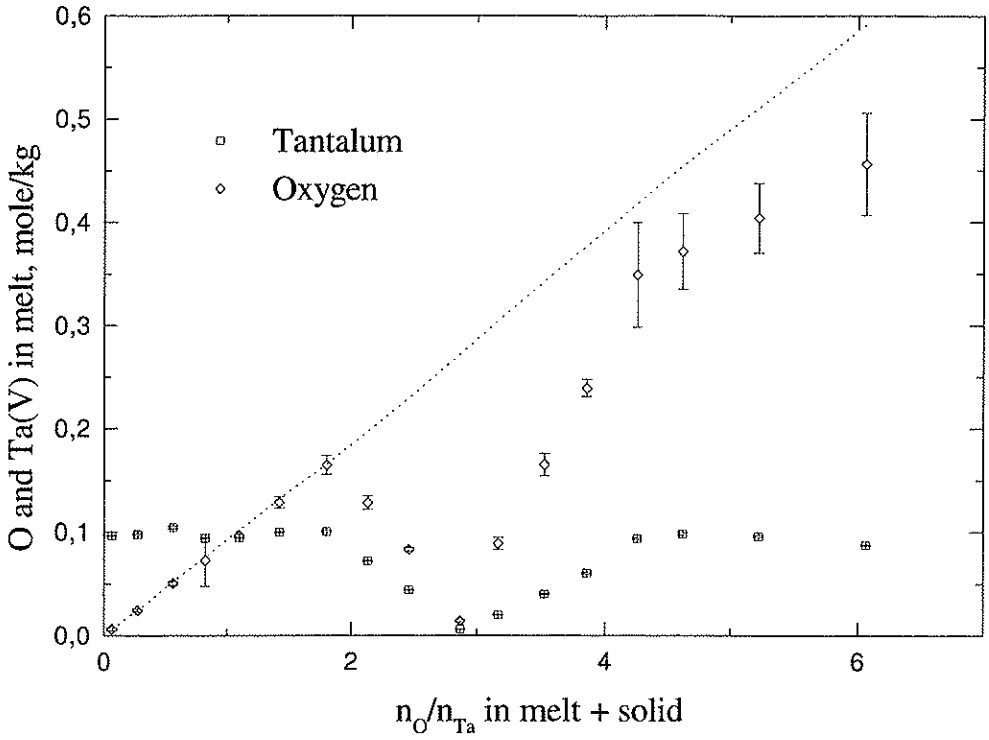

Figure 4.1: Oxide Na_2O and $Ta(V)$ concentrations in the liquid LiF-NaF-KF eutectic at 700 °C versus the molar ratio, n_O/n_{Ta}, in the melt and in the solid phases. $0 < n_O/n_{Ta} < 6.3$.

$\mathbf{0 < n_O/n_{Ta} < 2}$: The tantalum concentration in the melt is constant, and the oxygen concentration increases linearly as the ratio n_O/n_{Ta} increases. All the added oxide goes into solution, and no precipitation of solid compounds occur. The results are consistent with reaction 4.1

$$yO^{2-} + zTaF_7^{2-} = Ta_zO_yF_x^{(2y+x-5z)-} + (7z - x)F^- \qquad (4.1)$$

The formation of possible species of the type $TaOF_5^{2-}$ and $TaO_2F_4^{3-}$ as suggested by von Barner *et al.* [37] and Robert *et al.* [39] may therefore be reasonable. It should be noted that the oxygen concentration is, within the experimental errors, equal to the added amount of oxide, and not higher as was the case for the experiment described in chapter 3.1. The current solubility experiment with tantalum was performed with a high purity Na_2O (98.5%), which did not seem to contain much Na_2O_2.

Figure 4.1 does unfortunately not contain measurements at a ratio of oxygen to tantalum equal two, and it is difficult to say if the concentrations of oxygen and tantalum follows the mentioned trends all the way up to $n_O/n_{Ta} = 2$. The figure indicates that a decrease of both concentrations occur at a somewhat lower ratio $n_O/n_{Ta} \sim 1.8$. This could mean that precipitation of a solid compound starts before a total conversion of tantalum mono oxide to tantalum dioxo complexes has occured. In the related niobium system (see section 3.1), such precipitation started at around $n_O/n_{Nb} \sim 2.2$.

$\mathbf{2 < n_O/n_{Ta} < 3}$: As shown in figure 4.1, both the tantalum and the oxygen content of the melt decreases linearly as n_O/n_{Ta} increases. A minimum in solubility is reached at $n_O/n_{Ta} = 3$. Precipitation of a solid compound $AlkTaO_3$ seems to occur as indicated by reaction 4.2:

$$TaO_2F_4^{2-} + O^{2-} + Alk^+ = AlkTaO_3(s) + 4F^- \tag{4.2}$$

According to reaction 4.2, the slopes of the lines for the decreasing concentrations of $Ta(V)$ and O^{2-} should be close to -1 and -2, respectively. The lines in figure 4.1 show slopes of about -0.9 and -1.8. This small deviation from the theoretical values might be due to the presence of Na_2O_2 as was discussed for niobium in section 3.1, or to difficulties in measuring the slope correctly. As can be seen from figure 4.1, the solubility of oxygen and tantalum is very low at $n_O/n_{Ta} \sim 3$. It is therefore possible that precipitation of $AlkTaO_3$ according to reaction 4.2 starts before $n_O/n_{Ta} = 2$; before all the tantalum containing species are converted to a tantalum dioxo fluoride complex. To verify this, it is necessary to know the equilibrium constant of not only reaction 4.2, but also all the equilibrium constants of possible reactions in equation 4.1. This is not possible to obtain based on these data only.

The minimum in solubility was measured at $n_O/n_{Ta} = 2.9$ where the concentrations of oxygen and tantalum were 0.014 mole/kg melt and 0.0062 mole/kg melt respectively. This means that the solubility of the solid compound $AlkTaO_3$ is equal to or lower than 0.0062 mole/kg at $n_O/n_{Ta} = 3$ and 700 °C. Compared with the measured solubility of $AlkNbO_3$ of 0.045 mole/kg at 700 °C(see section 3.1), it is apparent that $AlkTaO_3$ is a lot less soluble in molten $FLiNaK$ at this temperature than the Nb-compound. No previous measurements of solubility of $AlkTaO_3$ in molten alkali fluoride have been found in the literature.

$\mathbf{3 < n_O/n_{Ta} < 6.5}$: Dissolution of the solid $AlkTaO_3$ compound occurs, and the concentration of tantalum and oxygen increases linearly up to a value of $n_O/n_{Ta} > 4$. The slopes of the increasing concentrations are 0.66 and 2.52 for tantalum and oxygen respectively. This indicate that about two thirds of the solid $AlkTaO_3$ dissolves, or that another solid tantalum oxide is formed upon addition of Na_2O. The slopes changes at a value of n_O/n_{Ta} slightly above four, and the formation of a tantalum tetra oxofluoride as indicated in reaction 4.3 is likely.

$$AlkTaO_3 + O^{2-} + xF^- = TaO_4F_x^{(3+x)-} + Alk^+ \tag{4.3}$$

The oxygen content continues to increase linearly when n_O/n_{Ta} increases further, but with a different slope than below $n_O/n_{Ta} = 4$. The increase is less than what would have been expected if all the added oxide dissolved completely. The tantalum concentration is slightly decreasing indicating a possible formation of another solid compound. Something similar was proposed for the related niobium system in section 3.1. It is impossible, however, to identify such a solid from the present data.

4.2 Solubility of Ta_2O_5 in $FLiNaK$

By adding small amounts of Ta_2O_5 to molten $FLiNaK$ at 700 °C, the dissolution process of the oxide was studied. The concentrations of oxygen and tantalum were measured as a function of the total amounts of oxide in the system. Data are given in figure 4.2. The initial oxide concentration in the purified melt was 0.0071 mole/kg melt. Values used to plot the figure are given in appendix B.

From figure 4.2 it can be seen that for small additions of Ta_2O_5, the oxygen and the tantalum concentrations increase linearly with the added amounts. The concentrations of O^{2-} and $Ta(V)$ are, however, lower than that represented by the added amounts of Ta_2O_5. The dissolution process is clearly accompanied by precipitation of a solid. Matthiesen *et al.* [31] performed a similar experiment with Nb_2O_5 in $FLiNaK$ at 700 °C, and found that precipitation of $AlkNbO_3(s)$ occured. By adding 1 mole of $Nb_2O_5(s)$, only 1 mole (50%) niobium and 2 mole (40%) oxygen dissolved. From the present results it can be seen that the precipitation is even larger. Addition of 1 mole $Ta_2O_5(s)$ increase the tantalum and oxygen content by approximately

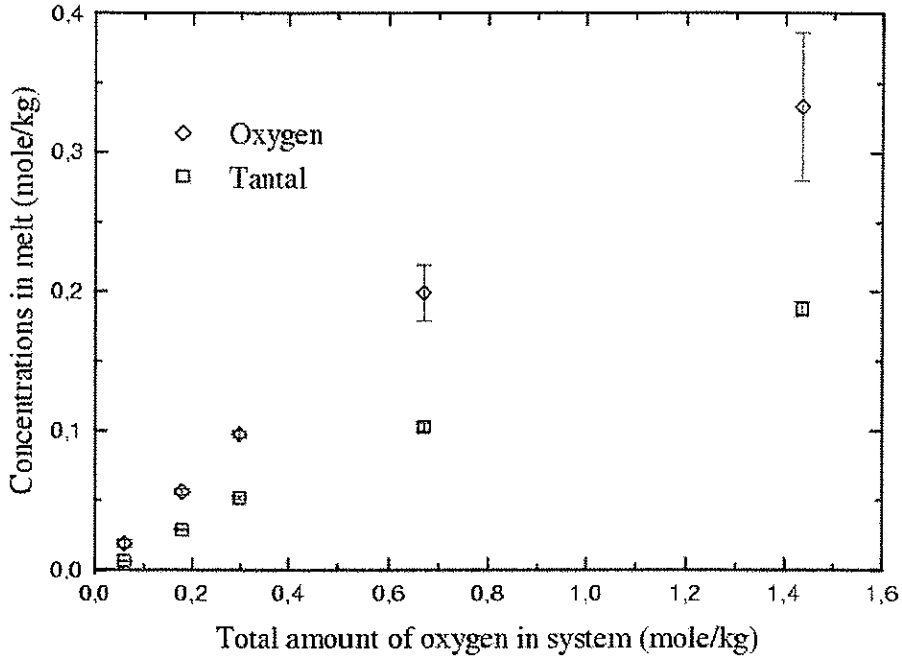

Figure 4.2: Oxide and $Ta(V)$ concentrations in the liquid LiF-NaF-KF eutectic at 700 °C versus added amounts of Ta_2O_5

0.96±0.03 (48±3%) and 1.66±0.11 mole (33±7%) respectively. 1.04±0.03 mole tantalum and 3.34±0.11 mole oxygen precipitate. The first three measurements in figure 4.2 were used to calculate these numbers. When subtracting the oxygen concentrations with the initial oxide content of 0.0071 mole/kg, the n_O/n_{Ta} ratio in the melt is between 1.7 and 1.8. This result can not simply be explained by formation of a tantalum dioxo fluoro complex and precipitation of $AlkTaO_3$ since this will give $n_O/n_{Ta} = 2$ in the melt. The calculated numbers rather indicate precipitation of a solid with an oxide to tantalum ratio higher than 3, and a co-formation of $TaOF_x^{(x-3)-}$ and $TaO_2F_x^{(1-x)-}$ complexes in the melt. This, however, does not fit with the solubility data presented in figure 4.1. The figure shows a clear minimum in solubility at $n_O/n_{Ta} \sim 3$, and suggests that the precipitating solid is $AlkTaO_3$. The discrepancy is probably due small errors in the concentrations of O^{2-} and $Ta(V)$ obtained in the solubility experiment with Ta_2O_5. The oxygen and tantalum contents are very low, and probably unfit for

a detailed determination of the $AlkTaO_3$ stoichiometry. When looking at the molar numbers 1.04±0.03 mole Ta and 3.34±0.11 mole O giving the precipitated amounts, this is rather close to precipitation of $AlkTaO_3$.

As briefly mentioned, the oxygen to tantalum ratio in the melt is clearly below 2 when Ta_2O_5 dissolves in $FLiNaK$. This fits well with the solubility experiment presented in figure 4.1. For the sample at $n_O/n_{Ta} = 2.46$ (based on total amounts in the system), it is found that the oxygen to tantalum ratio in the melt is 1.9. The results indicate a co-formation of $TaOF_x^{(x-3)-}$ and $TaO_2F_x^{(1-x)-}$ complexes. The data in figure 4.1 also indicate precipitation of $AlkTaO_3$ before $n_O/n_{Ta} = 2$. As Ta_2O_5 was further added to the melt, no clear evidence for absolute saturation was observed. Both the oxide and the tantalum concentration increase, however, less than for previous additions. Both the oxygen and the tantalum concentration was measured as a function of temperature when the total amount of Ta_2O_5 added was 1.44 mole/kg. Both concentrations increased with increasing temperature. Data are, however, not presented since this work was not completed.

4.3 Raman spectroscopic analysis of $Ta(V)$ in $FLiNaK$ with variations in oxygen content

Table 4.1 lists the main observed frequencies from the Raman spectra of $Ta(V)$ in $FLiNaK$-Na_2O mixtures at different temperatures and compositions. No fluorescence background (impurities) were detected in the measured spectra. A large number of spectra were recorded and only some are presented to give an overall structural picture of the liquid systems. Figure 4.3–4.6 show representative Raman spectra obtained for a series of $FLiNaK$-K_2TaF_7 liquid mixtures at different n_O/n_{Ta} ratios. These are spectra of the melt samples presented in figure 4.1. In addition to these, a few samples with higher tantalum concentration were prepared, and their Raman spectra are shown in figure 4.7. The main observed frequencies in figure 4.7 are presented in table 4.2. From this study the following general observations can be made:

Table 4.1: Observed Raman bands in melts with an initial concentration of tantalum 0.0956 mole/kg melt at different n_O/n_{Ta} ratios and temperatures. Numbers in parenthesis indicate shoulder bands and frequencies with an estimated error of 5 cm^{-1}, while other numbers have an estimated error of 1 cm^{-1}

n_O/n_{Ta}	T/°C	Main frequencies								
0.06	750		314		(600)	640			906	
0.26	750		314		600	640			906	
0.56	750		314		600	640		(870)	906	
0.82	750	306	(360)	585	600	(640)	790	870	906	
1.10	750	306	(360)	(550)	600	(640)	792	870	(906)	
1.43	750	306	360		(600)		790	870	(906)	(980)
1.80	850	306	360				790	870		
2.46	840	(306)	(360)				790	870		
2.87	940						865			980
3.17	930						850			
3.53	940						845			
3.86	940		(300)				843			
4.26	920		(300)			(740)	840			
4.63	940		(320)			740	840		1050	
5.22	850		320			740	840		1050	
6.06	900		320			740	840		1050	

Table 4.2: Observed Raman bands in melts with an initial concentration of tantalum 0.197 mole/kg melt at different n_O/n_{Ta} ratios and temperatures. Numbers in parenthesis indicate shoulder bands and frequencies with an estimated error of 5 cm^{-1}, while other numbers have an estimated error of 1 cm^{-1}

n_O/n_{Ta}	T/°C	Main frequencies						
0.04	750	306	(380)			(600)	640	904
0.16	750	314				(600)	640	904
0.26	750	314		(530)		600	640	904
0.46	750	314		(530)	(560)	600	640	904
0.69	650	314		(530)	(560)	600	640	904

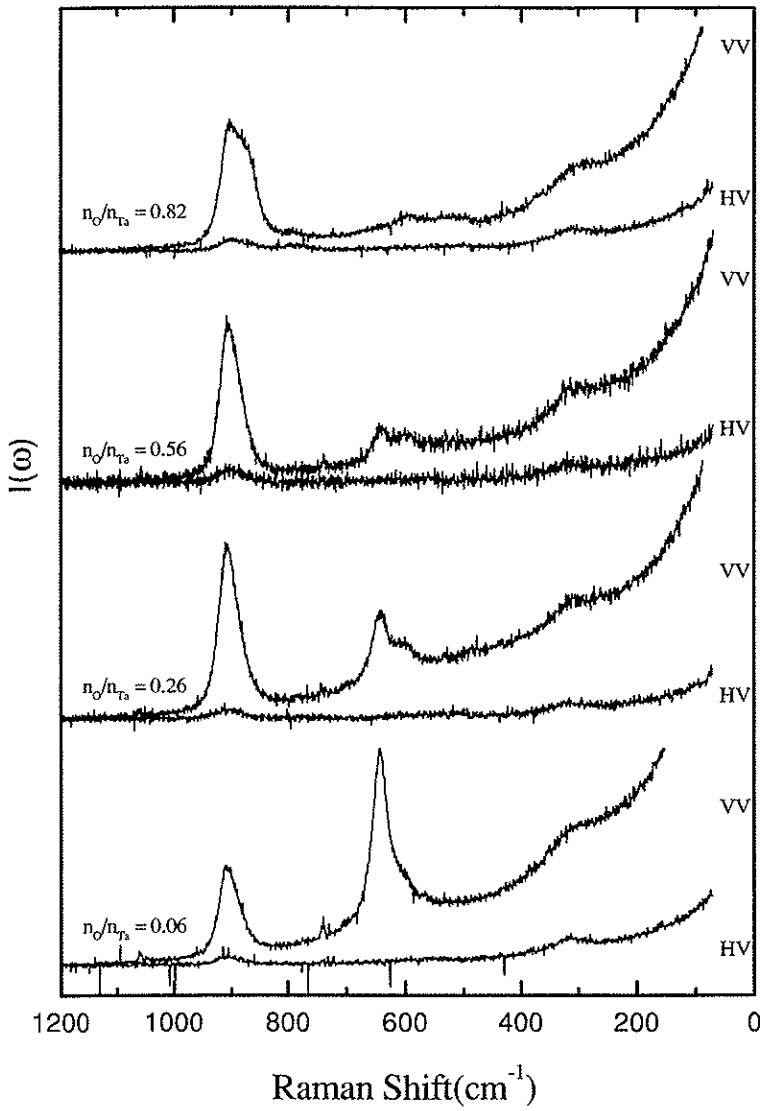

Figure 4.3: Raman spectra of 0.0956 mole/kg $Ta(V)$ in $FLiNaK$ melts with n_O/n_{Ta} ratios varying between 0.06 and 0.82

$0 < n_O/n_{Ta} < 3$: At n_O/n_{Ta} ratios close to one, the spectra are dominated by four main bands; three polarized at 906, 640, 600 cm^{-1} and one broad depolarized at 314 cm^{-1}. In addition to these, two depolarized bands at 306 and 380 cm^{-1} are probably present in the least oxide rich melts. As the oxide concentration increases, the intensity of the band at 640 cm^{-1} decreases, and almost vanishes at $n_O/n_{Ta} > 0.56$. At the same time, the depolarized band at 314 cm^{-1} is replaced by two new depolarized bands at

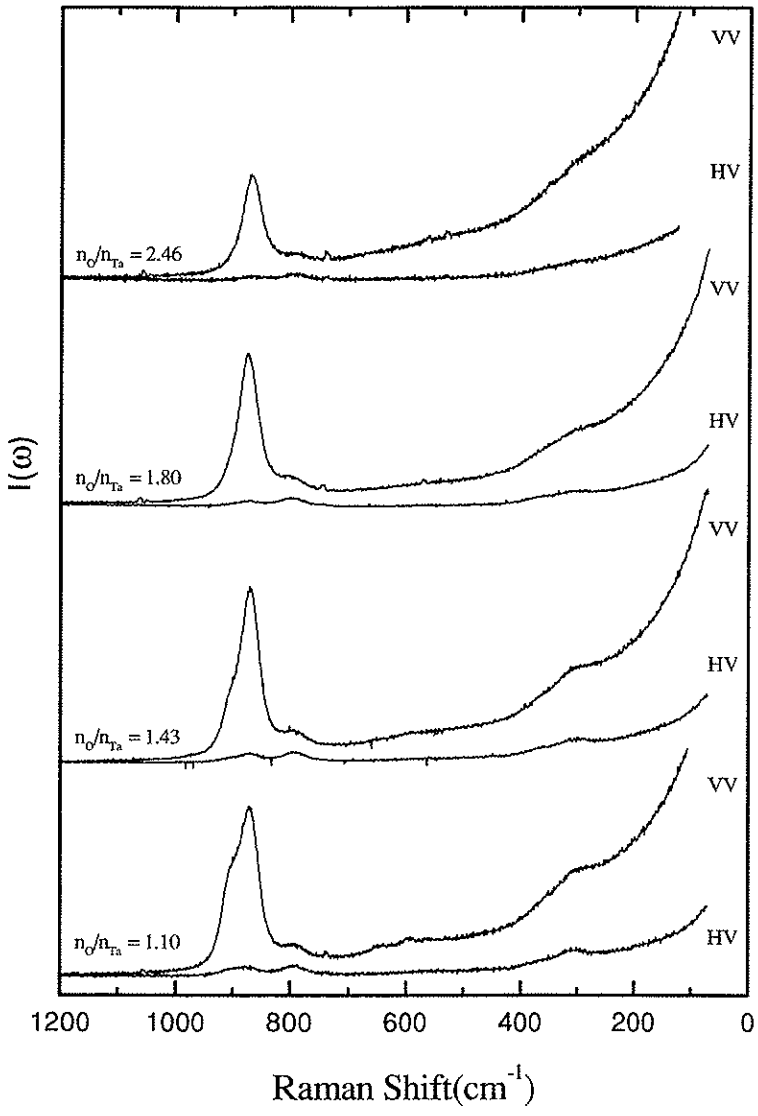

Figure 4.4: Raman spectra of 0.0956 mole/kg $Ta(V)$ in $FLiNaK$ melts with n_O/n_{Ta} ratios varying between 1.10 and 2.46

306 and 360 (broad) cm^{-1}, and two new bands at 790(dp) and 870(p) cm^{-1} appears. In addition to these, one or two broad polarized bands becomes visible in the range 550–590 cm^{-1}. This broad peak is only present in the melts of $n_O/n_{Ta} = 0.82$ and 1.10. Melts with $1.10 < n_O/n_{Ta} < 2.87$ are dominated by the four bands at 306(dp), 360(dp), 790(dp) and 870(p) cm^{-1}. A band at around 980 cm^{-1} is present at $n_O/n_{Ta} = 1.41$. The band is weak or absent in the spectra of melts with $1.41 < n_O/n_{Ta} < 2.87$, but appears

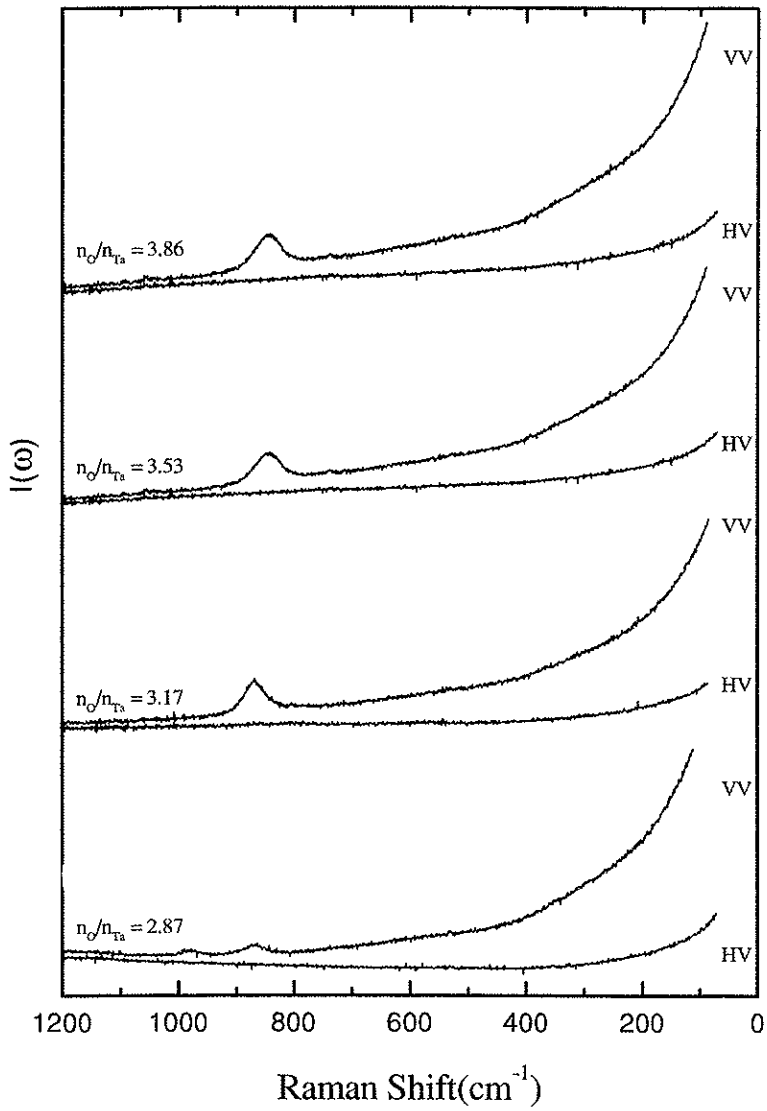

Figure 4.5: Raman spectra of 0.0956 mole/kg $Ta(V)$ in $FLiNaK$ melts with n_O/n_{Ta} ratios varying between 2.87 and 3.86

clearly in the spectrum at $n_O/n_{Ta} = 2.87$

$3 < n_O/n_{Ta} < 6.06$: Two polarized bands at 865 and 980 cm^{-1} are present in the spectrum at $n_O/n_{Ta} = 2.87$. When the oxide content in the melts increases, the band at 980 cm^{-1} disappears and the frequency of the other bands shifts continously down to 840 cm^{-1}. It is difficult to say whether this is a real shift or an overlapping effect of two bands at 840 and 865 cm^{-1}. In

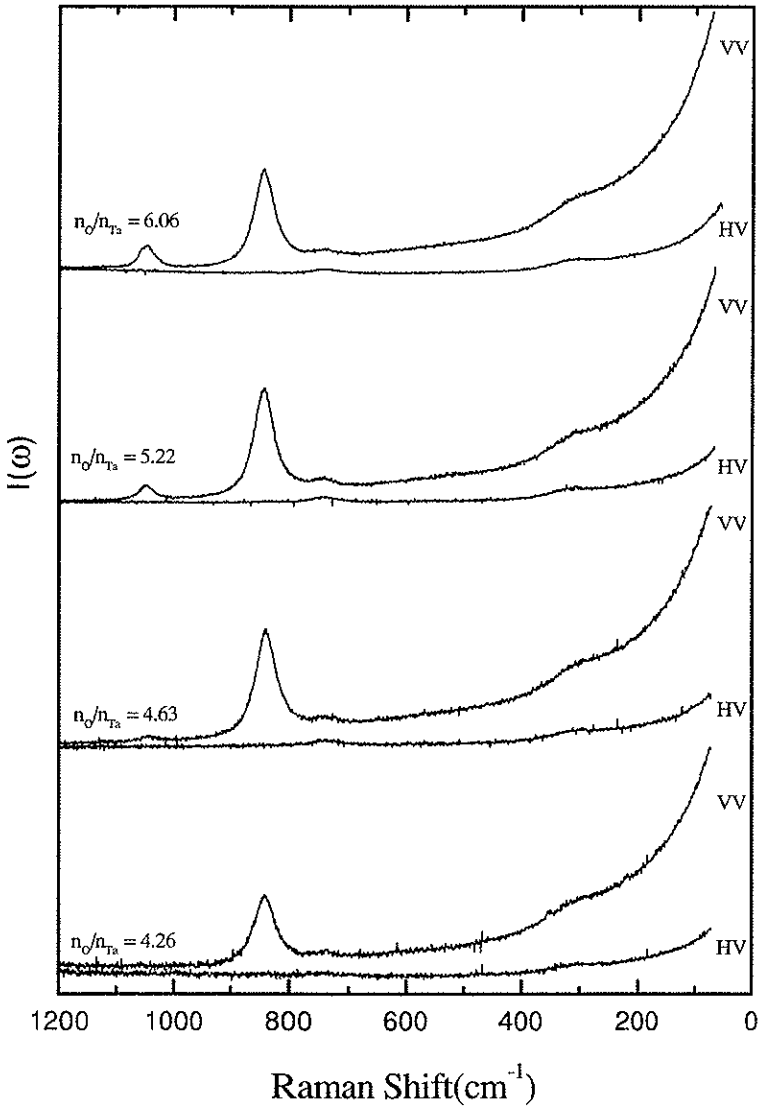

Figure 4.6: Raman spectra of 0.0956 mole/kg $Ta(V)$ in $FLiNaK$ melts with n_O/n_{Ta} ratios varying between 4.26 and 6.06

melts with a ratio n_O/n_{Ta} close to four, two depolarized bands at 320 and 740 cm^{-1} appears, and at even higher ratios a high frequency band at 1050 cm^{-1} is present. The intensity of the latter increases relative to the other three bands with increasing oxide content in the melts.

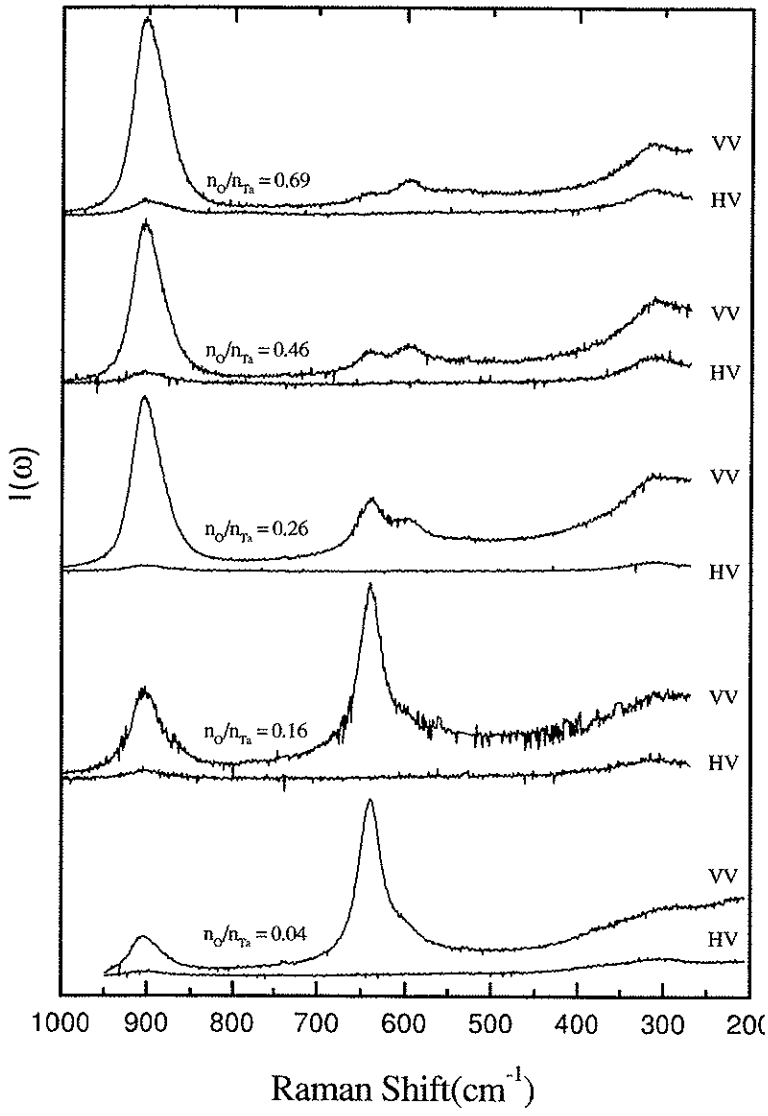

Figure 4.7: Raman spectra of 0.197 mole/kg $Ta(V)$ in $FLiNaK$ melts with n_O/n_{Ta} ratios varying between 0.04 and 0.69

4.4 Raman spectroscopic analysis of Ta_2O_5 dissolved in $FLiNaK$

The melt samples used to obtain Ta_2O_5 solubility data in figure 4.2 were also used to obtain Raman specta. The melt spectra are shown in figure 4.8. The different spectra are marked as sample 1, 2, 3 and 5, giving the same

samples as shown in figure 4.2 from left to right.

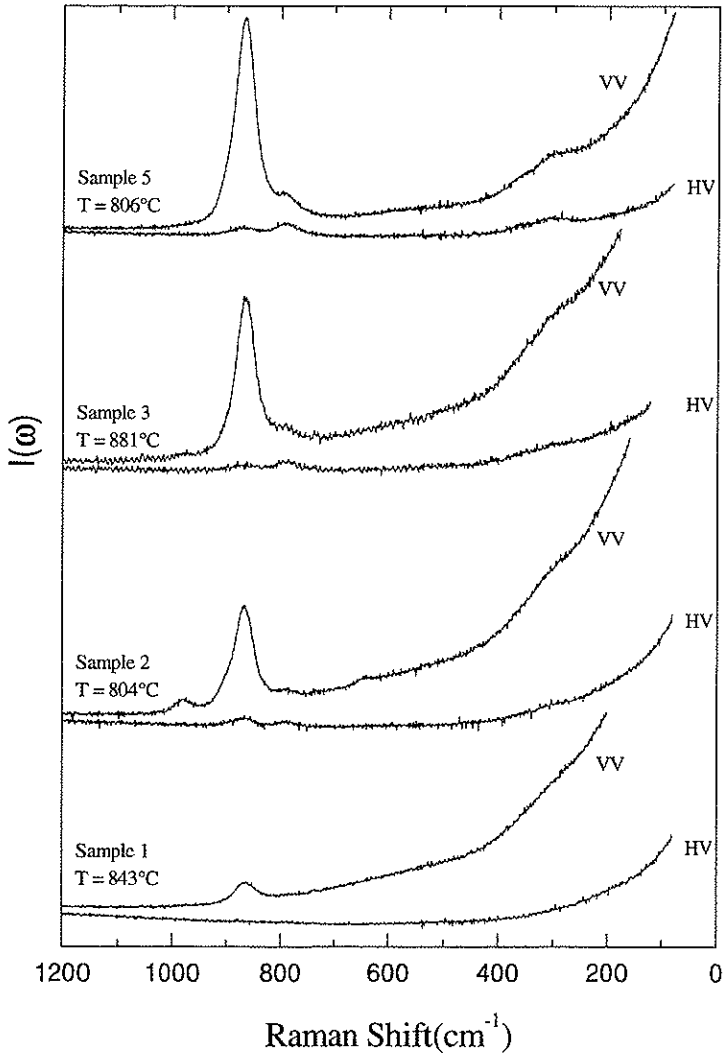

Figure 4.8: Raman spectra of Ta_2O_5 dissolved in $FLiNaK$. Sample 1, 2, 3 and 5 corresponds to melts presented in figure 4.2 where increasing number indicates increasing additions of oxide

A polarized band at 870 cm^{-1} appears after the first addition of Ta_2O_5. Its intensity increases upon further additions of the oxide. At the same time, three depolarized bands at 306, 360 and 790 cm^{-1} become visible, and their intensity seems to be proportional to the intensity of the 870 cm^{-1} band for sample 2, 3 and 5. Sample 2 furthermore contains two polarized bands at 640 and 980 cm^{-1}. The latter is visible in the spectrum of sample 3 and possibly

also in the spectrum of sample 5. While the intensity of the bands at 306, 360, 790 and 870 cm^{-1} increases upon additions of Ta_2O_5, the intensity of the 980 cm^{-1} band remains constant or decreases. The spectrum of sample 5 is totally dominated by these first four bands. A shoulder band is possibly present at the high frequency side of the 870 cm^{-1} band, and is probably due to the polarized band at 906 cm^{-1} that was described in section 4.3.

The most important result is the behavior of the 980 cm^{-1} band. Such a high frequency band was not observed when Nb_2O_5 was dissolved in *FLiNaK*, and is one clear difference between these otherwise very similar metals. The different $Ta(V)$ fluoro and oxofluoro complexes that form in molten *FLiNaK* will be discussed in the next sections.

4.5 The tantalum(V) fluoride complex in molten *FLiNaK*

As for the case of the niobium fluoride complex in molten *FLiNaK*, the Raman spectra of samples having a very low oxygen to tantalum ratio were very difficult to obtain. The spectrum representing a melt with $n_O/n_{Ta} = 0.06$ in figure 4.3 is rather noisy, and it is difficult to measure accurate frequencies for the bands below 400 cm^{-1}. The band at 906 cm^{-1} is due to an oxygen containing species as will be shown later. The spectrum of the melt with $n_O/n_{Ta} = 0.04$ in figure 4.7 is somewhat better. This was recorded in a single step with the monochromator centered at 580 cm^{-1}, and only frequencies between 200 and 950 cm^{-1} could be detected. This was due to limitations of the CCD detector (see section 2.3). All the spectra in figure 4.3 to 4.6 were recorded in two steps as described in section 2.3. Taking longer time, a reaction between the sample and the fused silica envelope was more difficult to avoid. The spectrum in figure 4.7 is therefore much less noisy than the $n_O/n_{Ta} = 0.06$ spectrum in figure 4.3, and the high frequency band at 906 cm^{-1} is less dominant. A weak depolarized band at around 380 cm^{-1} can be seen in addition to the band around 300 cm^{-1}. The spectral behavior of the bands at 640 and 380 cm^{-1} is therefore associated with the tantalum fluoride complex in *FLiNaK*. The origin of the depolarized band at 306 cm^{-1} that can be seen in the spectrum of the melt with $n_O/n_{Ta} = 0.04$, is somewhat uncertain. It appears to be rather broad, and is possibly a result of two overlapping bands. All the other bands in the spectrum are ascribed to oxygen containing tantalum complexes.

In the related niobium system, the NbF_7^{2-} and the NbF_6^- species could be present since no other configurations had been reported. The tantalum system is a bit more complex since the possible existence of TaF_6^-, TaF_7^{2-} TaF_8^{3-} and TaF_9^{4-} have been reported in various molten salt and aqueous media (see section 1.6.1). To determine the symmetry of the tantalum(V) fluoride complex in molten $FLiNaK$, it is reasonable to compare the measured spectra and the identified bands with results obtained in related systems. Table 4.3 lists relevant studies of tantalum complexes in solids, aqueous and molten states. The findings of TaF_9^{4-} by Varga and Freund [35] in perchloric acid solutions containing $Ta(V)$ and hydrofluoric acid were based on potential measurements rather than vibrational spectroscopy.

Table 4.3: Raman bands for tantalum fluoride complexes in various solid, aqueous and molten salt media

Complex	Medium	Vibrations cm^{-1}				Reference
TaF_6^-	HF-solution			585	696	[33]
TaF_6^-	$CsTaF_6(s)$		272	581	692	[33]
TaF_6^-	HF-solution		282	595	711	[34]
TaF_6^-	$KTaF_6(s)$		280	590	710	[34]
TaF_6^-	HF-solution		280		699	[134]
TaF_6^-	$CsTaF_6(s)$				685	[135]
TaF_7^{2-}	HF-solution	280	380	645		[33]
TaF_7^{2-}	$K_2TaF_7(s)$	275	392	640		[33]
TaF_7^{2-}	$K_2TaF_7(s)$	290	400	645		[34]
TaF_7^{2-}	HF-solution	280		645		[134]
TaF_7^{2-}	$K_2TaF_7(s)$		380	630		[135]
TaF_7^{2-}	$FLiNaK(l)$	276		640		[37]
TaF_7^{2-}	$FLiNaK(s)$		380	645		[38]
TaF_7^{2-}	$FLiNaK(s)$	290	380	645		[39]
TaF_7^{2-}	$FLiNaK(l)$		380	640		this work
TaF_8^{3-}	$Na_3TaF_8(s)$	371	411	461	614	[33]

The strongest Raman band for the TaF_6^-, TaF_7^{2-} and TaF_8^{3-} complexes occurs at 685–711 cm^{-1}, 630–645 cm^{-1} and 614 cm^{-1} respectively. Variations occur due to different media and experimental conditions. It is reasonable to first focus on this vibration, to find a symmetry for the tantalum fluoride complex in molten $FLiNaK$. As indicated in table 4.3, the observed band at

640 cm^{-1} is ascribed to the presence of a TaF_7^{2-} in molten *FLiNaK*. The band is very close to what has been observed for the complex in solid K_2TaF_7 by Keller and Strode [33], Matwiyoff *et al.* [34] and Babkin *et al.* [135]. It is furthermore very close to the measured band at 645 cm^{-1} that was associated to TaF_7^{2-} by Keller and Strode [33] and Tsikaeva *et al.* [134] in aqueous *HF*. The presence of TaF_7^{2-} in the melts of figure 4.3 and 4.7 is further supported by the observation of a weak depolarized band at 380 cm^{-1}. This band was observed in an aqueous tantalum containing *HF*-solution by Keller and Strode [33] and in solid K_2TaF_7 by Babkin *et al.* [135]. It should, however, be noted that Keller and Strode [33] and Matwiyoff *et al.* [34] found this band at a slightly higher frequency in this solid.

As mentioned in section 1.6.1, Fordyce and Baum [32] studied *Ta(V)*-fluoride complexes in molten alkali fluorides by means of infrared-reflection spectroscopy. TaF_7^{2-} was found to be the only stable species in *KF-LiF* melts. In the less polarizing *NaF-LiF* solvent both TaF_7^{2-} and TaF_6^- were observed. Their conclusion was that when *KF* was present in the system, TaF_6^- was no longer stable. This seems to be the case for molten *FLiNaK* as well. The six-coordinated complex would be expected to have a strong Raman band at around 700 cm^{-1}, and such a vibration is not present in figure 4.3 or 4.7. The existence of a TaF_8^{3-} complex would cause a band at around 610 cm^{-1}, and the intensity of this vibration would decrease with increasing oxide concentration. The band at 600 cm^{-1} is increasing when oxide is added to the system, and can not be due to an eight coordinated tantalum fluoride complex. It is therefore concluded that TaF_7^{2-} is the major species in molten *FLiNaK* at 750 °C.

Hoard [116] determined the structure of both NbF_7^{2-} and TaF_7^{2-} by means of XRD measurements, and found both to be of C_{2V} symmetry. As mentioned in section 3.5, Brown and Walker [117] showed that this might be inaccurate or incorrect for the niobium species. A similar study to that of Brown and Walker has not been found in the literature for the tantalum complex. This means that the bands at 640 and 380 cm^{-1} can not be ascribed to specific vibrations for a given point group. The polarized nature of the 640 cm^{-1} band does, however, indicate that it is due to a symmetric *Ta-F* stretching vibration of the TaF_7^{2-} complex. Similar for the depolarized 380 cm^{-1} band. It is probably due to an asymmetric bend or deformation mode in the same species.

The presence of TaF_7^{2-} in molten *FLiNaK* is in agreement with the findings of Fordyce and Baum [32] in molten *KF-LiF*, von Barner *et al.* [37] in

molten *FLiNaK* and by Bjerrum *et al.* [38] and Robert *et al.* [39] in solidified *FLiNaK*.

4.6 The di-tantalum(V) mono oxo fluoride complex in molten *FLiNaK*

The idea of having a $Ta_2OF_x^{(x-8)-}$ complex in molten *FLiNaK* was first introduced by Bjerrum *et al.* [38] in their Raman and IR study on solidified melts. This was done on the basis of a Raman active band at 600 cm^{-1}. The intensity of this vibration increased with increasing oxide additions up to a ratio $n_O/n_{Ta} = 0.5$, and decreased upon further oxide additions. The band had vanished at $n_O/n_{Ta} = 1$. This complex was once more studied by Robert *et al.* [39], who claimed the species to reach a maximum concentration at $n_O/n_{Ta} = 0.2 - 0.3$.

The spectral behavior of the 600 cm^{-1} band in figure 4.3 and 4.7 does indeed indicate that the vibration is due to a species with an oxygen to tantalum ratio between 0 and 1. The band appears as a weak shoulder in the spectra of the least oxygen rich melts, and its intensity increases upon addition of oxide. The increase is, however, not proportional to the high frequency band at 904 cm^{-1}. The latter reaches a maximum intensity as the ratio n_O/n_{Ta} approaches 1. It is therefore reasonable to attribute the 904 cm^{-1} band to a tantalum mono oxo fluoride complex. Sala-pala *et al.* [136] studied the solid $(Et_4N)_2[Ta_2OF_{10}]$ by means of Raman and IR spectroscopy. The compound was found to contain isolated $Ta_2OF_{10}^{2-}$ complexes of D_{4h} symmetry that showed strong Raman active bands at 270 and 669 cm^{-1}. The bands were ascribed to a symmetric *Ta-O-Ta* vibration and a symmetric *Ta-F* vibration respectively. It is therefore likely that the band 600 cm^{-1} observed in figure 4.3 and 4.7 is due a symmetric *Ta-F* vibration in an oxygen bridged $Ta_2OF_x^{(x-8)-}$ complex. A vibration due to the actual bridge is impossible to observe in the present spectra. This could be due to the noise in the spectra in the low-frequent region below 400 cm^{-1}. The spectra for $0.16 < n_O/n_{Ta} < 0.69$ in figure 4.7 are furthermore only measured down to $\sim 250\ cm^{-1}$.

4.7 The tantalum(V) mono oxo fluoride complex in molten *FLiNaK*

As mentioned in the previous section, the vibration at 904 cm^{-1} is attributed to the tantalum mono oxo fluoride complex. The polarized band is visible in all melts with $n_O/n_{Ta} \leqslant 1.8$, and is due to a symmetric $Ta = O$ stretching mode in the $TaOF_x^{(x-3)-}$ complex. This is similar to the 922 cm^{-1} band due to the $Nb = O$ symmetric stretching mode in the $NbOF_5^{2-}$ complex. The band at 314 cm^{-1} is present in the spectra of melts with $n_O/n_{Ta} < 0.82$, and is replaced by the bands at 306 and 360 cm^{-1} at higher ratios of oxygen to tantalum. At the same time, the bands at 870 and 790 cm^{-1} appears in the high frequency region. The four new bands are therefore ascribed to a new species with an oxide content higher than 1, and the 314 cm^{-1} band must therefore be due to the $TaOF_x^{(x-3)-}$ complex. A similar assignment was done by von Barner *et al.* [37] using molten *FLiNaK* and Robert *et al.* [39] using solidified *FLiNaK*. The groups measured Raman shifts at 312 and 319 cm^{-1} respectively. Robert *et al.* furthermore observed a weak band at 545 cm^{-1} that was ascribed to the same species. Such a band is possibly visible in the present work. The melts with a composition $n_O/n_{Ta} = 0.82$ and $n_O/n_{Ta} = 1.10$ in figure 4.3 and 4.4 showed a broad band in this region. The frequency of this band, or possibly bands, are uncertain, but Raman shifts of 585 and 550 cm^{-1} are indicated in table 4.1. The broadness of the wave and the low signal to noise ratio makes a more accurate determination of the frequency difficult. The bands seem to be polarized.

von Barner *et al.* [37] ascribed their depolarized band at 312 cm^{-1} to a *Ta-F* vibration of the $TaOF_x^{(x-3)-}$ complex. A similar band at 304 cm^{-1} was observed for the $NbOF_5^{2-}$ complex in the present work, and the nature of this band was discussed in section 3.6. It was showed that this low frequency band might not be due to an *Nb-F* (B_2) vibration but rather an *Nb-O-F* (E) bending mode of the species. Pausewang *et al.* [118] ascribed the band at 306 cm^{-1} in solid Cs_2NbOF_5 and the band at 310 cm^{-1} in solid Cs_2TaOF_5 to this type of vibration. It is therefore possible that the band at 312 cm^{-1} is due to a *Ta-O-F* bending mode, rather than a *Ta-F* vibration that was proposed by von Barner *et al.* [37]. The band at 904 cm^{-1} has already been ascribed to a $Ta = O$ vibration, but the weak band (or bands) in the range 550-600 cm^{-1} is yet to be discussed. Neither Bjerrum *et al.* [38] nor Robert *et al.* [39] ascribed this band to a specific mode in the $TaOF_x^{(x-3)-}$ complex. Pausewang *et al.* [118] did, however, measure a weak band at 595 cm^{-1} in the Cs_2TaOF_5 solid, and ascribed this to symmetric *Ta-F* vibration of the

TaF_4^+ entity. It is therefore likely that the weak band at around 550-600 cm^{-1} is of similar origin. A polarized band was observed at 640 cm^{-1} and attributed to a Ta-F vibration for the TaF_7^{2-} complex. As was seen in the case of niobium species, a red shift of about 45 cm^{-1} was observed in the Nb-F vibration when going from NbF_7^{2-} to $NbOF_5^{2-}$. A similar phenomenon can obviously be observed when going from TaF_7^{2-} to $TaOF_x^{(x-3)-}$, but the actual frequency difference is difficult to measure.

The value of x in the $TaOF_x^{(x-3)-}$ complex is yet to be determined, and $TaOF_4^-$, $TaOF_5^{2-}$ and $TaOF_6^{3-}$ are the most obvious candidates. No other ionic tantalum mono oxo fluoride species has been suggested in the literature. The $TaOF_4^-$ ion was studied in solid $CsTaOF_4$ by Buslaev and Kokunov [137] by means of IR spectroscopy, and a narrow intense band due to vibrations of the isolated $Ta = O$ group was observed at 955 cm^{-1}. Pausewang *et al.* [118] observed a similar band at 896 cm^{-1} in the IR spectra and 898 cm^{-1} in the Raman spectra for the $TaOF_5^{2-}$ in the solid Cs_2TaOF_5. The $TaOF_6^{3-}$ complex was studied by means of Raman spectroscopy in the solid $(NH_4)_3TaOF_6$ by Keller and Chetam-Strode [33], and a strong $Ta = O$ band was observed at 862 cm^{-1}. These studies clearly show that the Ta-O bond is weakened by the increasing number of fluorine ligands. The increasing electron density around the central nuclei reduces the effective charge of tantalum, and causes a reduced attraction to the negatively charged oxide atom. This subject was also discussed in section 3.6. It should be noted that a broad absorption band was observed in the range 620-710 cm^{-1} in the IR spectrum of solid $CsTaOF_4$, and this was attributed to vibrations of the TaO group in a Ta-O-Ta-O chain. This means that the solid does not contain discrete $TaOF_4^-$ ions. No bands in the present work indicate such bridging oxygen for the $TaOF_x^{(x-3)-}$ species, and the work by Buslaev and Kokunov [137] is not directly comparable to the present work. The band at 955 cm^{-1} in the $CsTaOF_4$ solid is, however, too far away from the band at 904 cm^{-1} in figure 4.3 or 906 cm^{-1} in figure 4.7 to make $x = 4$ a probable value for the $TaOF_x^{(x-3)-}$ complex. For the two other possibilities, $TaOF_5^{2-}$ seems more likely than $TaOF_6^{3-}$. The $Ta = O$ vibration of the former is very close to the measured value in the present work, and the same goes for the Ta-O-F mode at 310 cm^{-1} in solid Cs_2TaOF_5 and 314 cm^{-1} in figure 4.3. The band due to a Ta-F vibration is weak, and is not suitable for determination of x in the $TaOF_x^{(x-3)-}$ complex. It is therefore probable that the tantalum mono oxo fluoride complex in molten $FLiNaK$ is $TaOF_5^{2-}$. This is the same conclusion as drawn by Robert *et al.* [39].

4.8 The tantalum(V) dioxo fluoride complex in molten *FLiNaK*

As mentioned in the previous section, the four bands at 306(dp), 360(dp), 790(dp) and 870(p) cm^{-1} were ascribed to a tantalum oxofluoride complex with an oxide to tantalum ratio higher than 1. The bands first appear in the spectrum of the melt with $n_O/n_{Ta} = 0.8$ (figure 4.3), and their intensity continues to increase with increasing oxide contents (figure 4.4). The spectral behavior is very similar to that of the four bands at 290(dp), 368(dp), 816(dp) and 880(p) cm^{-1} for the $NbO_2F_4^{3-}$ complex (section 3.7). The four bands that dominate the spectrum of the melt with $n_O/n_{Ta} = 1.80$ in figure 4.4 are therefore ascribed to the presence of a tantalum dioxo fluoride complex of the type $TaO_2F_x^{(x-1)-}$. The spectrum of a melt with $n_O/n_{Ta} = 2.87$ indicates that the band at 980 cm^{-1} is of another origin. The spectrum is dominated by the former band and a band at around 865 cm^{-1} that might be the weak remains of the polarized band at 870 cm^{-1}. The concentration of tantalum containing species is very low in this sample, and the Raman spectrum has low intensity.

A detailed assignment of the four bands of the $NbO_2F_4^{3-}$ complex was given in section 3.7. Due to the spectral similarities of the niobium- and the tantalum dioxo fluoro complex, the band assignments will be covered only briefly. The polarized band at 870 cm^{-1} is assigned to a symmetric *Ta-O* vibration where the high frequency reflects the character of a strong double bond. The bond is weaker than the *Ta-O* bond of the $TaOF_5^{2-}$ complex, and the vibration of the dioxo complex occurs at a frequency about 35 cm^{-1} lower than for the mono oxo complex. This decrease is slightly lower than for the case of niobium mono/dioxo complexes, where a red shift of about 45 cm^{-1} was observed when one fluoride atom was replaced with one oxygen atom.

As in the case of the depolarized band at 815 cm^{-1} of the $NbO_2F_4^{3-}$ complex, the depolarized band at 790 cm^{-1} is ascribed to an asymmetric vibration of the TaO_2^+ entity. The band at 815 cm^{-1} was shown to be both IR and Raman active, and was used to exclude a center of symmetry in the niobium species. IR spectra of the different tantalum complexes have not been recorded in the present work, but Bjerrum *et al.* [38] measured Raman and IR spectra of tantalum in solidified *FLiNaK* melts with $0 < n_O/n_{Ta} < 2$. The IR spectrum of a sample with $n_O/n_{Ta} = 2$ had unfortunately very low intensity, and the different bands were difficult to resolve. The Raman spectrum of the same sample is furthermore rather different from that recorded

in the molten state. In addition to the four bands in the present work, the spectrum of Bjerrum *et al.* contains two bands at 620 and 700 cm^{-1}. It is therefore impossible to exclude a center of symmetry in the $TaO_2F_x^{(x-1)-}$ complex by using the mutual exclusion rule. This does, however, not mean that the complex necessarily has a symmetry center. As pointed out by Griffith and Wickins [127], the *cis* configuration is clearly preferred in d^0-complexes; complexes where the central atom lacks d-electrons. This is the case for both tantalum and niobium, and is an indication that the tantalum dioxo fluoro complex does not have a center of symmetry.

In accordance with the assignment of the band at 290 cm^{-1} to an asymmetric *Nb-O-F* vibration in the $NbO_2F_4^{3-}$ complex, the depolarized band at 306 cm^{-1} is assigned to an asymmetric *Ta-O-F* vibration in the $TaO_2F_x^{(x-1)-}$ complex. Compared with the depolarized *Ta-O-F* band of the $TaOF_5^{2-}$ complex, the frequency of the asymmetric vibration is reduced by 8 cm^{-1} (the reduction was about 15 cm^{-1} in the niobium case).

The origin of the band at 370 cm^{-1} for the $NbO_2F_4^{3-}$ complex was discussed thoroughly in section 3.7. It was shown that a deformation $\delta(MO_2)$ mode of the dioxo complex was a reasonable explanation. Adopting the same arguments, it is assumed that the depolarized band at 360 cm^{-1} for the $TaO_2F_x^{(x-1)-}$ complex has the same origin.

Determining the number of fluoride atoms in the niobium dioxo fluoride complex could be done by a comparison with the IR bands of the $Rb_2KNbO_2F_4$ solid measured by Pausewang and Rudorf [128]. IR or Raman measurements of a similar tantalum solid has, however, not been found in the literature and the number of fluoride atoms in the $TaO_2F_x^{(x-1)-}$ complex must be determined using other data. Griffith and Wickins [127], and Pausewang and Dehnicke [128] studied dioxo halide complexes of vanadium, molybdenum and tungsten in various alkali and ammonium solids. It was shown that the symmetric $\nu(MO_2)$ vibration occured at 965, 948 and 946 cm^{-1} for $(NH_4)_2[Mo(V)O_2F_3](s)$, $(NH_4)_2[Mo(VI)O_2F_4](s)$ and $(NH_4)_3[Mo(VI)O_2F_5](s)$ respectively. As expected, the frequency decreased with increasing number of fluorine atoms, but the difference between the last two compounds were very small. $(NH_4)_2[Mo(V)O_2F_3](s)$ contained six coordinated molybdenum atoms with bridging fluoride ligands, and was probably a dimeric species with two *cis*-dioxo groups. The fluorine bridge was, however, not visible in the Raman spectrum. A similar compound, $K_2VO_2F_3(s)$, was studied by Pausewang and Dehnicke [128] by means of IR spectroscopy, and was shown to contain chains of fluorine bridged $(VO_2F_4)_n$ groups. The $(NH_4)_3[Mo(VI)O_2F_5](s)$ compound was probably a double salt

with composition $(NH_4)_2[Mo(VI)O_2F_4]$, NH_4F, and did not contain seven-coordinated molybdenum. The work by Griffith and Wickins [127], and the examples above show that a coordination of six is clearly preferred for the dioxo complexes. Due to this, and the spectral similarities of $NbO_2F_4^{3-}$ and $TaO_2F_x^{(x-1)-}$, it is also likely that the latter has an octahedral coordination. As in the case of niobium, a possible fluorine bridge is impossible to detect since it is probably inactive in Raman. The lack of IR data of the $TaO_2F_x^{(x-1)-}$ complex in the molten state, makes it difficult to rule out such bridges. As already mentioned in this and the previous chapter, an oxygen bridged species would have a polarized Raman band in the range 600–800 cm^{-1}. Such a band is not found for the tantalum dioxo fluoro complex. It is therefore likely that the complex is either a monomeric specie $TaO_2F_4^{3-}$, or a fluorine bridged species similar to that of vanadium in $K_2VO_2F_3(s)$ or molybdenum in $(NH_4)_2[Mo(V)O_2F_3](s)$.

4.9 The band at 980 cm^{-1}

As mentioned in section 4.8, the band at 980 cm^{-1} is not due to the tantalum dioxo fluoro complex. The band occurs in melts with $1.43 \leqslant n_O/n_{Ta} \leqslant 2.87$, and is probably due to a species with oxygen to tantalum ratio within this range. It is therefore probably not due to a $TaO_3F_x^{(x+1)-}$ complex since the band is absent in the spectrum of the melt with $n_O/n_{Ta} = 3.17$. This fits with the solubility data, since the concentrations of oxygen and tantalum in the melt are very low at $n_O/n_{Ta} = 3$. It is indeed strange that the band appears in the melt with $n_O/n_{Ta} = 1.43$, then is absent, invisible or weak in the spectra of melts with $1.41 < n_O/n_{Ta} < 2.87$, just to reappear clearly in the spectrum of the melt with $n_O/n_{Ta} = 2.87$. This unsystematic behavior is probably due to experimental difficulties. The peak is very weak, and optimal optical conditions are probably required to record the vibration. The size of the hole in the windowless graphite cells used is probably an important factor.

The very high frequency and the polarized property of the band indicates that it is due to a $Ta = O$ symmetric vibration. The Ta-O bond is stronger than those in $TaOF_5^{2-}$ and $TaO_2F_4^{3-}$ which causes the symmetric vibration to occur at a significantly higher frequency. Apart from this, the band is difficult to assign.

4.10 Tantalum(V) oxo fluoride complexes with a ratio of n_O/n_{Ta} above 3 in molten $FLiNaK$

As mentioned in the previous section, the band at 980 cm^{-1} cannot be ascribed to a $TaO_3F_x^{(x+1)-}$ complex since the band is absent in the spectrum of the melt with $n_O/n_{Ta} = 3.17$. The band at around 865 cm^{-1} is therefore probably the remains of the polarized $Ta = O$ vibration of the $TaO_2F_4^{3-}$ complex. As seen in figure 4.5, the peak shifts to lower frequencies as oxide is added to the system, but then remains constant for melts with $n_O/n_{Ta} > 4$. The behavior of the spectra shown in figure 4.5 can probably be explained by $TaO_2F_4^{3-}$ coexisting with a tantalum oxo fluoride complex with n_O/n_{Ta} above 3.

Due to the low solubility of tantalum complexes in melts with n_O/n_{Ta} around 3, the general intensity of the Raman spectra in figure 4.5 is low. The spectra shown in figure 4.6 are, however, more intense. This fits well with the solubility data of figure 4.1 where the tantalum concentration is back to the initial value given by the added amount when $n_O/n_{Ta} \geqslant 4.26$. The spectra shown in figure 4.6 are characterized by four bands at 320(dp), 740(dp), 840(p) and 1050(p) cm^{-1}. The intensity of the latter increases relative to the other three when the oxide content increases in the melt, and seems very similar to the band 1045 cm^{-1} observed in the niobium case. As for the three other bands, their relative intensity seems to be constant and they are probably due to the same species. Their spectral behavior are similar to the bands at 310(dp), 750(dp) and 820(p) ascribed to a possible $NbO_4F_2^{5-}$ complex. The bands at 320(dp), 740(dp), 840(p) cm^{-1} are therefore probably due to a $TaO_4F_x^{(3+x)-}$ species. As in the case of the $TaO_2F_4^{3-}$ complex, the assignments of bands will be covered only briefly due to the similarities with the niobium system.

The polarized band at 840 cm^{-1} and the depolarized band at 740 cm^{-1} are probably of a similar origin as the two bands at 870 and 790 cm^{-1} observed for the dioxo fluoro complex. The bands appear as a pair, and are due to symmetric and asymmetric Ta-O vibrations, in this case probably in the TaO_4^{3-} entity. As mentioned in section 3.9, tetrahedral complexes are extremely rare for the cases of niobium and tantalum, and the value of x in $TaO_4F_x^{(3+x)-}$ is likely to be higher than 0. The band at 320 cm^{-1} is then probably due to a Ta-O-F bending vibration.

The absence of bands between 320 cm^{-1} and 740 cm^{-1}, makes the presence of oxide bridges unlikely in the $TaO_4F_x^{(3+x)-}$ complex. With no IR data available, it is difficult to determine whether or not there are bridging fluorines present in the species. The same problem was discussed for the $NbO_4F_2^{5-}$ complex, and it was assumed that the niobium species was a monomer like all the other $NbO_xF_y^{(2x+y-5)-}$ complexes found in molten $FLiNaK$. The same assumption is made for the $TaO_4F_x^{(3+x)-}$ ion. The number of fluorine atoms in the complex is also difficult to determine, but it is likely that the tantalum atom is octahedrally coordinated, meaning $x = 2$.

As already mentioned, the high frequency band at 1050 cm^{-1} must be due to a new tantalum complex. Since the intensity of the band continues to increase with oxide additions in melts with $n_O/n_{Ta} > 4$, it is probably due to an even more oxide rich species than $TaO_4F_2^{5-}$. From Raman spectroscopic studies on the high temperature β-Ta_2O_5 phase by Balachandran and Eror [138], it was shown that tantalum may form both five- and six-coordinated polyhedra with oxygen: "Chains of edge-shared pentagons are fused together with the formation of octahedral sites between adjacent chains. These distorted polyhedra are condensed with considerable variation in the bond lengths." In the corresponding $Nb(V)$ oxofluoride melts the band at 1044 cm^{-1} were assigned to the possible existence of $(NbO_6)_n$ network structures. The band at 1050 cm^{-1} is probably of a similar origin; a symmetric vibration of a very strong $Ta = O$ bond in a distorted five- and/or six-coordinated tantalum polyhedron.

4.11 Conclusions

Raman spectroscopy and oxide and Ta solubility measurements of Na_2O-$FLiNaK$-K_2TaF_7 melts show that at least five different tantalum oxo fluoro species are formed. The solubility data are indicating the formation of different $Ta_xO_yF_z^{(2y+z-5x)-}$ complexes where x, y and z takes values depending on the n_O/n_{Ta} ratio in the melt. From the Raman measurements, the existence of $TaF_7^{2-}(C_s)$, $Ta_2OF_x^{(x-8)-}$, $TaOF_5^{2-}(C_{4v})$ and $TaO_2F_x^{(x-1)-}$ at ratios up to 2 are well established. The dioxo fluoro complex is probably $TaO_2F_4^{3-}(C_{2v})$, and a polarized band at 980 cm^{-1} in these melts suggests the presence of yet another tantalum oxo fluoro complex. At $n_O/n_{Ta} = 3$ the solubility data indicates precipitation of a solid compound $AlkTaO_3$. At $n_O/n_{Ta} > 3$ the solubility data are consistent with a dissolution of the $AlkTaO_3$ solid, and a formation of a $TaO_4F_x^{(x+3)-}$ species. The tantalum

tetra oxo fluoride complex is possibly $TaO_4F_2^{5-}(C_{2v})$ The solubility data indicates a precipitation of an oxide rich solid at $n_O/n_{Ta} > 4$. The Raman spectra indicate the existence of $TaO_4F_2^{5-}$ species as well as $(TaO_5)_n$ or $(TaO_6)_n$ network structures in these melts.

Chapter 5

Concluding remarks

Senderoff and Mellors [6] and [7] were the first to demonstrate that it was possible to produce coherent coatings of niobium and tantalum by electroplating from a molten $FLiNaK$ electrolyte. As shown in chapter 1, this pioneering work was followed by a number of studies of similar nature. The purpose was to develop an industrial electroplating process of these refractory metals. Special attention has been given to the influence of oxide impurities in the electrolytes. This parameter has been shown to have a significant effect on current efficiency, coherence of the deposit and purity of the metal. The object of the present work was to study the solubility and structure of different $Nb(V)$ and $Ta(V)$ complexes in $FLiNaK$ melts with varying $n_{O^{2-}}/n_{M^{5+}}$ $(M = Nb, Ta)$ ratios.

5.1 Conclusions

The studies of structure and solubility of the different $Nb(V)$ and $Ta(V)$ complexes are summed up in section 3.11 and 4.11. The current section will focus on the similarities and differences observed for the two systems.

The K_2NbF_7-$FLiNaK$-Na_2O and K_2TaF_7-$FLiNaK$-Na_2O melts obviously have a lot in common. Both systems show a minimum in oxide and Nb/Ta solubility in melts with $n_O/n_M = 3$ which is due to a precipitation of a solid compound $AlkMO_3$. These solids starts to form in melts with a ratio n_O/n_M around 2, and the precipitation increases up to $n_O/n_M = 3$. The solids furthermore starts to dissolve when oxide is added beyond $n_O/n_M = 3$, and

almost all the added amounts of oxide and refractory metal are in the molten state at $n_O/n_M = 4$. A further increase of the n_O/n_M ratio is possibly accompanied by precipitation of another solid compound with an oxide to refractory metal ratio 6. The major difference between the niobium and the tantalum system is the solubility of the $AlkMO_3$ solid. The solubility of $AlkNbO_3$ in molten $FLiNaK$ at 700 °C was found to be more than 7 times larger than that of $AlkTaO_3$. The solubility data were not obtained exactly at $n_O/n_M = 3$ and the difference in solubility could be larger.

Both $Nb(V)$ and $Ta(V)$ form heptafluoro complexes in $FLiNaK$ melts with low oxide contents. The symmetry of these complexes are probably C_s, and can be understood as a four member fluorine square put on top of a 3 member fluorine triangle, with the central refractory atom placed between them. Both metals form MOF_5^{2-} complexes of C_{4v} symmetry and $MO_2F_4^{3-}$ complexes of C_{2v} symmetry when oxide is added to the melt. In addition to these, a dimeric tantalum species $Ta_2OF_x^{(x-8)-}$ is formed in melts with $n_O/n_{Ta} < 1.8$. A similar complex was not observed in the niobium containing melts. As allready mentioned, the solubility at $n_O/n_M = 3$ was significantly higher in the niobium system than in the tantalum system. A trioxo complex $NbO_3F_x^{(1+x)-}$ with a possible value of $x = 3$ was probably present in the $Nb(V)$ containing melts, while a similar tantalum species was not identified. $FLiNaK$ melts with $n_O/n_{Ta} \sim 3$ seemed to be a mixture of $TaO_2F_4^{3-}$ and complexes with $n_O/n_{Ta} > 3$. In addition, an unidentified tantalum complex was formed in these melts. This species had a polarized band at 980 cm^{-1}. The lack of a $TaO_3F_x^{(1+x)-}$ complex is probably the reason for the low solubility of the $AlkTaO_3$ solid. In systems with $n_O/n_M > 3$, $MO_4F_x^{(3+x)-}$ complexes with a possible value of $x = 2$ are formed for both $Nb(V)$ and $Ta(V)$. The symmetry of the species are possibly C_{2v}. This results in $NbO_4F_2^{5-}$ and $TaO_4F_2^{5-}$ complexes with the two fluorine atoms in *cis* position. These higly charged species reflect the remarkable complexing ability of niobium and tantalum. Other refractory metal species are also present in $Nb(V)$ and $Ta(V)$ melts with $n_O/n_{Ta} > 4$. These are probably distorted oxygen bridged $(NbO_6)_n$ and $(TaO_5)_n$ or $(TaO_6)_n$ polyhedra. One or two oxygen atoms are strongly bonded to the refractory metal atom, while the remaining oxygen form loosely bonded bridges.

The different ability of $Nb(V)$ and $Ta(V)$ to form trioxo fluoro complexes are also reflected in the solubility measurements of $Nb_2O_5(s)$ and $Ta_2O_5(s)$. By dissolving $Nb_2O_5(s)$ in molten $FLiNaK$, it was found that both $NbO_2F_4^{3-}$ and $NbO_3F_3^{4-}$ were formed. The ratio of oxide to $Nb(V)$ was about 2.1 in saturated melts. For the similar experiment with Ta_2O_5, the ratio of

oxide to $Ta(V)$ was below 2. These melts contained $TaOF_5^{2-}$, $TaO_2F_4^{3-}$ and an unidentified species with a Raman active band at 980 cm^{-1}. The Ta_2O_5-$FLiNaK$ melts studied were not saturated with Ta_2O_5.

5.2 Suggestions for further work

The main goal of the present work has been to investigate the structure and oxide solubility of K_2MF_7-$FLiNaK$ containing melts. Most of the complexes in the two systems were identified, and the solubility as a function of the ratio n_O/n_M was determined. It should, however, be possible to gain an even better understanding of the complex formation of these melts. This is especially true for the network structure that is probably present in both systems for high n_O/n_M ratios. High temperature O^{17} NMR has been proposed as a possible method to study these systems, but such analyzes are faced with extreme experimental difficulties and are very expensive to perform. This work is, however, in progress in cooperation with Catherine Bessada at CNRS-CRMHT in Orleans, France. It should furthermore be possible to isolate the solid that probably precipitates from the melts, and determine their composition and structure.

The $Nb(IV)$-O^{2-}-$FLiNaK$ system should probably be reexamined to clearify the discrepancies that was found between the work of Matthiesen, Jensen and Østvold [31] and Rosenkilde *et al.* [24]. The goal of this work would be to determine whether $Nb(IV)O_2F_x^{x-}$ is stable or not in molten $FLiNaK$. The dissolution study of NbO_2 in the present work indicates that the complex is unstable, but that the reaction to $Nb(V)O_2F_4^{3-}$ and Nb-metal is slow.

All the suggestions for further work mentioned above are merely for scientific interests. It should be emphasized how important basic research is for an improved understanding on these molten salt systems. Even though many of the conclusions drawn are uninteresting for the potential electroplating industry, the current research describes the remarkable ability of $Nb(V)$ and $Ta(V)$ to form highly charged complexes in oxide containing fluorides. As for the electroplating process, it should be noted that no major industry of this kind has been formed in the western world. It is now about 35 years since Senderoff and Mellors [6] published their work on coherent electrodeposition of niobium, but the ideas are yet to be commercially realized. Great progress in the understanding and development of this possible process has, however, been done during the last decade. This has led to pilot

plant projects currently under study by Professor N.J.Bjerrum at DTV in Denmark. It is now possible to produce refractory metal coatings of very high quality. The commercial success is dependant on the ability to compete with alternative processes like chemical vapour deposition. This alternative produces metal surfaces of lower quality, but is probably cheaper.

References

[1] S.Senderoff. Electrodeposition of refractory metals. *Metallurgical Reviews.*, 11:97–112, 1966.

[2] Tantalum-niobium international study center. www.tanb.org. 40 rue Washington, 1050 Brussels, Belgium.

[3] R.S.Sethi. Electrocoating from molten salts. *J. Appl. Electrochem.*, 9:411–426, 1979.

[4] C.W.Balke. Process for obtaining metallic tantalum. **U.S.Patent 1,799,403**, 1931.

[5] M.E.Sibert and M.A.Steinberg. Electrodeposition of titanium on base metals. *J. Electrochem. Soc.*, 102:641–647, 1955.

[6] G.W.Mellors and S.Senderoff. Electrodeposition of coherent deposits of refractory metals. *J. Electrochem. Soc.*, 112:266–272, 1965. I. Niobium.

[7] G.W.Mellors, S.Senderoff, and W.J.Reinhart. The electrodeposition of coherent deposits of refractory metals. *J. Electrochem. Soc.*, 112:840, 1965. II. The electrode reactions in the deposition of tantalum.

[8] G.W.Mellors and S.Senderoff. The electrodeposition of coherent deposits of refractory metals. *J. Electrochem. Soc.*, 113:60–66, 1966. III. Zirconium.

[9] S.Senderoff and G.W.Mellors. Electrodeposition of coherent deposits of refractory metals. *J. Electrochem. Soc.*, 114:556–560, 1967. V. Mechanism for the deposition of molybdenum from a chloride melt.

[10] S.Senderoff and G.W.Mellors. The electrodeposition of coherent deposits of refractory metals. *J. Electrochem. Soc.*, 113:66–71, 1966. IV. The electrode reactions in the deposition of niobium.

[11] G.W.Mellors and S.Senderoff. Coherent coatings of refractory metals. *Science*, 153:1475–1481, 1966.

[12] G.W.Mellors and S.Senderoff. Electrodeposition of refractory metals. **U.S.Patent 3,444,058**, 1969.

[13] S.Senderoff and A.Brenner. The electrolytic preparation of molybdenum from fused salts. *J. Electrochem. Soc.*, 101:16–27, 1954.

[14] U.Cohen. High rate electrodeposition of niobium from molten fluoride using periodic reversal steps and the effect on grain size. *J. Electrochem. Soc.*, 128:731–740, 1981.

[15] S.Senderoff, G.W.Mellors, and R.I.Bretz. Thermodynamic properties of molten mixtures of cerium chloride and calcium chloride. *J. Electrochem. Soc.*, 108:93–96, 1961.

[16] S.A.Kuznetsov. The effect of the second coordination sphere on the electroreduction of hafnium and rhenium complexes in salt melts. *Russ. J Electrochem.*, 32:1209–1214, 1996. Translated from Élektrokhimiya 32:1310-1316, 1996.

[17] J.S.Fordyce and R.L.Baum. Infrared-reflection spectra of molten fluoride solutions: $Nb(V)$ in $KF : LiF$. *J. Chem. Phys.*, 44:1166–1167, 1966.

[18] J.H.von Barner, E.Christensen, N.J.Bjerrum, and B.Gilbert. Vibration spectra of niobium(V) fluoro and oxo fluoro complexes formed in alkali-metal fluoride melts. *Inorg. Chem.*, 30:561–566, 1991.

[19] P.Los and J.Joslak. Electrodeposition of niobium from fluoride melts. *B. Electrochem*, 11:829–833, 1989.

[20] Z.Qiao and P.Taxil. Electrochemical reduction of niobium ions in molten *LiF-NaF*. *J. Appl. Electrochem.*, 15:259–265, 1985.

[21] P.Taxil and J.Mahenc. Formation of corrosion-resistant layers by electrodeposition of refractory metals or by alloy electrowinning in molten fluorides. *J. Appl. Electrochem.*, 17:261–269, 1987.

[22] E.Christensen, X.Wang, J.H.von Barner, T.Østvold, and N.J.Bjerrum. The influence of oxide on the electrodeposition of niobium in alkali fluoride melts. *J. Electrochem. Soc.*, 141:1212, 1994.

[23] F.Matthiesen, E.Christensen, J.H.von Barner, and N.J.Bjerrum. The redox chemistry of niobium(V) fluoro and oxofluoro complexes in *LiF-NaF-KF* melts. *J. Electrochem. Soc.*, 143:1793–1799, 1996.

[24] C.Rosenkilde, Aa.F.Vik, T.Østvold, E.Christensen, and N.J.Bjerrum. Electrochemical studies of the molten system K_2NbF_7-Na_2O-Nb-$(LiF\text{-}NaF\text{-}KF)_{eut}$ at 700 °C. *J. Electrochem. Soc.*, 147:3790–3800, 2000.

[25] L.M.Toth and L.O.Gilpatrick. The ligand-field spectrum of niobium(IV) in fluoride melts. *Inor. Chem.*, 15:243–244, 1976.

[26] L.O.Gilpatrick and L.M.Toth. Synthesis and ligand-field spectrum of potassium heptafluoroniobate(IV). *Inorg. Chem.*, 9:2242–2245, 1974.

[27] A.Robin, M.E.de Almeida, and A.F.Sartori. Formation of corrosion resistant niobium coatings by electrodeposition in fluoride melts. In M.Chemla and D.Devilliers, editors, *Molten salt chemistry and technology*, volume 73–75 of *Materials Science Forum*, pages 539–546, Segantinistr. 216, CH-8049 Zürich, Switzerland, 1991. Trans Tech publications Ltd.

[28] O.L.Keller Jr. Identification of complex ions of niobium(V) in hydrofluoric acid solutions by Raman and infrared spectroscopy. *Inorg. Chem.*, 2:783–787, 1963.

[29] K.B.Andersen, E.Christensen, R.W.Berg, N.J.Bjerrum, and J.H.von Barner. Infrared and Raman spectroscopic investigations of the $Nb(V)$ fluoro and oxofluoro complexes in the *LiF-NaF-KF* eutectic melt with development of a diamond IR cell. *Inorg. Chem.*, 39:3449–3454, 2000.

[30] V.I.Konstantinov, S.A.Kuznetsov, and P.T.Stangrit. Density of salt melts containing *KCl*, *KF*, K_2NbF_7 and Nb_2O_5. *Russ. J. Appl. Chem.*, 53:797–800, 1979. Translated from Zhurnal Prikladnoi Khimii 53:1029-1032, 1979.

[31] F.Matthiesen, P.T.Jensen, and T.Østvold. Oxofluoride complexes of niobium(IV,V) in the liquid eutectic *LiF-NaF-KF* melt at 700 °C with varying oxide-to-niobium molar ratios. *Acta Chem. Scand.*, 52:1000–1005, 1998.

[32] J.S.Fordyce and R.L.Baum. Infrared-reflection spectra of molten fluoride solutions: Tantalum(V) in alkali fluorides. *J. Chem. Phys.*, 44:1159–1167, 1966.

[33] O.L.Keller Jr. and C.Strode Jr. A study by Raman spectroscopy of complex ions formed by tantalum(V) in the system $Ta(V)$-HF-NH_4F-H_2O. *Inorg. Chem.*, 5:367–372, 1966.

[34] N.A.Matwiyoff, L.B.Asprey, and W.E.Wageman. Fluorine-19 nuclear magnetic resonance and Raman spectral studies of tantalum(V)-fluoride ion complexes in anhydrous hydrogen fluoride solutions. *Inorg. Chem.*, 9:2014–2019, 1970.

[35] L.P.Varga and H.Freund. The formation constants of the tantalum fluoride system. *J. Phys. Chem.*, 66:21–28, 1962. I. Potentiometric and anion exchange studies-evidence for species of coördination number nine.

[36] A.I.Agulyanskii. The influence of outher-sphere cations of the shift of ionic equilibrium involving tantalum(V) complexes in fluoride melts. *Russ. J Inorg. Chem.*, 25:1648–1650, 1980. Translated from Zhurnal Neorganicheskoi Khimii, 25:2988-3002, 1980.

[37] J.H.von Barner, R.W.Berg, N.J.Bjerrum, E.Christensen, and F.Rasmussen. Vibrational spectra of fluoro and oxofluoro complexes of $Nb(V)$ and $Ta(V)$. In M.Chemla and D.Devilliers, editors, *Molten salt chemistry and technology*, volume 73–75 of *Matererials Science Forum*, pages 279–284, Segantinistr. 216, CH-8049 Zürich, Switzerland, 1991. Trans Tech publications Ltd.

[38] N.J.Bjerrum, R.W.Berg, E.Christensen, D.H.Kerridge, and J.H.von Barner. Use of vibrational spectroscopy to determine oxide content of alkali metal fluoride-tantalum melts. *Anal. Chem.*, 34:2129–2135, 1995.

[39] E.Robert, E.Christensen, B.Gilbert, and N.J.Bjerrum. The effect of electrolysis of K_2TaF_7-LiF-NaF-KF Na_2O melts. *Electrochimica Acta*, 44:1689–1696, 1999.

[40] D.Inman, R.S.Sethi, and R.Spencer. The effects of complex ion formation and ionic adsorption on electrode reactions involving metals and metal ion in fused salts. *J. Electroanal. Chem.*, 29:137–147, 1971.

[41] A.Espinola, A.J.B.Dutra, and F.T.Silva. Mechanism of the electrochemical reduction of tantalum(V) in molten fluorides. *Anal. Chim. Acta*, 251:53–58, 1991.

[42] L.P.Polyakova, E.G.Polyakov, F.Matthiesen, E.Christensen, and N.J.Bjerrum. Electrochemical study of tantalum in fluoride and oxofluoride melts. *J.Electrochem. Soc.*, 141:2982–2988, 1994.

[43] P.Taxil and J.Mahenc. Formation of corrosion-resistant layers by electrodeposition of refractory metals or by alloy electrowinning in molten fluorides. *J. Appl. Electrochem.*, 17:261–269, 1987.

[44] V.I.Konstantinov, E.G.Polyakov, and P.T.Stangrit. Cathodic electrolysis on chloride-fluoride and oxofluoride-chloride melts of tantalum. *Electrochim. Acta*, 23:713–716, 1978.

[45] G.A.Voyiatzis, E.A.Pavlatou, G.N.Papatheodorou, M.Bachtler, and W.Freyland. Reduction products of pentavalent niobium and tantalum in fused chloride melts. In *Proc. Int. Symp. Molten Salt Chem. Techn.*, volume 9. Electrochem. Soc., 1993.

[46] W.Bues, F.Demiray, and H.A.Øye. Raman-spektroskopische untersuchungen von geschmolzenem $NbCl_5$. *Z. Phys. Chem. Neue Folge*, 84:18–24, 1973. [In German].

[47] G.J.Kipouros, J.H.Flint, and D.R.Sadoway. Raman spectroscopic investigation of alkali-metal hexachloro compounds of refractory metals. *Inorg. Chem.*, 24:3881–3884, 1985.

[48] S.A.Kuznetsov, A.G.Morachevskii, and P.T.Stangrit. Electrochemical behavior of niobium(V) in chloride melts. *Soviet Electrochem.*, 18:1357–1361, 1982. Translated from Élektrokhimiya 18:1522-1525, 1982.

[49] K.Zhou, T.Takenaka, N.Sato, and M.Nanjo. The electrochemical behavior of niobium ions in molten *LiCl-KCl* eutectic. *Denki Kagaku*, 59:981–987, 1991. [In japaneese]. Only abstract in english.

[50] G.Picard and P.Bocage. The niobium chemistry in molten *LiCl+KCl* eutectic. In M.Chemla and D.Devilliers, editors, *Molten salt chemistry and technology*, volume 73–75 of *Materials Science Forum*, pages 505–512, Segantinistr. 216, CH-8049 Zürich, Switzerland, 1991. Trans Tech publications Ltd.

[51] F.Lantelme, A.Barhoun, and J.Chevalet. Electrochemical behavor of solutions of niobium chlorides in fused alkali chlorides. *J. Electrochem. Soc.*, 140:324–331, 1993.

[52] M.Mohamedi, Y.Sato, and T.Yamamura. Examination of niobium electrochemistry from the reduction of Nb_3Cl_8 in molten *LiCl-KCl* eutectic. *Electrochim. Acta*, 44:1559–1565, 1999.

[53] J.Dartnell, K.E.Johnson, and L.L.Shreir. Electrochemistry of niobium in fused halides. *J. Less. Com. Mets.*, 6:85–93, 1964.

[54] Y.Saeki and T.Suzuki. Equilibrium between niobium and niobium subchloride in *LiCl-KCl* eutectic melt. *J. Less. Com. Mets.*, 9:362–366, 1965.

[55] B.Gillesberg, J.H.von Barner, N.J.Bjerrum, and F.Lantelme. Niobium plating processes in alkali chloride melts. *J. Appl. Electrochem.*, 29:939–949, 1999.

[56] S.A.Kuznetsov and V.V.Grinevich. Niobium interaction with its chloride, fluoride, and oxofluoride complexes in melts of alkali metal chlorides. *Russ. J. Appl. Chem.*, 67:1249–1255, 1994. Translated from Zhurnal Prikladnoi Khimii 67:1423-1430, 1994.

[57] S.A.Kuznetsov, S.V.Kuznetsova, and A.L.Glagolevskaya. The process of electroreduction of the niobium chloride complexes in the *NaCl-KCl* melt. *Russ. J. Electrochem.*, 32:981–987, 1996. Translated from Élektrokhimiya 32:1061-1067, 1996.

[58] A.Khalidi and J.Bouteillon. Comportment electrochimique de $NbCl_5$ en milieu *NaCl-KCl* pur et additionne d'ions fluorure. *J. Appl. Electrochem.*, 23:801–807, 1993. [In French]. Only abstract in English.

[59] I.Nakagawa and Y.Hirabayashi. Electrochemical study of a soluble niobium anode in molten salts. *J. Less. Com. Mets.*, 83:155–168, 1982.

[60] F.Lantelme and Y.Berghoute. Transient electrochemical techniques for studying electrodeposition of niobium in fused *NaCl-KCl*. *J. Electrochem. Soc*, 141:3306–3311, 1994.

[61] L.Arurault, J.Bouteillon, J.de Lepinay, A.Khalidi, and J.C.Poignet. Electrochemical properties of $NbCl_5$ or K_2NbF_7 dissolved in *NaCl-KCl* equimolar melts. In M.Chemla and D.Devilliers, editors, *Molten salt chemistry and technology*, volume 73–75 of *Materials Science Forum*, pages 305–312, Segantinistr. 216, CH-8049 Zürich, Switzerland, 1991. Trans Tech publications Ltd.

[62] I.R.Elizarova, E.G.Polyakov, and I.P.Polyakova. Electrochemical behavior of niobium in $CsCl$-KCl-$NbCl_5$ melts. *Russ. J. Electrochem.*, 27:581–587, 1991. Translated from Élektrokhimiya 27:640-647, 1991.

[63] I.Elizarova, E.Polyakov, and L.Polyakova. Electrochemical behavior of niobium in $CsCl$-KCl-$NbCl_5$ melt. In M.Chemla and D.Devilliers, editors, *Molten salt chemistry and technology*, volume 73–75 of *Materials Science Forum*, pages 393–400, Segantinistr. 216, CH-8049 Zürich, Switzerland, 1991. Trans Tech publications Ltd.

[64] U.Stöhr and W.Freyland. Electrochemical impedance investigations of redox mechanisms of refractory metal compounds in molten salts. *Electrochim. Acta*, 44:2199–2207, 1999. I. Niobium chloride and oxychloride in $CsCl$-$NaCl$ eutectic melt.

[65] C.Rosenkilde and T.Østvold. Chemistry of niobium chlorides in the $CsCl$-$NaCl$ eutectic melt. *Acta Chem. Scand.*, 49:85–95, 1995. 2. Voltammetric studies of niobium chlorides and oxochlorides in the $CsCl$-$NaCl$ eutectic melt.

[66] B.D.Vasin, S.V.Maslov, S.P.Raspopin, M.G.Kalinin, and D.B.Sukhinin. Electrochemical behavior of niobium in eutectic mixture of sodium and caesium chlorides. *Melts*, 4:40–44, 1990. Translated from Rasplavy 4:48-52, 1990.

[67] C.Rosenkilde, G.Voyatzis, V.R.Jensen, M.Ystenes, and T.Østvold. Raman spectroscopic and *ab initio* quantum chemical investigations of molecules and complex ions in the molten system $CsCl$- $NbCl_5$-$NbOCl_3$. *Inorg. Chem.*, 34:4360–4369, 1995.

[68] A.Sabatani and I.Bertini. Far-infrared spectra of oxochloro and oxobromo complexes of $Nb(V)$, $Mo(V)$ and $W(V)$. *Inorg. Chem.*, 5:204–206, 1966.

[69] E.Wendling. No 2.–données radiocristallographiques sur les chlorocomplexes des types $M_2(Me^{IV}Cl_6)$ $(Me = Ti, Nb, Mo, W)$, $M_2(Me^{IV}O_2Cl_4, H_2O)$ $(Me = Ti)$, $M_2(Me^{V}OCl_5)$ $(Me = V, Nb, Cr, Mo, W)$, $M_2(Me^{V}O_2Cl_5)$ $(Me = Nb, Ta)$, $M_2(Me^{IV}O_2Cl_4)$ $(Me = Mo)$ et $M_2(Me^{VI}O_3Cl_4)$ $(Me = Mo)$ $(M = NH_4, Rb, Cs)$. *Bull. Soc. Chim. de France*, pages 5–8, 1967. [In French].

[70] D.Brown. Some oxychloro-complexes of quinquevalent elements. *J. Chem. Soc. (A)*, pages 4944–4948, 1964.

[71] L.E.Ivanovskii and A.F.Plekhanov. Electrolysis of molten chloride melts using dissolving anodes made of a mixture of *NbO* and carbon. *Electrochemistry of molten and solid electrolytes*, 4:71–75, 1967.

[72] M.Bachtler, J.Rockenberger, W.Freyland, C.Rosenkilde, and T.Østvold. Electronic absorbtion spectra of reduction products of pentavalent niobium and tantalum in different alkali chloride and oxochloride melts. *J. Phys. Chem.*, 98:742–747, 1994.

[73] C.Rosenkilde and T.Østvold. Chemistry of niobium chlorides in the *CsCl-NaCl* eutectic melt. *Acta Chem. Scand.*, 49:265–270, 1995. 3. Solubility of Nb_2O_5 and *SrO* in the *CsCl-NaCl* eutectic melt with additions of $NbCl_x$ (x = 4, 5).

[74] C.Rosenkilde, G.A.Voyiatzis, and T.Østvold. Raman spectroscopic investigations of the molten *CsCl-*$TaOCl_3$*-*$TaCl_5$ system. *Acta Chem. Scand.*, 49:405–410, 1995.

[75] L.P.Polyakova, E.G.Polyakov, A.I.Sorokin, and P.T.Stangrit. Secondary processes during tantalum electroreduction in molten salts. *J. Appl. Electrochem.*, 22:628–637, 1992.

[76] T.Suzuki. Electrochemical study of tantalum tetrachloride in the *LiCl-KCl* eutectic melt. *Electrochimica Acta*, 15:303–313, 1970.

[77] R.A.Bailey, E.N.Balko, and A.A.Nobile. The anodization products of tantalum in the fused *LiCl-KCl* eutectic. *J. Inorg. Nucl. Chem.*, 37:971–974, 1975.

[78] A.N.Baimakov, S.A.Kuznetsov, E.G.Polyakov, and P.T.Stangrit. Electrochemical behavior of $Ta(V)$ in molten *LiCl-KCl* and the effect of fluoride ion on it. *Soviet Electrochem.*, 21:541–546, 1985. Translated from Élektrokhimiya 21:597-602, 1985.

[79] M.Bachtler, W.Freyland, G.A.Voyiatzis, and G.N.Papatheodorou. Electrochemical and simultaneous spectroscopic study of reduction mechanism and electronic conduction during electrodeposition of tantalum in molten alkali chlorides. *Ber. Bunsenges. Phys. Chem.*, 99:21–31, 1995.

[80] U.Stöhr, P.R.Bandi, F.Matthiesen, and W.Freyland. Electrochemical impedance and cyclic voltammetry study of the influence of oxide on the redox chemistry of niobium and tantalum in chloride melts. *Electrochimica Acta*, 43:569–578, 1998.

[81] Ts'ui Ping-hsin, V.I.Konstantinov, and N.P.Luzhnaya. Solubility and interaction of phases in systems of Ta_2O_5 with potassium and tantalum chlorides and fluorides. *Russ. J. Inorg. Chem.*, 8:204–208, 1963. [Translated from Zhur. Neorg. Khim. 8:389, 1963].

[82] J.H.von Barner, R.W.Berg, Y.Berghoute, and F.Lantelme. Investigation of the complex and redox chemistry of K_2NbF_7 dissolved in *NaCl-KCl* melts with oxide additions. In *Electrochemical technology of molten salts*, volume 1–2 of *Molten salt forum*, pages 121–126, Hardstratsse 13, CH-4714 Aedermannsdorf, Switzerland, 1993/1994. European workshop on electrochemical technology of molten salts, Trans Tech Publications Ltd.

[83] Z.A.Alimova, E.G.Polyakov, L.P.Polyakova, and V.G.Kremenetskii. The role of fluoride ions in the reduction-oxidation equilibria in *NaCl-KCl-NaCl-*K_2NbF_7 melts. *J. Fluorine Chem.*, 59:203–210, 1992.

[84] Z.A.Alimova, E.G.Polyakov, L.P.Polyakova, P.T.Stangrit, and V.G.Kremenetskii. Interaction of niobium with chloride-fluoride melts containing niobium. *Russ. J. Appl. Chem.*, 63:898–904, 1990. Translated from Zhurnal Prikladnoi Khimii 63:992-999, 1990.

[85] M.M.Wong and D.E.Kirby. Electrowinning of niobium. *J Electrochem. Tech.*, 6:119–123, 1968.

[86] S.A.Kuznetsov. Electrolytic production of niobium powder from chloride-fluoride melts containing compounds of niobium and zirconium. *Russ. J Electrochem.*, 36:509–515, 2000. Translated from Élektrokhimiya 36:573-580, 2000.

[87] M.Chemla and V.Grinevitch. Propriétés électrochimiques des fluoniobates en solution dans les chlorures alcalins fondus. *Bull. Soc. Chim. France*, pages 853–859, 1973. [In French].

[88] S.A.Kuznetsov, E.G.Polyakov, and P.T.Stangrit. Electrolytic deposition of niobium coatings from melts on long conductors. *Russ. J. Appl. Chem.*, 56:409–411, 1983. Translated from Zhurnal Prikladnoi Khimii 56:427-429, 1983.

[89] S.A.Kuznetsov, A.L.Glagolevskaya, and P.T.Stangrit. Influence of melt acid-base properties on the mechanism of electroreduction of the complex NbF_7^{2-} in an equimolar *NaCl-KCl* mixture. *Russ. J. Appl. Chem.*, 64:1689–1694, 1991. Translated from Zhurnal Prikladnoi Khimii 64:1838-1843, 1991.

[90] S.A.Kuznetsov, A.L.Glagolevskaya, V.V.Grinevich, and P.T.Stangrit. Kinetic parameters of niobium electroreduction from fluoride and oxyfluoride complexes in *NaCl-KCl* melts. *Russ. J. Electrochem.*, 28:1098–1105, 1992. Translated from Élektrokhimiya 28:1344-1351, 1992.

[91] S.A.Kuznetsov and P.T.Stangrit. Complex formation and stabilization of highest oxidation states of d- elements in salt melts. *Russ. J. Appl. Chem.*, 66:2036–2041, 1993. Translated from Zhurnal Prikladnoi Khimii 66:2702-2709, 1993.

[92] S.A.Kuznetsov, A.L.Glagolevskaya, V.V.Grinevich, and S.A.Kuznetsova. Electroreduction of niobium oxofluoride complexes in the *NaCl-KCl* melt. *Russ. J. Electrochem.*, 33:234–240, 1997. Translated from Élektrokhimiya 33:259-265, 1997.

[93] A.Barhoun, F.Lantelme, M.E.Roy, and J.P.Besse. Electroreduction of fluoniobate, K_2NbF_7, in fused *NaCl- KCl*. In M.Chemla and D.Devilliers, editors, *Molten salt chemistry and technology*, volume 73–75 of *Materials Science Forum*, pages 313–320, Segantinistr. 216, CH-8049 Zürich, Switzerland, 1991. Trans Tech publications Ltd.

[94] A.Barhoun, Y.Berghoute, and F.Lantelme. Electrodeposition of niobium from fluoroniobate K_2NbF_7 solutions in fused *NaCl-KCl*. *J. Alloys and compounds*, 179:241–252, 1992.

[95] L.Arurault, J.Bouteillon, and J.C.Poignet. Electrochemical study of the reduction of solutions obtained several hours after dissolving K_2NbF_7 in molten *NaCl-KCl* at 750 °C. *J. Electrochem. Soc.*, 142:3351–3356, 1995.

[96] F.Lantelme, Y.Berghoute, J.H.von Barner, and G.S.Picard. The influence of oxide on the electrochemical processes in K_2NbF_7-*NaCl-KCl* melts. *J. Elecotrchem. Soc.*, 142:4097–4102, 1995.

[97] V.I.Konstantinov, E.G.Polyakov, and P.T.Stangrit. Cathodic processes at electrolysis of chloride-fluoride and oxofluoride melts of niobium. *Electrochimica Acta*, 26:445–448, 1981.

[98] Z.A.Alimova, I.R.Elizarova, E.G.Polyakov, and L.P.Polyakova. Anodic dissolution of niobium in chloride and mixed chloride-fluoride melts. *Russ. J. Electrochem.*, 28:962–966, 1992. Translated from Élektrokhimiya 28:1165-1170, 1992.

[99] E.G.Polyakov, L.P.Polyakova, and I.R.Elizarova. Cathode processes in chloride-fluoride melts containing K_2NbF_7. *Russ. J. Electrochem.*, 31:457–464, 1995. Translated from Élektrokhimiya 31:502-509, 1995.

[100] B.Gillesberg, N.J.Bjerrum, J.H.von Barner, and F.Lantelme. Electrochemical investigation on the redox chemistry of niobium in *LiCl-KCl-KF-*Na_2O melts. *J. Electrochem. Soc.*, 144:3435–3441, 1997.

[101] L.Arurault, J.Bouteillon, and J.C.Poingnet. Chemical stability of solutions of niobium V in molten *NaCl-KCl* at 750 °C. *J. Electrochem, Soc.*, 142:16–19, 1995.

[102] S.A.Kuznetsov, E.G.Polyakov, and P.T.Stangrit. Current yield in the electrolysis of chloride-fluoroniobate melts. *Russ. J. Appl. Chem.*, 52:1238–1241, 1978. Translated from Zhurnal Prikladnoi Khimii 52:1308-1312, 1978.

[103] V.V.Grinevitch, V.A.Reznichenko, M.S.Model, S.A.Kuznetsov, E.G.Polyakov, and P.T.Stangrit. Oxydation-reduction processes in halide and oxohalide niobium containing melts. Part I: Interaction of fluoride-chloride and oxofluoride- chloride $Nb(V)$ melts with niobium oxides. *J. Appl. Electrochem.*, 29:693–702, 1999.

[104] A.I.Agulyanskii, S.A.Kirillov, and V.D.Prisyanzhnyi. This paper is written in russian, and is printed with Cyrillic letters. *Ukr. Khim. Zh.*, 46:457–460, 1980.

[105] Von P.Drossbach and P.Petrick. Zur kenntis der abscheidung von tantal durch elektrolyse geschmolzener salze. *Z. Elektrochem.*, 61:410–415, 1957.

[106] F.Lantelme, A.Barhoun, G. Li, and J.Besse. Electrodeposition of tantalum in *NaCl-KCl-*K_2TaF_7 melts. *J. Electrochem. Soc.*, 139:1249–1255. 1992.

[107] R.M.Bergman and C.E.Mosheim. Tantalum powder process. **U.S.Patent 4,684,399**, 1987.

[108] S.Pizzini and R.Morlotti. Oxygen and hydrogen electrodes in molten fluorides. *Electrochimica Acta*, 10:1033–1041, 1965.

[109] D.R.Lide, editor. *CRC Handbook of Chemistry and Physics.* CRC Press LLC, 78 edition, 1997–1998.

[110] H.Mediaas, J.E.Vindstad, and T.Østvold. Solubility of MgO in $MgCl_2$-$NaCl$-NaF melts. *Light metals*, pages 1129–1137, 1996.

[111] H.Mediaas, J.E.Vindstad, and T.Østvold. Solubility of MgO in mixed chloride-fluoride melts containing $MgCl_2$. *Acta Chem. Scand.*, 51:501–514, 1997.

[112] B.Gilbert, G.Mamantov, and G.M.Begun. A simple Raman cell and furnace usable at temperatures higher than 1000 °C for corrosive melts. *Applied Spectroscopy*, 29:276–278, 1975.

[113] B.Gilbert and T.Materne. Reinvestigation of molten fluoroaluminate Raman spectra: The question of the existence of AlF_5^{2-} ions. *Applied Spectroscopy*, 44:299–305, 1990.

[114] V.Dracopoulos and G.N.Papatheodorou. In H.C.Delong, S.Deki, P.C.Trulove, R.W.Bradshaw, and G.R.Stafford, editors, *Eleventh International Symposium on Molten Salts*, Pennington NJ, 1998. The Electrochemical Society.

[115] S.A.Kuznetsov, A.L.Glagolevskaya, S.V.Kuznetsova, A.T.Belyaevskii, and P.T Stangrit. Preparation of high-melting metal carbide coatings in molten salts using disproportionation reactions. *Russ. J. Appl. Chem.*, 63:1920–1921, 1990. Translated from Zhurnal Prikladnoi Khimii 63:2078-2080, 1990.

[116] J.L.Hoard. Structures of complex fluorides. Potasium heptafluocolumbiate and potasium heptafluotantalate. The configuration of the heptafluocolumbiate and heptafluotantalate ions. *J. Am. Chem. Soc.*, 61:1252–1259, 1939.

[117] G.M.Brown and L.A.Walker. Refinement of the structure of potasium heptafluoroniobate, K_2NbF_7, from neutron-diffraction data. *Acta. Cryst*, 20:220–229, 1966.

[118] von G.Pausewang, R.Schmitt, and K.Dehnicke. Schwingungsspektren von oxofluorokomplexen der spezies $NbOF_5^{2-}$, $TaOF_5^{2-}$, $MoO_2F_4^{2-}$, $WO_2F_4^{2-}$, $NbOF_6^{3-}$ und $MoO_2F_5^{3-}$. *Z. Anorg. Allg. Chem.*, 408:1–8, 1974. [In German].

[119] G.Pausewang. Zur struktur der verbindungen A_2NbOF_5 und $A_2MoO_2F_4$ mit $A = Rb, Cs, NH_4$. *Z. Naturforsch*, 26b:1218–1220, 1971. [In german].

[120] G.Pausewang. Neue $A_2M(O,F)_6$ verbindungen mit K_2GeF_6-struktur. *Z. Naturforsch*, 29b:49–51, 1971. [In german].

[121] A.M.Srivastava and J.F.Ackerman. Synthesis and luminescence properties of Cs_2NbOF_5 with isolated $[NbOX_5]^{-2}(X = F^-, Cl^-)$ octahedra. *Mat. Res. Bull.*, 26:443–448, 1991.

[122] T.G.Burke, D.F.Smith, and A.H.Nielsen. The molecular structure of MoF_6, WF_6 and UF_6 from infrared and Raman spectra. *J. Chem. Phys.*, 20:447–454, 1952.

[123] L.E.Alexander, I.R.Beattie, A.Bukovszky, P.J.Jones, and C.J.Marsden. Vapour density and vibrational spectra of $MoOF_4$ and WOF_4. The structure of crystalline WOF_4. *J. Chem. Soc. Dalton*, pages 81–84, 1974.

[124] J.H.Holloway, H.Selig, and H.H.Claasen. Vibrational spectra of IOF_5, $OsOF_5$ and $ReOF_5$. *J. Chem. Phys.*, 54:4305–4311, 1971.

[125] I.R.Beattie, K.M.S.Livingston, D.J.Reynolds, and G.A.Ozin. Vibrational spectra of some oxide halides of the transition elements with particular reference to gas-phase and single-crystal Raman spectroscopy. *J. Chem. Soc. (A)*, pages 1210–1216, 1970.

[126] J.A.S.Howell and K.C.Moss. Nuclear magnetic resonance studies of fluorine-containing compounds. Part III. The tetrafluorooxovandate(V) ion. *J. Chem. Soc.(A)*, pages 270–272, 1971.

[127] W.P.Griffith and T.D.Wickins. *cis*-Dioxo and trioxo-complexes. *J. Chem. Soc.(A)*, pages 400–404, 1968.

[128] G.Pausewang and W.Rudorf. $A_3MeO_xF_{6-x}$-verbindungen mit $x = 1, 2, 3$. *Z. Anorg. Allg. Chem.*, 364:69–87, 1969.

[129] M.D.Fontana, G.E.Kugel, J.Vamvakas, and C.Carbatos. Long wavelength phonons in the different phases of $KNbO_3$. *Phys. Stat. Sol.*, 103:211–219, 1981.

[130] A.A.Mc.Connel, J.S.Anderson, and C.N.R.Rao. Raman spectra of niobium oxides. *Spectr. Acta*, 32A:1067–1076, 1976.

[131] D.A.Edwards and R.T.Ward. Some reactions of rhenium(V) chloride. *J. Chem. Soc. (A)*, pages 1617–1620, 1970.

[132] U.Balachandran and N.G.Eror. Raman spectrum of the high temperature form of Nb_2O_5. *J. Mat. Sci. Letts.*, 1:374–376, 1982.

[133] S.Boghosian, F.Borup, and R.W.Berg. Stoichiometry, vibrational modes and structure of molten Nb_2O_5-$K_2S_2O_7$ mixtures. A Raman spectroscopic study. In P.C.Trulove, H.C.DeLong, G.R.Stafford, and S.Deki, editors, *Molten Salts XI*, volume 98-11, pages 536–543. The electrochemical society, Pennington, New Jersey, 1998.

[134] D.V.Tsikaeva, S.D.Nikitina, A.I.Agulyanskii, and V.T.Kalinnkov. Vibrational spectra of niobium and tantalum complexes in hydrofluoric acid. *J. Gen. Chem. USSR*, 5:866–870, 1987. Translated from Zh. Obshch. Khim, 5:974-976, 1987.

[135] A.G.Babkin, A.I.Nikolaev, and E.V.Shevyreva. The re-extraction of fluoro-complexes of niobium and tantalum from neutral oxygen-containing solvents. *Russ. J Inorg. Chem.*, 31:1412–1413, 1986. Translated from Zh. Neorg. Khim. 31:2444-2445, 1986.

[136] J.Sala-pala, J.Y.Calves, and J.E.Guerchais. A study of the ion $[Ta_2OF_{10}]^{2-}$. *Can. J. Chem.*, 56:1545–1548, 1978.

[137] Yu.A.Buslaev and Yu.V.Kokunov. Inner-sphere reactions of transition metal alkoxide halides. *Proc. USSR Acad. Sci., Inorg. Mater.*, 4:461–464, 1968. [Translated from Izv. Akad. Nauk. SSSR, Neorg. Mater. 4:537-540, 1968].

[138] U.Balachandran and N.G.Eror. A study of the crystal structure of B-Ta_2O_5 by vibrational spectroscopy and X-ray diffraction. *J. Mat. Sci. Letts.*, 1:219–222, 1982.

Appendices

Appendix A

Solubility data for $Nb(V)$

Experimental results from solubility measurements with $Nb(V)$

Tabel A.1 shows analyzed values of oxygen and niobium in melt samples from liquid $FLiNaK$ at 700 °C. The samples are withdrawn at various molar ratios, n_O/n_{Nb}, in the melt and in the solid phases. The data were used to make figure 3.1.

Table A.1: Concentrations of oxygen and niobium that were used to create figure 3.1

Oxygen mole/kg	SD mole/kg	Niobium mole/kg	SD mole/kg	n_O/n_{Nb}	SD
0,0098	0,0013	0,2148	0,0034	0,0427	0,0058
0,0988	0,0063	0,2014	0,0014	0,3883	0,0059
0,2138	0,0163	0,2283	0,0032	0,7943	0,0061
0,2988	0,0109	0,2375	0,0028	1,1627	0,0063
0,3793	0,0126	0,2241	0,0036	1,4825	0,0066
0,4617	0,0044	0,2248	0,0020	1,7670	0,0067
0,4770	0,0262	0,2206	0,0026	2,0188	0,0073
0,3581	0,0738	0,1864	0,0017	2,2835	0,0097
0,2644	0,0056	0,0993	0,0008	2,6070	0,0099
0,1678	0,0095	0,0441	0,0004	2,9393	0,0100
0,4232	0,0219	0,1095	0,0013	3,2870	0,0104
0,6613	0,0256	0,1691	0,0029	3,6086	0,0109
0,8388	0,0494	0,1959	0,0012	3,9412	0,0122
0,8640	0,0469	0,2006	0,0020	4,2709	0,0134
0,9075	0,0250	0,2185	0,0019	4,5825	0,0141

Tabel A.2 shows analyzed values of oxygen and niobium in melt samples from liquid *FLiNaK* at 700 °C. The samples are withdrawn at various molar ratios, n_O/n_{Nb}, in the melt and in the solid phases. The data were used to make figure 3.2.

Table A.2: Concentrations of oxygen and niobium that were used to create figure 3.2

Oxygen mole/kg	SD mole/kg	Niobium mole/kg	SD mole/kg	n_O/n_{Nb}
0,4356	0,0318	0,2320	0,0018	1,9744
0,1508	0,0080	0,0453	0,0004	2,9699
0,5594	0,0500	0,1578	0,0008	3,4749
0,7731	0,0519	0,2060	0,0015	3,9050
0,8188	0,0625	0,2040	0,0018	4,4555
0,9241	0,0780	0,2079	0,0014	5,0082
1,0438	0,0625	0,2106	0,0015	5,6157
0,9850	0,0144	0,2134	0,0015	6,2106
1,2063	0,1313	0,2028	0,0018	6,8226
1,3750	0,0750	0,1841	0,0022	7,6345
1,6438	0,1375	0,2197	0,0024	8,6162

Tabel A.3 shows analyzed values of oxygen and niobium in melts samples from liquid *FLiNaK* saturated with Nb_2O_5. Samples were withdrawn at different temperatures. The data were used to make figure 3.4.

Table A.3: Concentrations of oxygen and niobium that were used to create figure 3.4

Temperature °C	Oxygen mole/kg	Niobium mole/kg
550	0,164	0,0769
650	0,664	0,307
700	1,169	0,544
800	1,879	0,747

Appendix B

Solubility data for $Ta(V)$

Experimental results from solubility measurements with $Ta(V)$

Tabel B.1 shows analyzed values of oxygen and tantalum in melt samples from liquid *FLiNaK* at 700 °C. The samples are withdrawn at various molar ratios, n_O/n_{Ta}, in the melt and in the solid phases. The data were used to make figure 4.1.

Tabel B.2 shows analyzed values of oxygen and niobium in melts samples from liquid *FLiNaK* with dissolved Ta_2O_5. Samples were withdrawn at 700 °C. The data were used to make figure 4.2.

Table B.1: Concentrations of oxygen and tantalum that were used to create figure 4.1

Oxygen mole/kg	SD mole/kg	Tantalum mole/kg	SD mole/kg	n_O/n_{Ta}	SD
0,0061	0,0012	0,0966	0,0006	0,0642	0,0125
0,0244	0,0014	0,0980	0,0007	0,2647	0,0125
0,0504	0,0019	0,1046	0,0012	0,5602	0,0128
0,0729	0,0250	0,0943	0,0005	0,8200	0,0132
0,0966	0,0001	0,0946	0,0004	1,1002	0,0146
0,1289	0,0056	0,0999	0,0007	1,4278	0,0149
0,1649	0,0091	0,1006	0,0008	1,7994	0,0155
0,1285	0,0065	0,0723	0,0006	2,1320	0,0161
0,0833	0,0016	0,0442	0,0003	2,4635	0,0166
0,0141	0,0001	0,0062	0,0001	2,8704	0,0168
0,0891	0,0057	0,0198	0,0003	3,1700	0,0169
0,1654	0,0108	0,0402	0,0003	3,5282	0,0171
0,2393	0,0082	0,0604	0,0006	3,8579	0,0176
0,3486	0,0508	0,0937	0,0008	4,2592	0,0182
0,3713	0,0366	0,0983	0,0013	4,6250	0,0208
0,4038	0,0337	0,0962	0,0009	5,2173	0,0257
0,4563	0,0496	0,0875	0,0005	6,0627	0,0283

Table B.2: Concentrations of oxygen and tantalum that were used to create figure 4.2

Total O mole/kg	Oxygen mole/kg	SD mole/kg	Tantalum mole/kg	SD mole/kg
0,0614	0,0189	0,0028	0,0064	0,0001
0,1801	0,0562	0,0019	0,0288	0,0008
0,2979	0,0974	0,0024	0,0518	0,0013
0,6698	0,1989	0,0201	0,1029	0,0026
1,4347	0,3329	0,0532	0,1879	0,0052